Development of a biodegradable contact lens system for ocular drug delivery

by

Piyush Garg

A thesis

presented to the University of Waterloo

in fulfillment of the

thesis requirement for the degree of

Doctor of Philosophy

in

Vision Science

Waterloo, Ontario, Canada, 2025

© Piyush Garg 2025

Examining Committee Membership

The following served on the Examining Committee for this thesis.

External Examiner	Debarun Dutta Senior Lecturer
Internal-External Examiner	Elizabeth Prince Assistant Professor
Supervisors	Lyndon Jones University Professor
	Chau-Minh Phan Research Assistant Professor
Internal Members	Marc G. Aucoin Professor
	Denise Hileeto Clinical Associate Professor
	William Ngo Assistant Professor

Author's Declaration

This thesis consists of material all of which I authored or co-authored: see Statement of Contributions included in the thesis. This is a true copy of the thesis, including any required final revisions, as accepted by my examiners.

I understand that my thesis may be made electronically available to the public.

Statement of Contributions

Piyush Garg was the sole author for Chapters 1, 2, and 7, which were written under the supervision of Dr. Lyndon Jones, Dr. Chau-Minh Phan and Dr. Parvin Shokrollahi and were not written for publication.

This thesis consists of four manuscripts written for publication. Exceptions to sole authorship of material are as follows:

Research presented in Chapter 3:

This research was conducted at the Centre for Ocular Research & Education (CORE) at the University of Waterloo under the supervision of Dr. Lyndon Jones. The study was designed and carried out by Parvin Shokrollahi, Piyush Garg, David Wulff, Chau-Minh Phan, and Lyndon Jones. Parvin Shokrollahi, Piyush Garg, and David Wulff contributed to concept/design, data acquisition, analysis, manuscript writing, and final review. Chau-Minh Phan and Lyndon Jones contributed to conceptualization and manuscript reviewing.

Citation: Shokrollahi P, Garg P, Wulff D, Hui A, Phan CM, Jones L. Vat photopolymerization 3D printing optimization: Analysis of print conditions and print quality for complex geometries and ocular applications. *Int J Pharm.* 2025; 668: 124999.

Research presented in Chapter 4:

This work was conducted at the University of Waterloo under the supervision of Dr. Chau-Minh Phan and Dr. Lyndon Jones. Piyush Garg is responsible for the majority of study design, data acquisition, analysis, manuscript writing and final review. Haile Darge contributed to data acquisition related to cell culture experiments. Parvin Shokrollahi, Chau-Minh Phan and Lyndon Jones contributed to the conceptualization of the project and manuscript review.

Citation: Garg P, Shokrollahi P, Darge HF, Phan CM, Jones L. 3D-printed contact lenses to release polyvinyl alcohol as a therapeutic agent for the treatment of dry eyes. *Pharmaceutics.* 2025; 17(2): 219.

Research presented in Chapter 5:

This work was conducted at the University of Waterloo under the supervision of Dr. Chau-Minh Phan and Dr. Lyndon Jones. Piyush Garg and Parvin Shokrollahi are responsible for the majority of study design,conceptualization, data acquisition, analysis, manuscript writing and final review. Haile Darge contributed to data acquisition related to cell culture experiments. Chau-Minh Phan and Lyndon Jones contributed to the final manuscript review.

Citation: Garg P, Shokrollahi P, Darge HF, Phan CM, Jones L. Controlled PVA release from chemical–physical interpenetrating networks to treat dry eyes. *ACS Omega.* 2024; 10(1): 1249–1260.

Research presented in Chapter 6:

This research was conducted at the University of Waterloo under the supervision of Dr. Lyndon Jones. The study, focusing on biodegradable 3D-printed conjunctival inserts for the treatment of dry eyes, was conceptualized and designed by Piyush Garg and Parvin Shokrollahi, with contributions from Chau-Minh Phan and Lyndon Jones. Data acquisition, analysis, manuscript writing was carried out by Piyush Garg with supervision of Parvin Shokrollahi. Chau-Minh Phan and Lyndon Jones also provided supervision and assisted with manuscript revisions. The manuscript was drafted by Piyush Garg, with input and revisions from all co-authors.

Citation: Garg P, Shokrollahi P, Phan CM, Jones L. Biodegradable 3D-printed conjunctival inserts for the treatment of dry eyes. *Polymers*. 2025; 17(5): 623.

As lead author of these experimental chapters, I was responsible for contributing to conceptualizing study design, carrying out data collection and analysis, and drafting and submitting manuscripts. My coauthors provided guidance during each step of the research and provided feedback on draft manuscripts.

Abstract

Purpose:

The aim of this thesis was to develop a biodegradable ocular drug delivery system (comprising contact lenses and conjunctival inserts), with the ability of controlled release of PVA using a physical crosslinking method.

Methods:

In the first experimental chapter (Chapter 3), a commercially available 3D printer was modified and the 3D printing process with a gelatin methacrylate (GelMA) biomaterial ink was optimized. GelMA biomaterial ink was selected as a base material owing to its biocompatibility and demonstrated high levels of controllability. In the second experimental chapter (Chapter 4), the shape fidelity of the 3D printed contact lenses loaded with polyvinyl alcohol (PVA) as a therapeutic agent was evaluated. In the third experimental chapter (Chapter 5), a physical crosslinking strategy was evaluated as a potential modification to prolong the release of PVA from the GelMA network. In the final experimental chapter (Chapter 6), the degradation mechanism of GelMA-based conjunctival inserts in the presence of a matrix metalloproteinase enzyme (MMP9) is described, along with its correlation with the release of PVA.

Results

The results demonstrate that by tuning the printing conditions and ink parameters, soft biomaterials from a GelMA ink of higher shape fidelity and accuracy can be efficiently printed even on low-cost 3D printers. Moreover, a fine interplay between the dye concentration (C_{Dye}) and exposure time is key to effective polymerization and resolution, ensuring successful printing of the hydrogel biomaterials with higher structural integrity. It is further possible to add PVA to these lenses and the PVA release curves showed that about 1300 µg of PVA was released over the study duration of 24 hrs. PVA can act as a viscosity enhancer and protect corneal cells against dry eye related desiccation stress. These results were confirmed with the help of non-invasive keratograph break-up time measurements on a 3D printed eyeball model, where 1.4% (w/v) PVA solution displayed significantly higher tear break-up time compared to a control ($p<0.05$).

The release rate of PVA from these biomaterials can be controlled by applying short freeze thaw cycles, which induces formation of crystalline domains in the interpenetrating network. The appearance

of endothermic peaks at 48 ℃ and 60 ℃ in differential scanning calorimetry (DSC) thermograms and 20°-2θ peaks in X-ray diffraction (XRD) patterns suggest the formation of these crystalline domains. The release profiles of the PVA containing hydrogels prove that crystalline domain formation could support sustained PVA release and control its initial burst release. The release profiles displayed highest linearity with the Korsmeyer-Peppas model ($0.9944<R^2<0.9952$), indicating that these systems follow non-Fickian or anomalous transport.

The results from this thesis highlight the versatility of 3D printing to fabricate GelMA-based conjunctival inserts. There are different factors that influence the MMP-mediated degradation of GelMA hydrogels, and that the degradation rate is a function of MMP9 enzyme concentration. The 3D printed GelMA/PVA inserts formed a semi-interpenetrating network. The results from the biodegradation study show that about 59.6% and 83.3% of the P-Gel-5% hydrogel was degraded at the end of 8 hrs and 12 hrs in the presence of 50 µg/ml MMP9 enzyme solution. Similarly, about 47.0%, 50.2% and 81.7% % of the P-Gel-5% hydrogel was degraded at the end of 8 hrs, 12 hrs, and 24 hrs, respectively, in the presence of 25 µg/ml MMP9 enzyme solution. However, no degradation was observed in the control group incubated with PBS at the end of the study duration of 24 hrs. The PVA release graphs demonstrate that 222.7±20.3 µg, 265.5±27.1 µg and 242.7±30.4 µg of PVA was released at 25 µg/ml, 50 µg/ml and 100 µg/ml MMP9 enzyme concentrations after 24 hrs. These results suggest that degradation rate of GelMA is a function of MMP9 enzyme concentration and the PVA release profiles of these inserts in the presence of different concentrations of MMP9 showed highest linearity with the Korsmeyer-Peppas model.

Conclusions

This thesis has investigated 3D printed CLs and conjunctival inserts for controlled ocular drug delivery. Several important findings have been reported, and the shortcomings have been discussed in this thesis. With the advancements in 3D printing, personalized ophthalmic devices fabricated from 3D printing could be a commercially viable option, but the cost and transparency need to be considered.

Acknowledgements

Mom & Dad, I did it!

As I reach the end of this extraordinary journey, I am filled with gratitude for the countless individuals who have made this accomplishment possible.

"A PhD is not the solitary achievement of an individual's effort, but a rich tapestry woven from the threads of relentless endeavor and collaborative contributions of many."

First and foremost, I must extend my deepest thanks to my advisors, Lyndon Jones and Chau-Minh Phan (and Parvin Shokrollahi: Yes, although you were not my official supervisor, the depth of your mentorship has been equivalent to that of a supervisor in my journey). Your unwavering belief in me, your profound wisdom, and your constant encouragement have been my guiding light throughout this process. The patience and dedication you have shown me have not only shaped this thesis but have also deeply inspired me. You have all helped me realize that I can achieve far more than I could ever imagine a few years ago. I am forever grateful for the countless hours you all have invested in my growth and success.

To my committee members, Marc Aucoin, Denise Hileeto and William Ngo, your invaluable feedback and unwavering support have been pivotal. Your insightful critiques and thoughtful suggestions have enriched this research. I am deeply appreciative of your commitment and expertise.

I would like to extend my deepest gratitude to my grandmom, dad, mom, my brother, and sister-in-law whose unwavering love, boundless encouragement, and steadfast belief in me have been my greatest sources of strength throughout this journey. Your sacrifices and support have provided me with the foundation to pursue my dreams and reach this milestone. I am grateful for your patience, understanding, and the endless support you have given me. This achievement is a testament to your unwavering faith in my abilities and your unconditional love and is as much yours as it is mine.

My heartfelt thanks go to my friends at Waterloo: Shreya, Deepak, Shilpa, Pranav, Vasisht, Athira, Ujwal, Jean, Adrian, Mattie, James, Navya, Irina and others; whose support made this journey not just bearable but truly memorable. A huge thanks to my friends Shubham, Devansh, Anshul, Joslia, Keerthana, Robin, Gopal, Mani, Lalit, Mohit, Vishal, and many others for supporting me throughout

from miles apart. Special thanks go to CORE members and my lab colleagues David, Haile, and Nijani (for her intellectual discussions regarding how to make colorful graphs) made this journey fun. Another thanks to the Immigration Consultants at the University of Waterloo especially Shannon Chung and Clint MacPhee for providing unwavering support.

I would also like to thank everyone who has touched my life in significant ways throughout this journey including Monalisa Mukherjee, Rohan Bhattacharya, Shivani Chandra, Pooja Vijayaraghavan, Harsh Chauhan, Anuj Kumar Poonia, Yogesh Kumar Verma, and Subodh Kumar. Your support, whether through guidance, encouragement, or simple acts of kindness, has meant the world to me and helped me in reaching where I am today.

Another huge thanks to Art, Ciara, Emily and all the members of my exceptional Mambo Club family. My words cannot express the depth of my gratitude. Your unconditional support, whether through guidance, encouragement, or simple acts of kindness, has meant the world to me and have reshaped me into a better individual. And of course, Lachlan and Arwen, you both have been a source of comfort and joy, and I cherish the moments we spent together.

A sincere thank you to Priyum for your unwavering professional support and for being an amazing host. I will always treasure the memories of my 27th birthday spent with you in Boucherville. And a big shout-out to Daria for supporting me during my busiest schedules and making my internship experience truly enjoyable.

I am grateful to all the funding agencies and institutions for their generous support in the form of research grants, scholarships, awards, internships and part-time roles: Ontario Graduate Scholarship, NSERC's Collaborative Research and Training Experience (CREATE) trainee grant, School of Optometry of 1948 Graduate Scholarship, Entrepreneurial PhD Fellowship, W.S. Rickert Fellowship in Science, Desmond Fonn Contact Lens Research Award, Daytech Manufacturing Ltd. Prize, Canadian Optometric Education Trust Fund (COETF), Mitacs Accelerate Fellowship, University of Waterloo Campus Housing, and the National Research Council of Canada (NRC).

Thank you all for being the pillars of support that have carried me through. This accomplishment is a testament to your belief in me, and I am forever grateful for the role each of you has played in this journey.

Lastly, I would like to acknowledge my own perseverance and commitment throughout this research journey. There were personal and professional moments when the challenges seemed overwhelming, and doubts about the feasibility of completing this thesis surfaced. However, through sustained effort and belief in the process, I managed to overcome these obstacles and continue working towards my goal. The dedication to pushing through difficult times has been a crucial part of this achievement. Finally, I am happy to see my work come to fruition and feel satisfied with the outcome of my hard work and dedication.

Dedication

To the vision that was once debated,

and the realities we now created.

To the experiences we never planned,

and the paths that led us hand in hand.

To the friends and family, we found along the way,

every Wednesday, dancing our hearts away!

Table of Contents

Examining Committee Membership ii
Author's Declaration iii
Statement of Contributions iv
Abstract ivi
Acknowledgements viiii
Dedication xi
List of Figures xvii
List of Tables xxx
List of Abbreviations xx
List of Symbols xxixi
Chapter 1 Rationale and Objectives 1
Chapter 2 Introduction 4
2.1 Drug delivery to the eye, challeges and solutions 4
2.2 Polyvinyl alcohol (PVA) 10
2.3 Biodegradable polymers 14
2.4 3D printing 25
2.5 Concluding remarks: Thesis directions and plan 27
Chapter 3 – 3D printing of a prototype biodegradable contact lens using gelatin methacrylate 28
3.1 Abstract 29
3.2 Introduction 30
3.3 Materials and methods 32
3.3.1 GelMA synthesis 32
3.3.2 Biomaterial ink preparation 32
3.3.3 Designing of CAD models 33
3.3.4 3D printing process 33
3.3.5 Shape fidelity evaluation 34
3.4 Results and Discussion 36

3.4.1 3D printing process 36
3.4.2 Effect of dye concentration on print quality 37
3.4.3 Effect of exposure time on print quality 38
3.4.4 Putting it all together: 3D printed contact lenses 40
3.5 Conclusion 41
Chapter 4 – 3D Printed Contact Lenses to Release PVA as a Therapeutic Agent for the Treatment of Dry Eyes 42
4.1 Abstract 43
4.2 Introduction 44
4.3 Materials and methods 46
4.3.1 GelMA synthesis 46
4.3.2 Preparation of GelMA and P-Gel inks 46
4.3.3 3D printing of contact lenses 47
4.3.4 Print Quantification 47
4.3.5 Light Transmittance 48
4.3.6 PVA release from 3D printed CL 48
4.3.7 Drug Release Kinetics via Mathematical Modeling 49
4.3.8 Viscosity Measurements 50
4.3.9 Non-Invasive Keratograph Break-up Time 50
4.3.10 Simulating Dry Eye Conditions via Desiccation Stress on HCECs 51
4.3.11 Statistical Analysis 51
4.4 Results and Discussion 52
4.4.1 3D printing of Contact Lenses 52
4.4.2 Print Quantification Analysis 53
4.4.3 Light Transmittance and Optical Transparency 55
4.4.4 PVA release 56
4.4.5 NIKBUT measurements 57
4.4.6 Viscosity Measurements 58
4.4.7 Ability of PVA to protect HCEC against desiccation stress 59

4.5 Conclusion 61
Chapter 5 – Controlled PVA Release from Chemical-Physical Interpenetrating Networks to Treat Dry Eyes 62
5.1 Abstract 63
5.2 Introduction 64
5.3 Materials and methods 66
5.3.1 GelMA synthesis 66
5.3.2 Preparation of GelMA and GelMA/PVA Hydrogel Discs 66
5.3.3 Morphological Characterization 67
5.3.4 Chemical Characterization 67
5.3.5 Thermal Analysis 68
5.3.6 Swelling Behaviour 68
5.3.7 Mechanical Properties 68
5.3.8 Release and Detection of PVA 69
5.3.9 Drug Release Kinetics via Mathematical Modeling 69
5.3.10 Cytocompatibility Evaluation 71
5.3.11 Statistical Analysis 71
5.4 Results and Discussion 72
5.4.1 Morphological Characterization 72
5.4.2 Chemical Characterization 74
5.4.2.1 Fourier Transform Infrared (FTIR) Spectroscopy 74
5.4.2.2 Nuclear Magnetic Resonance (NMR) 75
5.4.2.3 X-Ray Diffraction (XRD) 76
5.4.3 Thermal Analysis 77
5.4.4 Swelling Behaviour 77
5.4.5 Mechanical Properties 79
5.4.6 Release of PVA 79
5.4.7 Drug Release Kinetics via Mathematical Modeling 81
5.4.8 Cytocompatibility Evaluation 83

5.5 Conclusion 84
Chapter 6 – Biodegradable 3D printed conjunctival inserts for the treatment of dry eyes 85
6.1 Abstract 86
6.2 Introduction 87
6.3 Materials and methods 90
6.3.1 GelMA synthesis 90
6.3.2 Preparation of P-Gel-5% ink 90
6.3.3 3D printing of P-Gel-5% conjunctival inserts 90
6.3.4 Mechanical testing 91
6.3.5 Equilibrium swelling 92
6.3.6 Water Contact Angle 92
6.3.7 Biodegradation of P-Gel-5% inserts by MMP9 91
6.3.8 Scanning Electron Microscopy 93
6.3.9 Release and Detection of PVA 93
6.3.10 Drug release kinetics via mathematical modeling 94
6.3.11 Statistical Analysis 95
6.4 Results and Discussion 96
6.4.1 3D printing of Ocular Inserts 96
6.4.2 Mechanical Testing, Equilibrium Water Content (EWC), and Water Contact Angle 97
6.4.3 PVA Release from P-Gel-5% inserts in presence of MMP9 99
6.4.4 Biodegradation of P-Gel-5% inserts in presence of MMP9 100
6.4.5 Release Kinetics in the presence of MMP9 enzymes 106
6.5 Conclusion 110
Chapter 7 – General Discussion, Limitations and Conclusions 111
Copyrights permission 120
References 125

List of Figures

Chapter 2

Figure 1. Anatomy and physiological barriers in ocular drug delivery.
Figure 2. Concept of drug eluting contact lenses.
Figure 3. Schematic display of tear evaporation in the pathogenesis of dry eye disease.
Figure 4. Active agents used for tear film-oriented therapy for dry eye disease.
Figure 5. Biomedical applications of freeze-thawed PVA hydrogels.
Figure 6. Strategy for using freeze-thawed PVA hydrogels for drug delivery.
Figure 7. Mechanisms of hydrogels degradation.
Figure 8. Factors affecting different properties of GelMA hydrogels.
Figure 9. Schematic illustration of enzyme diffusion and degradation reaction in the biodegradable polymer.
Figure 10. Scheme for fabrication of CLs from stereolithography-based 3D printing.
Figure 11. Summary of key properties to be considered during bioink development for 3D printing, including printability assessment.

Chapter 3

Figure 1. The CAD designs of solid cubes with and without a hollow conduit in the centre, an object with radial spokes, and a contact lens.
Figure 2. 3D printing process for fabricating a contact lens.
Figure 3. Scheme of preparation of GelMA prepolymer solution for 3D printing of CLs.
Figure 4. Effect of Tartrazine dye concentration (C_{Dye}) print quality. Scale bars represent 10mm.
Figure 5. Effect of exposure time (t_{EXP}) on the print quality. The spokes model comprises of 18 radial lines of 600µm width and 100µm height.
Figure 6. 3D printed contact lens and CAD design.

Chapter 4

Scheme 1. Scheme of preparation of P-Gel prepolymer solution for 3D printing of CL
Figure 1. Comparative optical clarity of (a) commercially available Dailies Aqua Comfort Plus™ CL and (b,c) 3D printed PVA-loaded CL (P-Gel-1.5% and P-Gel-3%). The images were taken on a 3D printed eye model mimicking the human eye to show the fitting of these lenses and their optical clarity.
Figure 2. 3D printed contact lenses (a) before and (b) after washing and post curing
Figure 3. Analysis of Shape Fidelity and Circularity of the 3D printed contact lenses (calculations based on 2D top view).
Figure 4. (a) Optical transparency of 3D printed CLs on a colored background (b) Optical transmittance curves of GelMA, P-Gel-1.5% and P-Gel-3%.
Figure 5. (a) Cumulative PVA release curves of P-Gel-1.5% and P-Gel-3% (b) Instantaneous release of PVA (µg/ml) from P-Gel-1.5% and P-Gel-3% (c) Modelling of the PVA release data using the Korsmeyer-Peppas model (R^2=0.9806 and R^2=0.9864 for P-Gel-1.5% and P-Gel-3% respectively)

Figure 6. Subjective assessments of non-invasive keratograph break-up time (NIKBUT) of PBS, 1.4% (w/v) PVA and Refresh Classic eye drops on a 3D printed eye model (*n*=5).
Figure 7. Statistical analysis for the tear break up times.
Figure 8. Graph representing viscosity as a function of PVA concentration.
Figure 9. Effect of PVA and Refresh Classic eye drops on HCEC and resistance against desiccation stress.

Chapter 5

Scheme 1. Schematic illustration for the formation of PVA/GelMA hydrogel networks.
Figure 1. Cross sectional SEM images of the freeze dried (a) GelMA (b) P-Gel (c) P-Gel-1FT, and (d) P-Gel-2FT hydrogels showing a highly interconnected porous structure. The pore architecture becomes more uniform with the addition of PVA.
Figure 2. Pore size distribution of (a) GelMA (b) P-Gel (c) P-Gel-1FT, and (d) P-Gel-2FT. GelMA shows a broad pore size distribution with pores sizes ranging from 1 to 90 μm, with most pores ranging from 15-20 μm. The P-Gel samples showed more uniform pore sizes with mean pore size of 10-25 μm.
Figure 3. FTIR spectra of GelMA prepolymer solution, GelMA hydrogels, P-Gel prepolymer solution, P-Gel hydrogels and PVA powder.
Figure 4. ^{1}HNMR of gelatin and GelMA.
Figure 5. (a) XRD patterns of GelMA, PVA, P-Gel, P-Gel-1FT, and P-Gel-2FT samples. (b) DSC thermogram of GelMA and P-Gel-2FT samples for the first (~200 °C) and second heating (~ 250 °C) cycle.
Figure 6. (a) Equilibrium Swelling of GelMA, P-Gel and freeze thawed hydrogels. (b) Swelling kinetics analysis based on power law. (c) Stress Strain curves and (d) Young's modulus for GelMA, P-Gel and freeze thawed hydrogels.
Figure 7. PVA release curves and the effect of freezing times on the release rate of PVA (per 100mg hydrogel). The freeze thawed samples show lower release of PVA than the P-Gel samples, supporting the concept of using freeze thaw cycles to control release rates.
Figure 8. PVA release profiles per time point showing the effect of freezing thaw cycle on the release of PVA.
Figure 9. Modelling of the PVA release data on well-known mathematical models: (a) zero order, (b) first order, (c) Higuchi's model, and (d) Korsmeyer-Peppas model.
Figure 10. MTT assay for GelMA, PVA, P-Gel and P-Gel-2FT

Chapter 6

Figure 1. Fabrication of GelMA and P-Gel-5% conjunctival inserts using 3D printing
Figure 2. 3D printing of PVA-loaded conjunctival inserts.
Figure 3. (a) Mechanical strength and (b) equilibrium swelling graphs for GelMA and P-Gel-5% samples.
Figure 4. Water contact angle for GelMA and P-Gel-5% conjunctival inserts.

Figure 5. PVA release curves of 3D printed conjunctival inserts in the presence of varying concentrations of MMP9 enzyme.
Figure 6. Biodegradation profiles of 3D printed conjunctival inserts in the presence of varying concentrations of MMP9 enzyme.
Figure 7. Morphological changes in GelMA inserts before and after exposure to 100µg/ml MMP9 enzyme for 24 hrs.
Figure 8. Morphological changes in P-Gel-5% inserts before and after exposure to 100µg/ml MMP9 enzyme for 24 hrs.
Figure 9. Correlation between the biodegradation profiles and PVA release curves of 3D printed conjunctival inserts in presence of varying concentrations of MMP9 enzyme.
Figure 10. Modelling of the PVA release data on well-known mathematical models: (a) zero order, (b) first order, (c) Higuchi's model, and (d) Korsmeyer-Peppas model.
Figure 11. Modelling of the PVA release data on well-known mathematical models: (a) zero order, (b) first order, (c) Higuchi's model, and (d) Korsmeyer-Peppas model using non-linear regression.

List of Tables

Chapter 3

Table 1. Various ink and process parameters affecting the print quality in 3D printing.
Table 2. Parameters used for 3D printing using GelMA
Table 3. Circularity values for different dye concentrations (v/v)
Table 4. Effect of dye concentration on print quality.
Table 5. Effect of exposure time on print quality.

Chapter 4

Table 1. Calculations for Shape Fidelity and Circularity of the 3D printed CL.
Table 2. Curve fitting of various models for drug release kinetics
Table 3. The coefficient of determination (R^2) values of P-Gel-1.5% and P-Gel-3% calculated using different kinetic models.
Table 4. First tear break up time (in seconds)

Chapter 5

Table 1. Curve fitting of various models for drug release kinetics
Table 2. Young's Modulus
Table 3. Compressive Strength
Table 4. The coefficient of determination (R^2) values of P-Gel, P-Gel-1FT, and P-Gel-2FT calculated by using different kinetic models.

Chapter 6

Table 1. Curve fitting of various models for drug release kinetics
Table 2. The coefficient of determination (R^2) values of PVA release from P-Gel-5% in PBS and MMP9 (25 µg/ml, 50 µg/ml and 100 µg/ml) calculated by using different kinetic models.

List of Abbreviations

3DP	3-dimensional printing
CLs	Contact lenses
mSLA	Masked stereolithography
GelMA	Gelatin methacrylate
PVA	Polyvinyl alcohol
HPMC	Hydroxypropyl methylcellulose
PVP	Polyvinyl pyrrolidone
CMC	Carboxymethylcellulose
UV	Ultraviolet
C_{Dye}	Dye/photo-absorber concentration
T_{Layer}	Layer thickness
t_{EXP}	UV exposure time
STL	Stereolithography
RH	Relative humidity
HCECs	Human corneal epithelial cells
NIKBUT	Non-invasive keratograph break up times
P-Gel	PVA/GelMA hydrogels
P-Gel-5%	5% (w/v) PVA/10% (w/v) GelMA hydrogels
FT	Freeze thaw
P-Gel-1FT	PVA/GelMA hydrogels freeze thawed for 1hr
P-Gel-2FT	PVA/GelMA hydrogels freeze thawed for 2hr
SEM	Scanning electron microscopy
FTIR	Fourier transform infrared spectroscopy
XRD	X-Ray diffraction
NMR	Nuclear magnetic resonance
DSC	Differential scanning calorimetry
R^2	Coefficient of determination
MMPs	Matrix metalloproteinases

List of Symbols

%	percentage
ºC	degrees centigrade
g	gram
h	hours
L	liter
M	molar
mg	milligram
mL	milliliter
mm	millimeter
min	minutes
nm	nanometer
pH	negative logarithm hydrogen ion concentration
µg	microgram
ng	nanogram
µl	microliter
µm	micrometer

Chapter 1

Rationale and Objectives

Conventionally, eye drops have been used to administer >90% of eye medications.[1] There are several factors such as low bioavailability, low patient compliance, incorrect dose administration, and repeated daily administration that contribute to the inefficiencies of conventional eye drops.[2,3] Contact lens-based drug delivery is an emerging field in ophthalmology that aims to provide a more effective and convenient alternative to traditional eye drops. In recent decades, there has been an enormous interest in using contact lenses as drug delivery devices for treating a variety of ocular diseases. Mathematical model simulations suggest that roughly 50% of the drugs released from CLs can diffuse into the cornea, resulting in approximately 35 times greater efficiency compared to delivery by eye drops.[4] Thus, in theory, CLs can act as drug reservoirs to release drugs over an extended period of time, resulting in higher drug residence time and drug penetration into the eye. In addition to increasing the drug penetration into the eye, it is also important to gain control over the drug release rate from these CLs[5] while ensuring that the drug is delivered at therapeutically effective levels.

While there are different techniques, such as encapsulation, chemical modification of the drug, hydrophobic/hydrophilic balancing, molecular imprinting, and complexation, reported in the literature proposed to extend the drug release from contact lenses;[6-10] they all continue to demonstrate some degree of burst release, an initial phase of rapid release of drug molecules from the drug loaded contact lenses. This is an issue as it causes drugs to be released at an uncontrollable rate over the initial few hours, lowering the therapeutic efficacy and potentially leading to systemic side effects. In addition, these techniques may also lead to changes in important properties of the contact lenses including transparency, swelling, and hydrophilicity.

Therefore, an ideal drug delivery system should be able to regulate the drug release rate to maintain therapeutic levels over an extended period and minimize the burst release, thus improving the safety and efficacy of the treatment. In this regard, biodegradable polymers can be engineered to degrade over a specific time frame, allowing for precise control over drug release rates and can be used as a potential method to deliver ocular drugs. Of note, biodegradable polymers offer several advantages such as controllable drug release profiles, biocompatible nature, and reduced systemic toxicity, which makes them valuable in designing drug delivery systems. However, the degradation of biodegradable polymers during storage is a matter of concern, therefore they could be fabricated using an on-demand approach.

To this end, 3D printing may offer a viable solution, enabling on-demand fabrication of a biodegradable contact lens system. Moreover, 3D printing offers several advantages such as taking precise control over object dimensions using computer aided design models and fabricating personalized and custom-fit CLs for an individual patient.[6] The customization could be in terms of patient-specific fitting factors (especially related to diameter or base curve radius), as well as factors related to various drug concentrations, depending on the ocular condition being treated for an individual. Stereolithography (SLA)-based 3D printing makes it possible to use different photopolymerizable materials loaded with therapeutics of interest to fabricate CL with desired functionalities. This technique also offers freedom of design fabrication, higher resolution, and improved shape fidelity.[5] As an added benefit, 3D printing can also be leveraged to incorporate spatial design elements such as drug reservoirs and microfluidic channels to enhance drug delivery. Interestingly, 3D printing opens new avenues for rapid prototyping of designs, allowing for quick iteration and prototype development.[13]

This leads to the title of this thesis:

'Development of a 3D printed biodegradable contact lens system for ocular drug delivery'

To this end, the aims and objectives of this thesis are as follows:

1. Optimize 3D printing for gelatin methacrylate biomaterial ink for a low-cost 3D printer.
2. 3D printing of contact lens to release PVA as a therapeutic agent.
3. Controlling the burst release of PVA from GelMA via a physical crosslinking method.
4. 3D printing of biodegradable conjunctival inserts for the treatment of dry eyes

In ***Chapter 3*** of this thesis, 3D printing method is optimized, which enables a time-efficient and reliable determination of printing conditions for complex geometries such as contact lenses using gelatin methacrylate hydrogel biomaterial ink. The impact of printing direction on the print quality will be also examined in terms of object/print thickness and aspect ratio. Moreover, the effects of dye concentration, exposure time, and layer thickness on print quality will be evaluated. Overall, the optimized ink parameters and print conditions will be for the 3D printing in this thesis. Of note, herein, we aim to print objects using a vat-based low-cost (~CA$ 300) commercial 3D printer as opposed to expensive 3D printers available in the market.

Chapter 4 of this thesis aims to 3D print a prototype contact lens with PVA as a wetting agent. To evaluate the print quality of the 3D printed CL, circularity will be used to evaluate the shape fidelity in 3D printing. PVA release from these lenses will be assessed along with its role to act as a viscosity enhancer. The effect of PVA will be further analysed by a dry eye disease (desiccation stress) cell model and its role

to stabilize the tear film will be studied by using the non-invasive keratograph break-up time measurements on a 3D printed eyeball model.

Chapter 5 of this thesis aims to control the burst release of PVA by forming a chemical-physical (double) interpenetrating network. PVA was specifically used as part of these degradable hydrogels because of its dual nature, to act as a wetting agent as well as its ability to be physically crosslinked using freeze thaw cycles, forming a drug-loaded interpenetrating network where the unbound PVA acts as 'drug'. Using various chemical characterization techniques, this chapter also describes the mechanism of the chemical-physical interpenetrating network in controlling the release of PVA. The release kinetics will be studied using various mathematical models.

While contact lenses offer a promising platform for ocular drug delivery, they come with inherent limitations—they must maintain optical transparency, mechanical strength, oxygen permeability, and overall comfort to ensure patient safety and wearability. These stringent design requirements can constrain material choices and drug loading strategies. In contrast, ocular inserts are not subject to the same optical or mechanical demands, allowing for greater flexibility in material selection and drug release design. This makes them especially suitable for incorporating biodegradable polymers, which can provide sustained drug delivery without the need for removal. The concept of biodegradability, therefore, extends naturally to ocular inserts, where self-degrading materials can enhance patient compliance, reduce intervention, and improve therapeutic outcomes—supporting the broader objective of developing advanced, low-maintenance ocular drug delivery systems.

Therefore, ***Chapter 6*** of this thesis focusses on the biodegradable conjunctival inserts. The chapter dives deeper into the mechanism of degradation of GelMA based hydrogels by ocular enzymes such as matrix metalloproteinases and its correlation with the release PVA, which is a well-known wetting agent. The versatile 3D printing abilities of GelMA will be used to leveraged to design conjunctival inserts with higher precision which also overcomes the decrease in transparency caused with addition of PVA to GelMA hydrogels. Interestingly, these collagenolytic enzymes are elevated in certain ocular conditions such as dry eye and can be utilized as a feedback mechanism for regulating the degradation rate of PVA from these conjunctival inserts.

Chapter 2

General Introduction

2.1 Drug delivery to the eye, challenges and solutions

2.1.1 Anatomy of eye

Eye health and vision have widespread implications in many facets of life and health. The ocular surface consists of a complex network of ocular tissues including the cornea, conjunctiva, lids, and lacrimal and secretory system as well as endocrine, nervous, and immune systems that work together to mediate the function of the tear film.[1] The tears on the ocular surface are present in three major compartments: the fornical compartment (between fornix and the retrotarsal space), the tear menisci and the preocular tear film.[2] The corneal surface and conjunctival epithelium contains transmembrane mucins[3] which are facilitates the spread of the tears on the ocular surface. These transmembrane mucins are attached to the microplicae of the epithelial cells and also constitute a line of defense for the epithelial cells against any infection (*Figure* 1).[4,5]

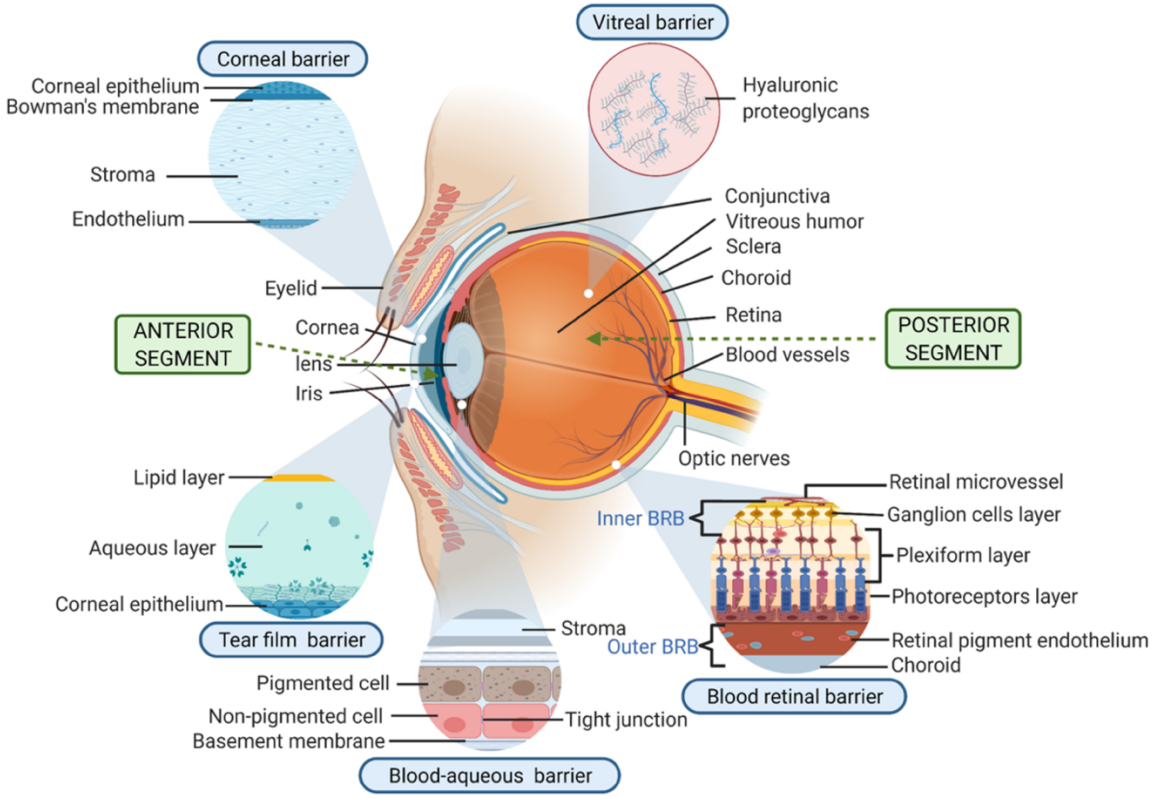


***Figure* 1.** Anatomy and physiological barriers in ocular drug delivery[6]

2.1.2 Tear Film

The tear film is a thin, multi-layered fluid that coats the surface of the eye, playing a vital role in maintaining ocular health and clear vision. It is approximately 3 to 10 μL in volume, 3 μm thick, and secreted at a rate of 1 to 2 μL/min.[7] The tear film acts as a lubricant, reducing friction during blinking, and provides a smooth, refractive surface for optimal light transmission. Additionally, it protects the eye from debris and pathogens with its mechanical barrier and antimicrobial properties. The tear film is comprised of three main layers: an outer lipid layer that is composed of lipids secreted by the meibomian glands, this layer reduces tear evaporation and provides a smooth surface for light refraction; a middle aqueous layer, secreted mainly by the lacrimal glands and contains water, electrolytes, proteins (including antimicrobial agents), and mucins, which provides lubrication, nutrition, and antimicrobial protection; and an inner mucin layer, composed of membrane-associated mucins produced by corneal and conjunctival epithelial cells and gel-forming mucins secreted by goblet cells in the conjunctiva, helps the tear film adhere to the hydrophobic corneal epithelium, creating a hydrophilic interface that allows uniform spreading of the aqueous layer.

In summary, the tear film is essential for maintaining the health, clarity, and overall function of the eye. Disruptions to the tear film can lead to discomfort, dryness, and an increased risk of infections.[2]

2.1.3 Conventional eye drops and their disadvantages

Conventionally, eye drops have been used to administer eye medications and they account for approximately 90% of ophthalmic medications.[8] Other methods include ointments, gels, intraocular and periocular injections, implants and inserts, contact lenses, punctal plugs, and systemic medications. However, several factors such as low bioavailability, low patient compliance, incorrect dose administration, repeated daily administration and many more contribute to the inefficiencies of conventional eye drops.[9] The low bioavailability is exacerbated by tear dilution, reflex tearing, reflex blinking, and unidirectional drainage of fluid through the nasolacrimal duct.[10] Despite high drug concentrations for short periods in the eye, a considerable portion of the drug is removed through the vascularized conjunctiva, further decreasing corneal bioavailability.[11] Apart from the higher permeability of the conjunctiva compared to cornea, the conjunctival area is 16-18 times larger than the corneal area, leading to more drug flux into the conjunctiva than the cornea.[12] Also, the short tear film residence time (about 2-3 min) necessitates for a recurrent dosing regimen.[12] However, sustained drug concentrations cannot be maintained on the ocular surface by frequent use of eye drops.[10] Additionally, the toxicity concerns pertaining to the target tissue need to be factored in while determining the maximum drug exposure from a single drop.[11] The volume discrepancy between an eye drop (about 30 μL) and the tear film (about 7 μL) results in low residence time of the eye drops, leads to a rapid drainage of the drugs from the eye, and is another reason for low corneal bioavailability (less than

5%) of the administered drug.[11] All these factors lead to daily multiple instillations of drops throughout the day for treating various eye diseases, leading to poor patient compliance.

2.1.4 Contact lenses and drug delivery

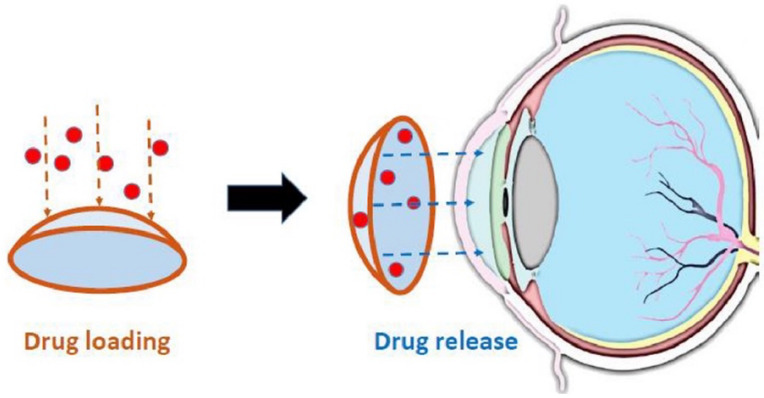


***Figure* 2.** Concept of drug eluting contact lenses[13]

Presently, innovation and research are steered towards simplifying the treatment regimen and reducing the frequency of drop administration. An ideal ocular drug delivery system should overcome the limitations of conventional eye drops and maintain appropriate pharmacokinetics.[12] Moreover, it should be bestowed with properties such as good comfort, biocompatibility, easy administration, and no adverse effects on normal eye functions like blinking or vision.[12] In recent decades, there has been an enormous interest in using CLs as drug delivery devices for treating a variety of ocular diseases (*Figure* 2). There are over 150 million CL wearers in the world[14] and the global CL market is expected to rise to over 19 billion US dollars by 2024.[15] In contrast to eye drops that get rapidly removed from the eye, drugs released from CLs into the post-lens tear film avoid ocular removal mechanisms such as blinking, tear dilution and drainage. Using a mathematical model, it has also been postulated that, with contact lenses, nearly 50% of a drug would be absorbed by the cornea.[16] Therefore, drug delivery using CLs results in higher drug residence time and drug penetration into the eye in comparison to traditional drop formulations.

Despite the encouraging outcomes, wearing contact lenses presents inherent drawbacks, including dry eye syndrome and discomfort.[17-19] Reportedly, wearing of contact lenses disrupts the physiological process of natural blinking, consequently impeding the effective preservation of moisture on the corneal surface and contributing to accelerated tear film evaporation.[20,21] CL wear is also associated with a decrease in tear film stability and tear volume as well as increased friction between the lens and the lid wiper and lens edge and the bulbar conjunctiva.[22] Also, the tear evaporation rates are higher with the use of CLs, potentially leading to greater CL discomfort (*Figure* 3).[20]

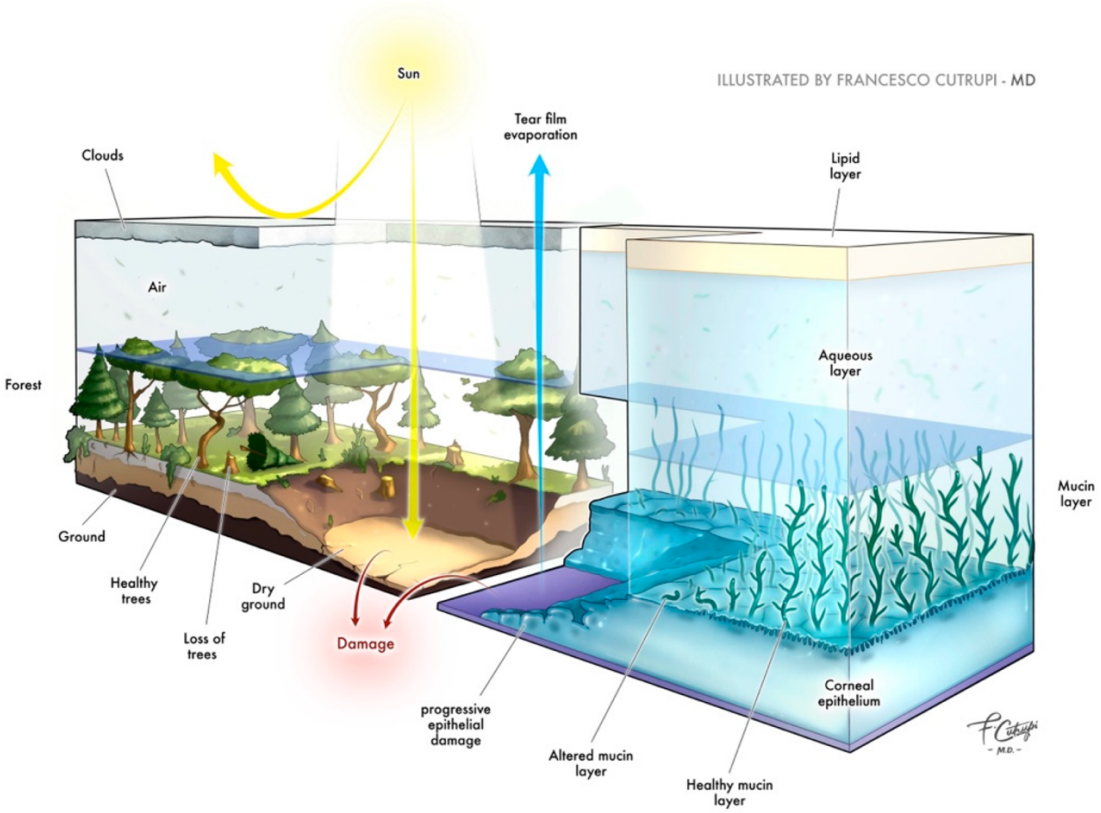


***Figure* 3.** Schematic display of tear evaporation in the pathogenesis of dry eye disease.[1]

2.1.5 Strategies to treat dry eye (Tear Film Oriented Dry Eye Therapy)

Dry Eye Disease is a multifactorial ocular surface disorder characterized by tear film instability and ocular surface inflammation. Dry eye treatment involves identifying a correct treatment strategy based on where the abnormality relating to dry eye is in the tear film and epithelium, with this concept being termed "tear film-oriented therapy" (*Figure* 4).[23]

Figure 4 outlines a scientific framework for the classification and function of tear substitutes in the management of dry eye disease (DED). Tear substitutes are categorized into three primary groups based on their therapeutic roles: wetting/lubricating agents, multiple-action tear substitutes, and ocular surface modulators. These categories align with specific pathophysiological features of DED, including tear film instability (due to increased evaporation, aqueous deficiency, and decreased wettability), tear film hyperosmolarity, ocular surface cell apoptosis, and ocular inflammation. Corresponding classes of active ingredients are employed to address these conditions. For instance, oily agents stabilize the lipid layer to reduce evaporation, viscosity-enhancing agents and electrolytes support the aqueous layer, and osmo-protectants like trehalose and L-carnitine mitigate cellular stress. Additionally, antioxidants, cytoprotective

agents, wound-healing promoters, and anti-inflammatory compounds help restore ocular surface integrity and function. The image also connects these ingredients to the layered architecture of the tear film—lipid, aqueous, and mucin layers—highlighting the importance of a targeted, multi-mechanistic approach in DED therapy.

Current strategies to treat dry eye include the use of artificial tears, aqueous secretagogues, mucin secretagogues, and anti-inflammatory drugs.[23] Of these, treatments involving the use of artificial tears is most commonly used. Artificial tear supplements often use viscosity-building macromolecules such as polyvinyl alcohol, sodium hyaluronate, carbomers, and natural gums to prolong the symptomatic relief provided by eye drops.[24]

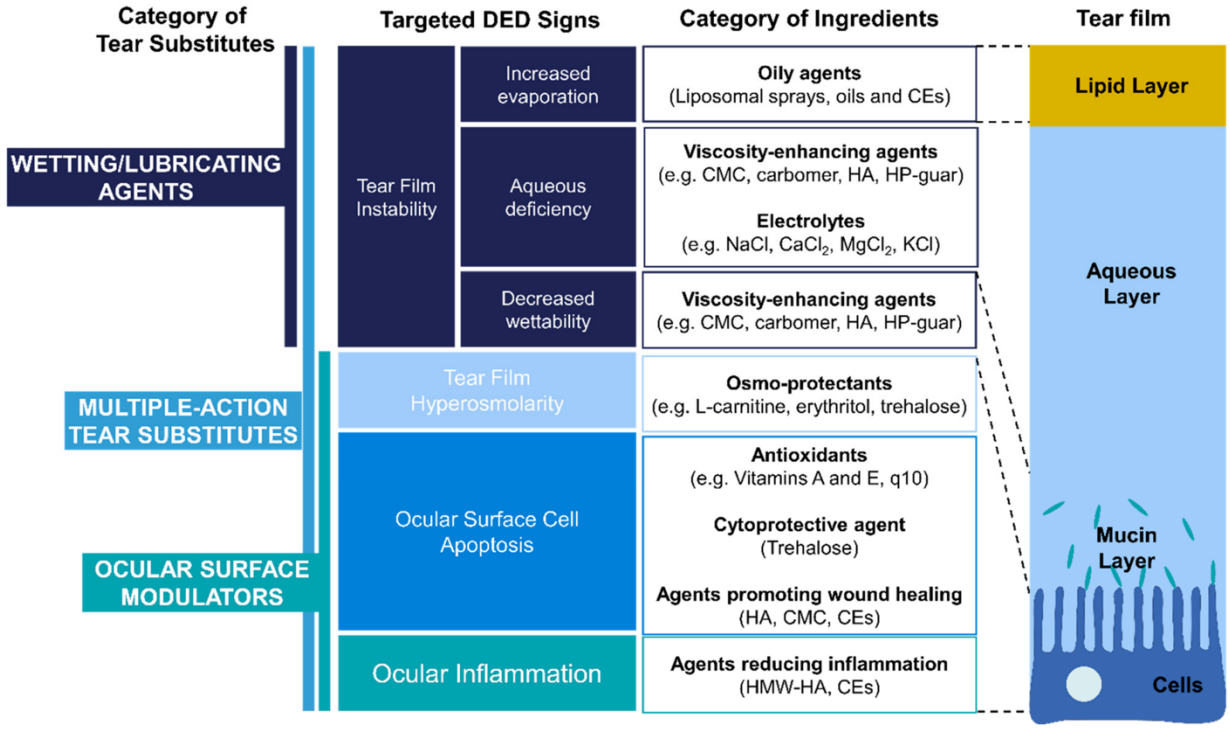


***Figure* 4.** Active agents used for tear film oriented therapy for dry eye disease (ADDE = Aqueous Deficiency Dry Eye; CEs = Cationic emulsions; CMC = Carboxymethylcellulose; EDE = Evaporative Dry Eye; HA = Hyaluronic acid; HMW = high molecular weight; HP-guar = hydroxypropyl guar).[24]

In addition, the viscosity building macromolecules also form a protective layer over the ocular surface, thereby reducing ocular surface desiccation. These viscosity enhancing agents are efficient at replenishing and stabilizing the aqueous layer in the tear film. Artificial tear solutions containing viscosity enhancing agents and electrolytes mimics the composition of the natural aqueous layer and are classified

as wetting agents.[24,25] However, the major drawback of viscous solutions is that they can cause an initial blurring of vision upon instillation. In the case of the abnormality in the lipid layer, the use of oily agents and surfactants could be beneficial[26] or osmo-protectants could be used to counteract the hyperosmolarity of the tear film.[24] Such tear substitutes can be considered as 'multi-action tear substitutes' as they perform more than one action, apart from replenishing the aqueous layer of the tear film. Another class of tear substitutes include antioxidants, cationic emulsions, and hyaluronic acid, which can be considered as ocular surface modulators. These chemical components can prevent cell apoptosis caused by oxidative stress, reduce expression and secretion of pro-inflammatory factors, thus reducing the ocular inflammation and promote wound healing.[24]

2.1.6 Treating dry eyes with lubricating agent releasing CLs

CLs have been studied for the topical delivery of various therapeutic agents such as ocular lubricants (polyvinyl pyrrolidone, hyaluronic acid, hydroxy propyl methylcellulose), cyclosporine A and dexamethasone, antibiotics, antifungals, antivirals, corticosteroids, and antiglaucoma agents.[27] Soft CLs can be impregnated with internal wetting agents to reduce the discomfort associated with CL wear.[28] For instance, incorporation of hyaluronic acid into silicone hydrogel CLs increases their hydrophilicity and equilibrium water content without affecting their transparency.[29] The incorporation of these internal wetting agents can be confirmed by attenuated total reflectance, Fourier transform infrared spectroscopy, confocal laser scanning microscopy and X-ray photoelectron spectroscopy.[28] An inherent PVA releasing CL material is commercially available, nelfilcon A (Alcon, Ft Worth, TX), which releases PVA from the lenses due to the natural blinking action of the eye, and which has been shown to stabilize the tear film while improving comfort towards the end of the day.[30,31] Additionally, the blister pack solution of this lens contains other moisturizing agents that are added during the packaging process (hydroxypropyl methylcellulose and polyethylene glycol) and PVA, which is released from the lens material due to simple diffusion when in the blister pack.

While PVA is a well-recognized ophthalmic demulcent used for the management of DED, it is one of many lubricating agents approved under section 349.12 of the FDA monograph for ophthalmic drug products. This regulation outlines several classes of active ingredients that function as demulcents—substances that soothe and protect the ocular surface by forming a lubricating film. Cellulose derivatives, such as carboxymethylcellulose sodium (CMC), hydroxyethyl cellulose, hypromellose, and methylcellulose (all in the 0.2–2.5% range), are among the most commonly used agents due to their high viscosity, prolonged ocular retention, and mucoadhesive properties. Dextran 70 (at 0.1%) is often used in

combination with other polymers to enhance tear film stability. Gelatin (0.01%) has limited use but can provide viscosity enhancement. Polyols such as glycerin, polyethylene glycols (300 and 400), polysorbate 80, and propylene glycol (each 0.2–1%) act as humectants and moisture retainers, offering relief from dryness and discomfort. Povidone (0.1–2%) provides surface coating properties, mimicking mucin and stabilizing the tear film. Together, these agents represent a broad pharmacological toolkit for formulating artificial tears that cater to the diverse etiologies and severities of DED, each contributing uniquely to tear film stability, retention, and ocular surface protection. [32]

2.2 Polyvinyl alcohol (PVA)

2.2.1 Polymers for (ophthalmic) drug delivery

In ocular drug delivery, polymers are a key component of the formulation toolbox and can overcome the challenge of rapid clearance from the eye by prolonging the residence time of the drug in the cornea and the conjunctival epithelium.[33] They can be used to address the formulation challenges and improve drug retention, along with several other benefits such as inhibiting crystallization, acting as solubilizers, serving as lubricants, and stabilizing the formulation. The main categories of polymers that could be used for ophthalmic formulations come from natural, semi-synthetic and synthetic origins. As such, natural polymers lack batch-to-batch consistency, which is a key component of any pharmaceutical formulation. Moreover, controlling the microbial load in such polymers can be challenging. Examples of these polymers include guar gum, gellan, and hyaluronic acid. Similarly, semi-synthetic polymers which include carboxymethyl cellulose, hydroxypropyl methylcellulose, and hydroxyethyl cellulose suffer from problems such as high batch-to-batch variability. However, synthetic polymers which include PVA, carbomers, and polyvinyl pyrrolidone offer a narrow range of viscosity and high reproducibility.

2.2.2 PVA for biomedical (ocular) applications

PVA is a biocompatible synthetic polymer which is formed by polymerization of vinyl acetate and partial hydrolysis of the resulting esterified polymer. It has been used for decades in various biomedical applications (*Figure* 5).

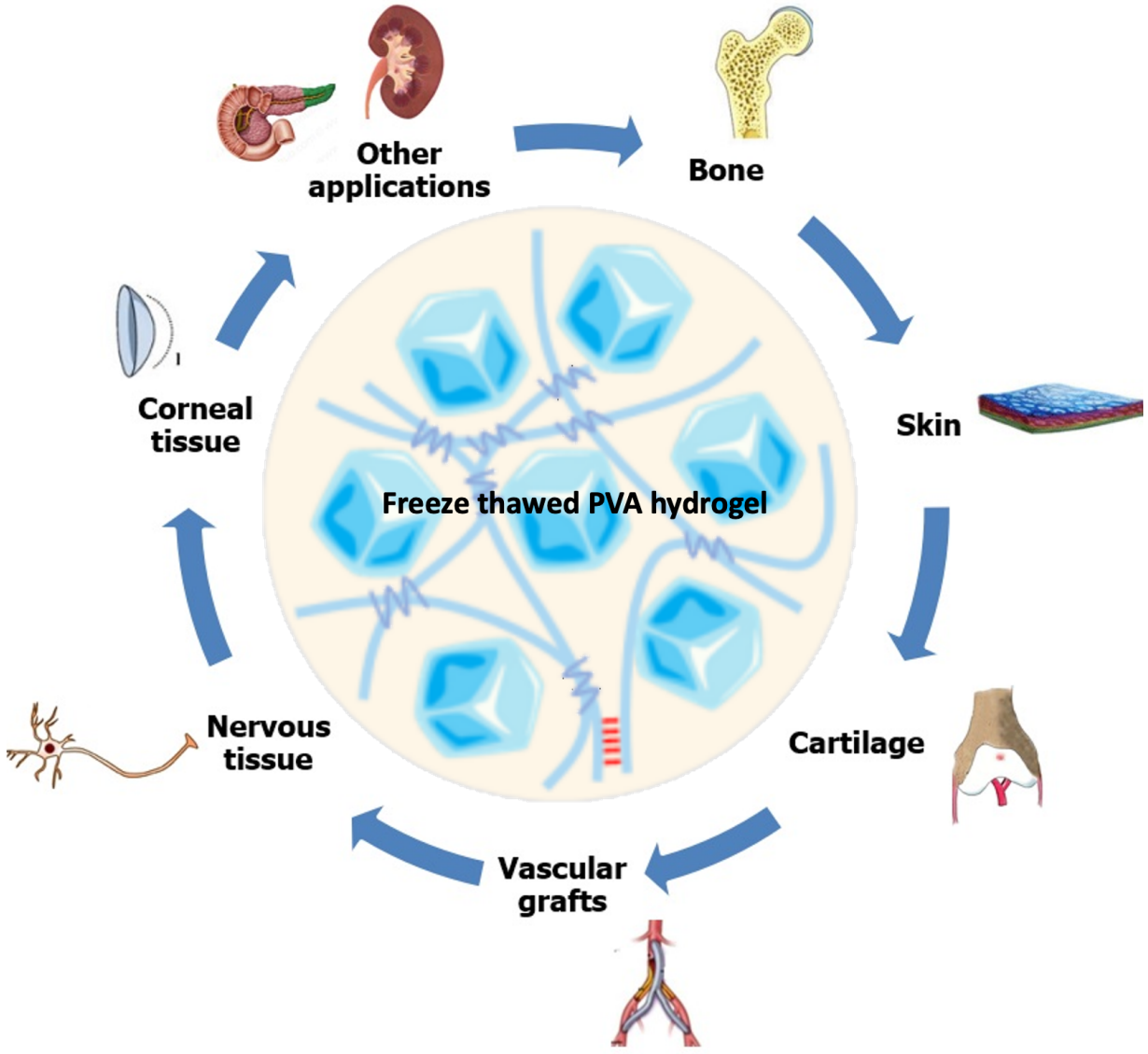


***Figure* 5.** Biomedical applications of freeze-thawed PVA hydrogels.[34,35]

PVA exhibits excellent biocompatibility with ocular tissues, minimizing the risk of irritation, inflammation, or other adverse reactions. This biocompatibility stems from PVA's hydrophilic nature and resistance to protein adsorption, reducing the likelihood of triggering immune responses.[36] The mechanical properties of PVA hydrogels can be readily tailored by adjusting parameters like polymer concentration, molecular weight, and crosslink density. This tunability allows for the creation of hydrogels with desired mechanical strength, stiffness, and degradation rates, enabling customized drug release profiles and residence times within the eye. PVA hydrogels can be engineered to provide sustained drug release, a significant advantage over conventional eye drops that suffer from rapid drainage and clearance. This sustained release characteristic is achievable through various mechanisms, including diffusion-controlled

release from the hydrogel matrix, degradation-mediated release, or a combination of both.[37] The inherent transparency of PVA hydrogels makes them ideal for ocular applications, as they do not interfere with vision.

2.2.3 Freeze thawed PVA hydrogels for biomedical applications

Freeze-thawed PVA hydrogels are a subset of biomaterials, particularly appealing for their biocompatibility and diverse applications in the biomedicine.[38] These hydrogels are formed through a cyclical process of freezing and thawing aqueous PVA solutions. This process leverages the inherent properties of PVA, inducing the formation of crystalline junctions between the polymer chains through hydrogen bonding. These junctions act as physical crosslinks, leading to the development of a three-dimensional network structure. The beauty of this technique lies in its simplicity and controllability. By adjusting parameters such as the concentration of the PVA solution, the molecular weight of the PVA used, and the number of freeze-thaw cycles employed, the properties of the resulting hydrogel can be tailored. For instance, increasing the PVA concentration generally leads to a hydrogel with higher mechanical strength and a denser network.[38] Similarly, a higher number of freeze-thaw cycles can result in smaller pore sizes within the hydrogel.[38]

These tunable properties make freeze-thawed PVA hydrogels incredibly versatile for various biomedical applications. Their high-water content mimics the natural environment of many tissues, while their biocompatibility minimizes adverse reactions. These characteristics, combined with their controllable degradation rates, make them ideal candidates for drug delivery systems, where the hydrogel can act as a carrier, gradually releasing the drug over time (*Figure* 6).

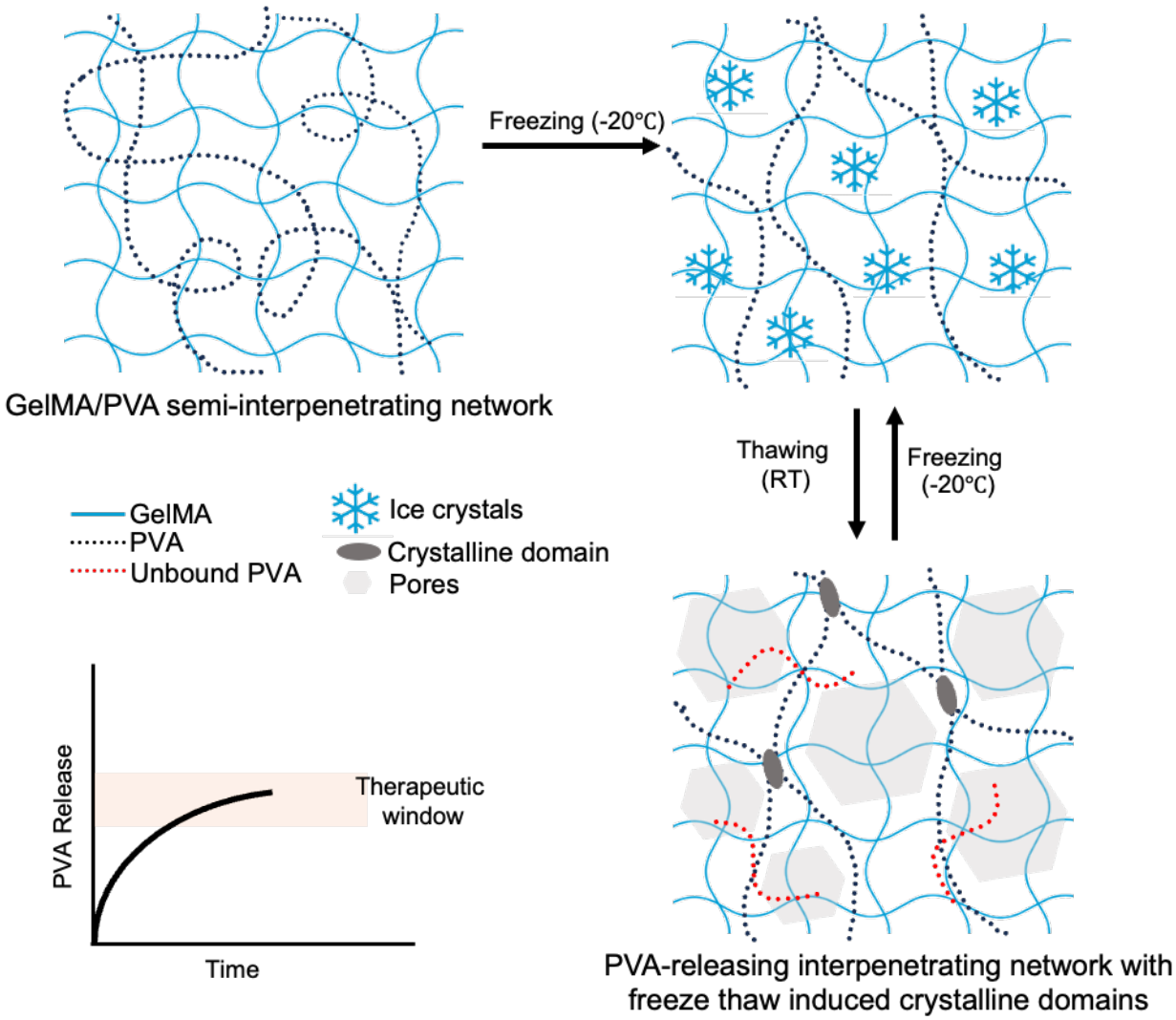


***Figure* 6.** Strategy for using freeze-thawed PVA hydrogels for drug delivery.

The porous nature of these hydrogels allows for cell infiltration and nutrient diffusion, making them suitable for wound healing applications. The hydrogel can provide a moist environment conducive to tissue regeneration, while protecting the wound site. In the realm of tissue engineering, freeze-thawed PVA hydrogels have shown promise as scaffolds for cartilage regeneration. Their mechanical properties can be tailored to match that of natural cartilage, providing structural support while allowing for cell growth and differentiation.[36,38]

2.2.4 PVA Selection/Grades and role of PVA as a viscosity enhancer/lubricating agent

PVA is generally recognized as safe by the US Food and Drug Administration.[39] In ophthalmic formulations, PVA offers several benefits, such as a precise range of viscosity, which can be used on the ocular surface. Interestingly, PVA forms transparent solutions along with higher precorneal residence time[40], which are two of the key parameters for ophthalmic formulations. Importantly, it also inhibits crystallization, thus helping to retain the solubility of various pharmaceutical ingredients in dosage forms. PVA is an approved over-the-counter ophthalmic demulcent at concentrations of 0.1% to 4% as indicated by the 21 Code of Federal Regulations (CFR) section 349.12.[32]

PVA is available in a variety of grades, based on parameters such as viscosity, size of polymer chains, and degree of hydrolysis. Another important consideration when using PVA is the purity because of the possible presence of crotonaldehyde, an impurity generated during its synthesis. Owing to the strict regulatory requirements in the medical devices segment, it is critical to select the right polymer. There are different grades of PVA available in the market and the choice is a key parameter in controlling the final product performance in terms of desired physicochemical properties. For instance, low viscosity grades could be used for lubricant activity and a higher viscosity grade PVA is more suitable as a viscosity enhancer. Similarly, PVA is also available in different hydrolysis grades, which refer to the amount of unhydrolyzed acetate groups in the polymer chains. Higher hydrolysis grades of PVA can improve the mechanical and tensile strength of the hydrogels via H-bonds, however, lower hydrolysis grades might help in the delivery of poorly water-soluble drugs.[40]

PVA was first used in the field of ophthalmics in the 1960s to increase solution viscosity and prolong the precorneal residence time.[41] Owing to its excellent lubricating properties, PVA is a promising candidate for lubricating eye drops. Generally, lubricant drops to treat moderate dry eye such as Refresh™ and Liquifilm™ (Allergan, Irvine, CA) contain approximately 1.4% PVA.[42]

2.3 Biodegradable polymers

2.3.1 Biodegradable polymers in Biomedical and Ocular applications

Owing to their biocompatible nature, both synthetic and naturally occurring biodegradable polymers have been used for a plethora of biomedical applications, including: tissue engineering,[43] regenerative medicine,[44] 3D bioprinting,[45,46] and drug delivery.[47]

Biodegradable polymers have gained significant attention for 3D printing of ocular drug delivery systems due to their ability to provide controlled degradation, biocompatibility, and structural versatility. Among these, poly(lactic-co-glycolic acid) (PLGA) is widely used owing to its FDA approval, tunable

degradation rates, and capacity to encapsulate both hydrophilic and hydrophobic drugs.[48] Polycaprolactone (PCL), with its slower degradation profile, is suited for long-term implants and has been used in scaffolds for ocular tissue engineering.[49] Polylactic acid (PLA) offers good mechanical properties and is often blended with other polymers to optimize printability and degradation kinetics. Natural polymers like gelatin, chitosan, and hyaluronic acid are also integrated into 3D printing inks for their mucoadhesive and bioactive properties, supporting corneal epithelial regeneration and anti-inflammatory effects.[50] PVA, while synthetically derived, is water-soluble and biodegradable under certain conditions, and has been employed in contact lens matrices for sustained drug release. These polymers can be tailored in formulation and printing parameters (e.g., fused deposition modelling, inkjet, or stereolithography) to produce customized ocular inserts, microneedles, or lens-based systems, enhancing therapeutic precision for dry eye and other ocular conditions.

Drug release from polymers can be exercised either *via* temporal or distribution control. In temporal control, the drug is released over an extended period and is favorable for drugs that are quickly metabolized and eliminated from the body after administration, whereas distribution control over the drug release allows the drug to be precisely delivered to its molecular site of action.[51]

The use of biodegradable polymers for drug delivery provides a more predictable drug release profile, in which the drug release rate can be proportional to the degradation of the material. Drug delivery systems utilizing biodegradable polymers offer a significant advantage due to their inherent ability to break down into non-toxic byproducts within the body. This biodegradability ensures that the drug carrier itself does not accumulate and pose long-term risks, enhancing the safety profile of the treatment. As the polymer degrades, it releases the therapeutic agent in a controlled manner, potentially allowing for sustained drug release and targeted delivery to specific sites. This controlled degradation, coupled with the biocompatibility of the resulting byproducts, makes biodegradable polymers a valuable tool in developing safer and more effective drug delivery strategies (*Figure* 7).

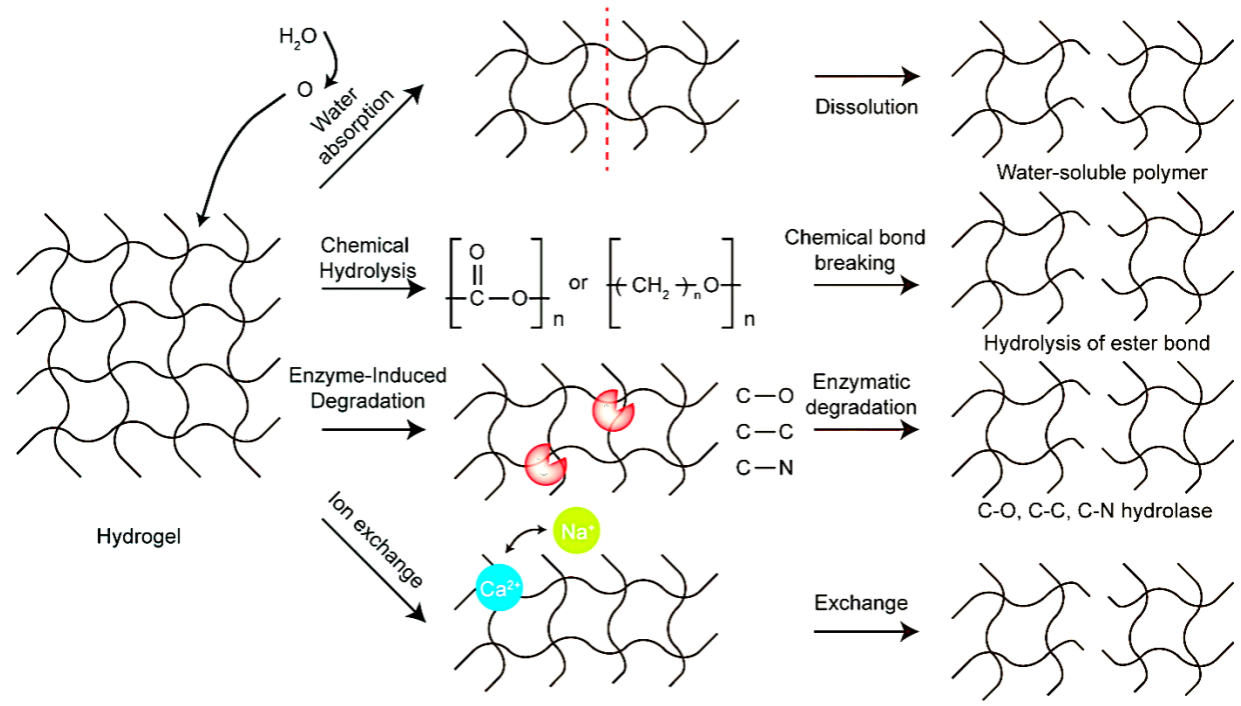


***Figure* 7.** Mechanisms of hydrogels degradation.[52]

Depending on the intended use, different products may require different stability or degradation properties.[53] For instance, in the case of chronic implantable biomedical devices, the polymers must be stable in biological environments for the device to perform its optimal function for a specified time period, which could last for few years. Contrary to this, the degradation time for polymers used to design tissue engineering scaffolds should be comparable to the tissue healing process, which could last from a few weeks to months. Similarly, the optimal degradation time frame for polymers used in drug delivery applications may range from a few hours to a few weeks. Several factors can control the rate of degradation of polymeric biomaterials, such as crosslink density, degree of substitution, and the presence or absence of pendant groups. However, when hydrolysis of the polymer reaches a critical point, there might be a burst phase. For ocular drug delivery, the degradation of the polymers should not cloud vision. Potentially, the drug release profile should display a linear zero order release kinetics, wherein drug release is constant per unit of time.[54]

2.3.2 Gelatin methacrylate (GelMA) hydrogels

Gelatin-based hydrogels are biodegradable, non-toxic, and biocompatible in nature and one of the most utilized polymers in biomedical applications. Gelatin hydrogels can be physically, chemically, or enzymatically crosslinked and are widely used in drug delivery.[55] Gelatin derivatives, in particular, GelMA hydrogels, are attractive candidates for biomedical use due to their outstanding biocompatibility[56] and can

easily form a 3D network via physical or chemical crosslinking.[55] GelMA is derived from gelatin and has methacrylate anhydride substituted with the free amine groups of gelatin. GelMA has integrin recognition RGD motifs along its backbone, which are important for effective crosstalk of biomaterials with cells.[57]

GelMA hydrogels possess excellent biocompatibility, tunable mechanical properties, and can be easily modified for various applications, including drug delivery and tissue engineering, and a variety of biomedical applications. Of note, the photo crosslinking method used to crosslink GelMA can be performed in mild crosslinking conditions (room temperature, neutral pH, in aqueous environments, etc.), with a short reaction time and low cytotoxicity.[56,58] Interestingly, GelMA hydrogels can be used for 2D cell seeding[59] and 3D cell encapsulation.[60] Additionally, the degree of crosslinking can be tuned to control the stiffness of the GelMA hydrogel (*Figure* 8).

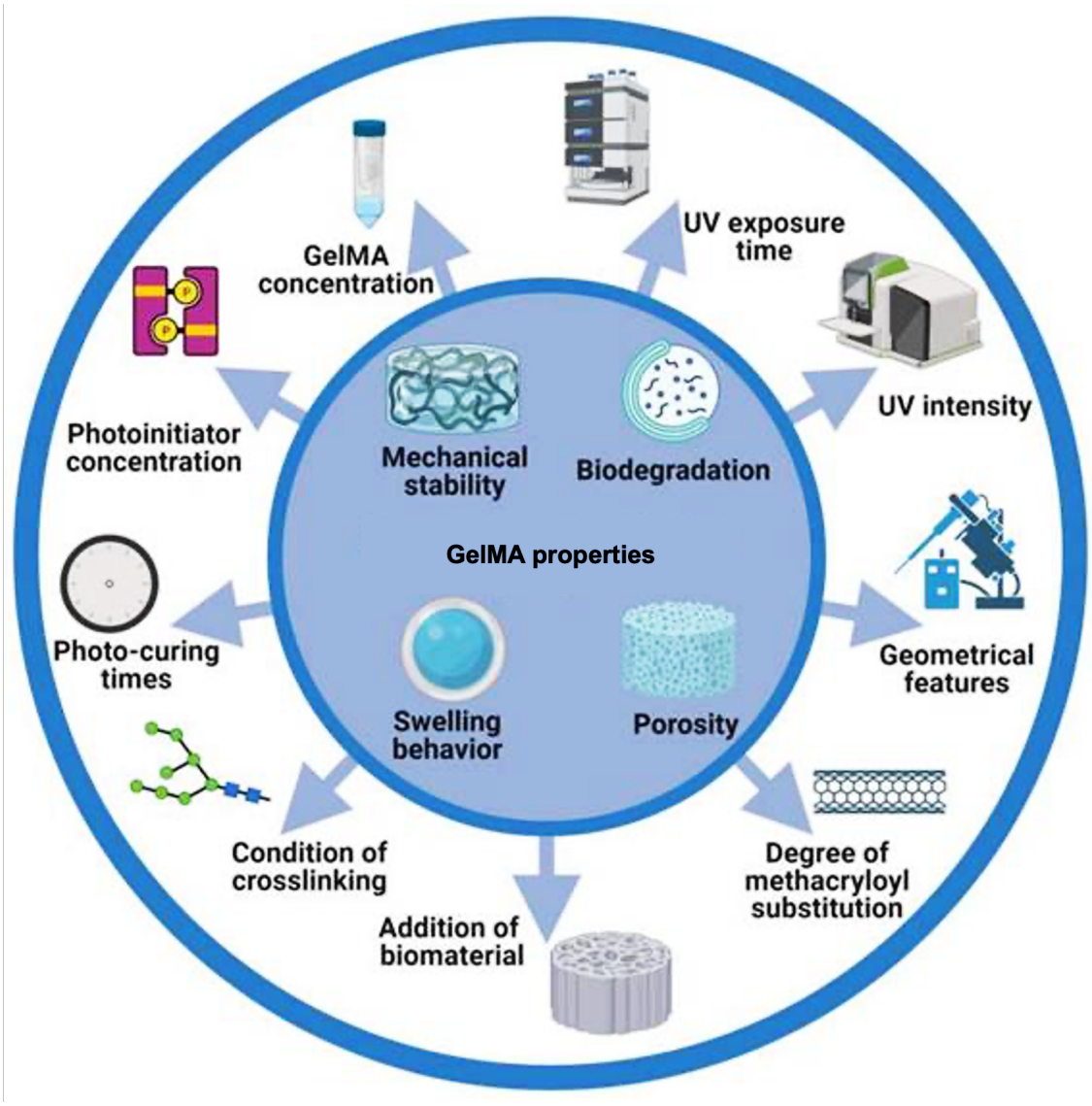


***Figure* 8.** Factors affecting different properties of GelMA hydrogels.[61]

However, their poor mechanical strength limits their applications as medical devices such as CLs for drug delivery. Therefore, to overcome this problem, a GelMA hydrogel can be combined with other photopolymerizable polymers such as polyethylene glycol diacrylate (PEGDA) and hydroxyethyl(methacrylate) (HEMA). Interestingly, GelMA degrades in the presence of collagenases or matrix metalloproteinases (MMPs) enzymes, which are found on the ocular surface.[62]

2.3.3 Enzymatic degradation of GelMA; Matrix metalloproteinases (MMPs) enzymes

MMPs belong to a large family of zinc-dependent endopeptidases. Their primary role is to break down various components of the extracellular matrix, the structural framework surrounding cells.[63] Based on the substrate preference and domain organization, MMPs are grouped membrane-type MMPs, collagenases, gelatinases, and stromelysins.[64] Despite variations in domain organization among MMP subgroups, several key domains are highly conserved. These domains, arranged from the N-terminal to the C-terminal end, typically include a pro-peptide, a catalytic domain, a linker region of variable length, and a hemopexin-like domain.[64] MMPs are essential for tissue remodeling, wound healing, cell migration, and other biological processes. Interestingly, MMPs are also linked to the pathophysiology of various diseases affecting the ocular surface.[65]

2.3.4 Role of MMPs in Biodegradation of Gelatin Methacrylate Hydrogels

There are different factors that influence the MMP-mediated degradation of GelMA hydrogels. Different MMPs have varying affinities for GelMA and degrade it at different rates. Moreover, the concentration of specific MMPs in the surrounding environment influences the degradation kinetics. As enzymes move through the polymer matrix, they break down cross-links, effectively reducing the cross-link density ($\rho(r,t)$). This reduction leads to an expansion of the polymer mesh. Eventually, the degradation process reaches a critical point known as the reverse gelation point, defined by $\rho(r,t)=\rho_c$. At the reverse gelation point, the polymer undergoes a drastic shift in its structural integrity. The connectivity of the network declines sharply, causing a transition from a gel-like state to a more fluid-like state. The critical cross-link density (ρ_c) represents the minimum number of cross-links required to maintain the structural integrity of the polymer network. It is often determined by the ratio $1/\beta$, where β represents the minimum network connections needed for structural integrity. Given an initial cross-link density of ρ_0 in the non-degraded state, ρc can be expressed as $\rho_c=\rho_0/\beta$. The interplay between enzyme diffusion and the subsequent

polymer degradation can be movement of enzymes, while enzyme-mediated kinetics describe the degradation of the polymer (*Figure* 9).[66]

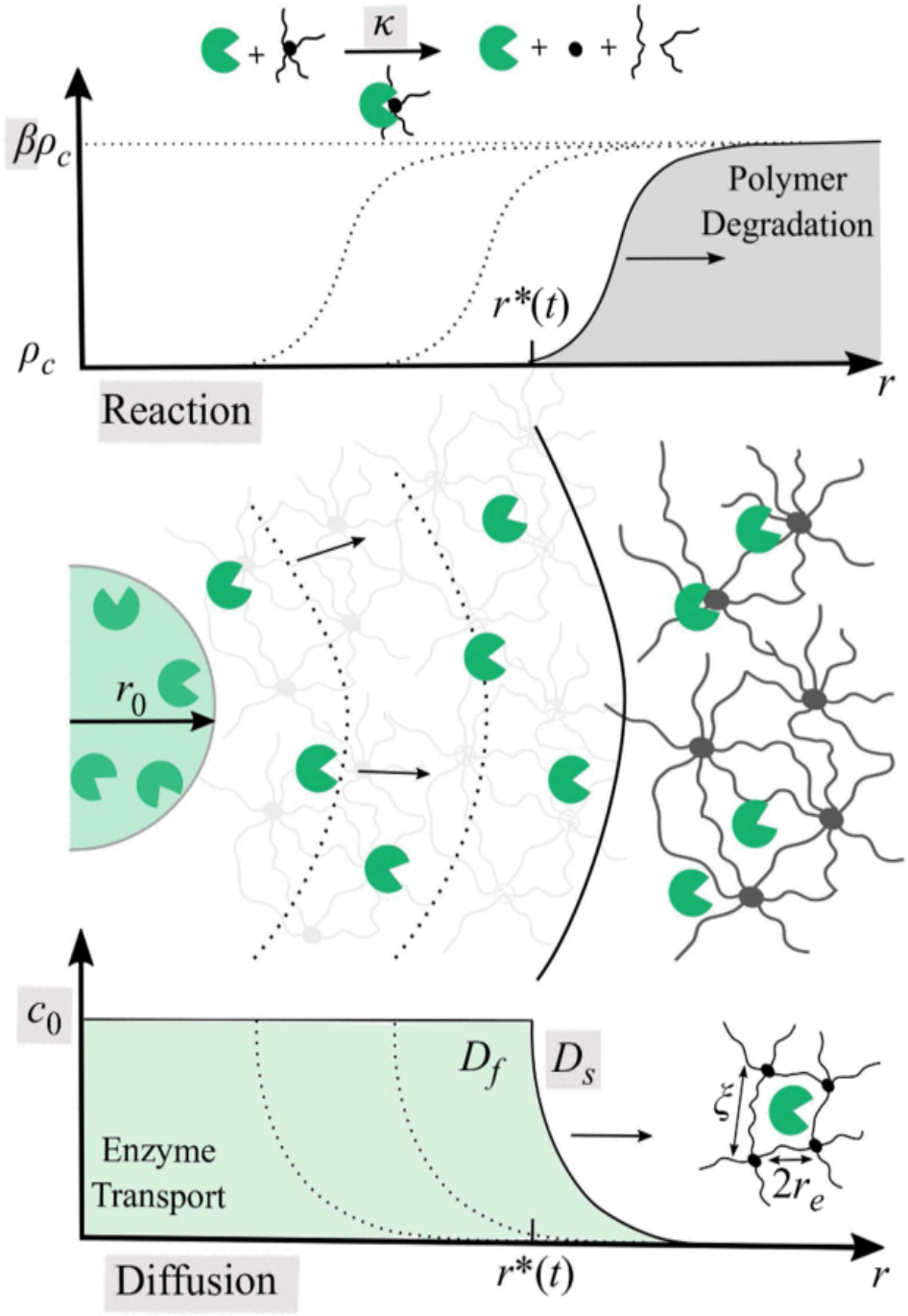


***Figure* 9.** Schematic illustration of enzyme diffusion and degradation reaction in the biodegradable polymer. The evolution of polymer cross-link density ρ (ρ_c corresponds to reverse gelation) and enzyme concentration (c) are illustrated. The highlighted parameters β (network connectivity), κ (reaction rate

constant for degradation), c_0 (enzyme source concentration), and Ds (enzyme diffusivity in the polymer mesh) are the key features of the model.[66]

Interestingly, GelMA properties such as degree of methacrylation, crosslinking density, and environmental factors including pH, temperature, and the presence of MMP inhibitors or activators can all modulate the degradation process. By incorporating MMP-cleavable peptides into GelMA hydrogels, drug release can be coupled to the presence and activity of MMPs. This is particularly useful for targeted drug delivery to sites of disease or injury where MMPs are upregulated. MMP-mediated degradation also allows GelMA hydrogels to break down in a manner that mimics natural ECM turnover, promoting tissue regeneration and integration. For instance, GelMA hydrogels have been designed to be degraded by MMPs and show promise for wound healing applications. The MMP-cleavable linkages in these hydrogels can be used to control the release of growth factors that promote tissue repair. As MMPs are naturally upregulated during wound healing, the hydrogel degrades in sync with the healing process, providing temporary support and gradually giving way to new tissue. Understanding the interplay between MMPs and GelMA degradation is crucial for designing biomaterials with tailored degradation profiles for drug delivery, tissue engineering, and other biomedical applications.

2.3.5 MMP-Mediated Degradation of GelMA Hydrogels: A Mechanistic Perspective

While GelMA is derived from denatured collagen (gelatin), it retains a significant portion of the native collagen's amino acid sequence, particularly within the triple-helical region. This makes it susceptible to hydrolysis by MMPs exhibiting collagenolytic activity. MMPs, particularly MMP-2 (gelatinase A) and MMP-9 (gelatinase B), recognize specific amino acid motifs within the gelatin backbone. These motifs often involve glycine residues in the P1′ position and hydrophobic amino acids in the P2′ and P3′ positions. The canonical cleavage site for MMP-2 and MMP-9 in collagen is Gly-Ile/Leu-Gly, but these enzymes can also cleave at other Gly-X-Y sequences within GelMA. These two MMPs, known as gelatinases, exhibit particularly high activity towards gelatin and GelMA. They cleave peptide bonds adjacent to glycine residues, which are abundant in gelatin. While collagenases and gelatinases are key, other MMPs, like MMP-1, MMP-3, and MMP-7, can also contribute to GelMA degradation, although at slower rates. Interestingly, MMP enzymes are also found on the ocular surface and their levels are elevated in certain ocular conditions such as corneal wound healing, ulceration, and uveitis and they show collagenolytic activity.[67] Research suggest that MMP-9 is elevated in the tears of dry eye patients.[68,69] The gelatinase MMP9 enzyme cleaves collagen chains α1(V) and α(XI) between Gly-439 and Val-440 and the α2(V) chain between Gly-445 and Leu-446.[70,71]

The MMP-mediated degradation process occurs in following steps:

1. **Diffusion:** MMPs from the surrounding environment or secreted by encapsulated cells diffuse into the GelMA hydrogel.
2. **Cleavage Site Recognition:** MMPs recognize and bind to specific amino acid sequences within the gelatin chains.
3. **Hydrolysis:** The enzyme's catalytic domain, containing a zinc ion, facilitates the hydrolysis of peptide bonds at the cleavage site.
4. **Fragmentation:** The gelatin chains are broken down into smaller peptides and amino acids.
5. **Erosion and Dissolution:** As degradation progresses, the hydrogel network weakens, leading to erosion and eventual dissolution of the material.

Additionally, there are some structural features of GelMA that influence the degradation rate. Degree of methacrylation, a critical parameter in GelMA synthesis, can significantly influence MMP-mediated degradation. Higher methacrylation degrees can mask MMP cleavage sites, hindering enzyme access, leading to slower degradation kinetics. Conversely, lower methacrylation degrees expose more cleavage sites, rendering the hydrogel more susceptible to enzymatic degradation. Similarly, lower crosslinking density allows for easier diffusion of MMPs into the hydrogel and faster degradation whereas higher density creates a tighter network that restricts MMP movement and slows down degradation. Additionally, the pore size of the GelMA hydrogel influences the diffusion of both MMPs and the cleaved degradation products. Larger pore sizes and higher pore interconnectivity allow for more rapid enzyme diffusion and product removal, accelerating the overall degradation process. The degree of crystallinity within the GelMA network is another factor that can also impact the degradation rates. Crystalline regions, characterized by tightly packed polymer chains, hinder enzyme access and slow down degradation. Conversely, amorphous regions, with their more loosely arranged chains, are more susceptible to enzymatic attack. Understanding the intricacies of MMP-mediated GelMA degradation allows for the rational design of hydrogels with tailored degradation profiles for a wide range of biomedical applications. Different characterization techniques can be used to study MMP-mediated GelMA degradation:

- **Zymography:** This technique allows for the visualization and quantification of MMP activity within or surrounding the GelMA hydrogel. By analyzing the characteristic banding patterns on zymograms, the presence and activity of specific MMPs involved in degradation can be assessed.[72]
- **Mass Spectrometry:** Mass spectrometry techniques can be employed to identify and quantify the specific degradation products generated during MMP-mediated hydrolysis of GelMA. This provides insights into the cleavage sites targeted by MMPs and the kinetics of degradation.[73]

- **Rheology:** Rheological measurements can be used to monitor changes in the viscoelastic properties of GelMA hydrogels during enzymatic degradation. As MMPs cleave the gelatin backbone, the hydrogel's storage modulus and loss modulus decrease, reflecting the loss of structural integrity.[74]
- **SEM:** SEM primarily provides qualitative information about the hydrogel's morphology. However, it cannot directly quantify the extent of hydrogel degradation**.** SEM is most useful for comparing the microstructure of hydrogels at different time points during degradation. By imaging samples at regular intervals, the degradation of the hydrogel's microstructure can be tracked.[75]

As previously mentioned, CLs have been proposed as ocular drug delivery devices to treat various ocular conditions.[76] Commercialization of the first contact lens for drug delivery has recently (March 2021) been achieved by Johnson & Johnson (Acuvue Theravision™), which delivers ketotifen to treat ocular allergies. Of note, an ideal ocular drug delivery system should overcome the limitations of conventional eye drops, such as low bioavailability, while maintaining appropriate pharmacokinetics.[9] Unlike eye drops, drugs released from CLs remain within the post-lens tear film, evading ocular removal mechanisms such as blinking, tear dilution and drainage. Therefore, drug delivery using CLs results in higher drug residence time and drug penetration into the eye compared to traditional drop formulations. However, a central concern in ocular drug delivery is to deliver the drugs in a sustained and prolonged manner and CLs often suffer from problems such as low drug absorption and high burst release. Some techniques used for sustained drug release, which include the inclusion of nanoparticles, liposomes, and vitamin E coatings,[77] have been proposed to deliver drugs from CLs. Even though these techniques show some degree of sustained drug release, they still exhibit a pattern of significant burst release.[78] This is an issue because it causes drugs to be released at an uncontrollable rate over the initial few hours of wear, decreasing the therapeutic effect of the drug after 5-6 hours of use and raises safety concerns due to potential excessive release and subsequent toxicity to the ocular surface. In this regard, biodegradable polymers for fabricating a drug delivery system can help us to build up on the science of controlled drug delivery and have an even greater impact on the healthcare sector.[47] According to International Union of Pure and Applied Chemistry, 'degradable polymers' are the ones that can undergo in vivo degradation resulting solely from hydrolysis by the water present in tissues and organs, referred to as hydrolysis or hydrolytic degradation.[79] The following is the structural classification of polymeric devices for sustained release:[80]

- Monolithic type, in which there is homogeneous mixture of drug and polymers.
- Binding type, where polymer binds to drugs through chemical or ionic binds.
- Reservoir type, where drugs are stored within polymers.

In case of polymer erosion, a water insoluble material is converted to a water-soluble material. There are three different types of polymer erosion processes:[54]

- **Type I erosion:** Type I erosion occurs by the cleavage of the water-soluble backbone when crosslinked networks of water-soluble macromolecules are placed in the aqueous environments. In such hydrogel systems, the water solubility of the incorporated drug becomes an important factor. These polymers are mainly used to deliver drugs. For example, polyacrylamides, PVA, and PVP.
- **Type II erosion:** In type II erosion, water-insoluble macromolecules are converted to water-soluble macromolecules by hydrolysis, ionization, or protonation of pendant groups. However, no backbone cleavage occurs in this case and such materials are useful in topical applications. For example, alkyl monoesters of poly (vinyl methyl ester/maleic anhydride).
- **Type III erosion:** In this type of erosion, conversion of high molecular weight water insoluble macromolecules takes place into water-soluble molecules by a hydrolytic cleavage of labile bonds in the polymer backbone. Such systems are used for administering drugs to intramuscular, subcutaneous, or intraperitoneal implantation sites where the degradation products should be non-toxic. The polymers that undergo type III erosion include polylactic acid, polyglycolide, poly lactic-co-glycolic acid.

2.3.6 3D printed biodegradable CLs for ocular drug delivery

Although biodegradable polymers such as GelMA have benefits in ocular drug delivery, the main challenge is that they degrade in storage, so they must either be stored in a dried form or fabricated on-demand. To this end, 3D printing may offer a viable solution, enabling on-demand fabrication of contact lens and ocular inserts that could also be customized for an individual patient. Commercial CLs are manufactured via mainly molding methods, and to a lesser extent by spin-casting and lathe machining. However, this large-scale fabrication makes it unsuitable for customization to meet the needs of an individual patient, an approach towards so-called “personalized medicine”. This customization could relate to patient-specific fitting factors (especially related to diameter or base curve radius), as well as factors related to various drug concentrations, depending on the ocular condition being treated for an individual. For example, a patient with severe dry eye due to autoimmune disease (e.g., Sjögren’s syndrome) may require a higher concentration and longer duration of anti-inflammatory drug release compared to someone with mild, environmentally induced dry eye. Similarly, post-surgical patients might need short-term, high-dose corticosteroid delivery, whereas chronic dry eye patients may benefit from low-dose, sustained immunomodulators like cyclosporine. These scenarios illustrate how drug type, concentration, and release

duration should be tailored to the underlying condition and disease severity. However, realizing personalized medicine also presents challenges. Key barriers include the lack of quantitative biomarkers to guide dosing and the variability in patient response. While MMP9 levels offer some diagnostic value, they are typically measured qualitatively. Determining patient-specific dosage would require integrating biomarker data into predictive models. Until such tools are available, a stratified approach, where inserts are tailored to disease severity (e.g., mild, moderate, severe), may offer a practical path forward.

Current treatments, such as eye drops, are often limited not by the drug itself, but by inefficient delivery, including low bioavailability, short residence time, and frequent dosing requirements. These challenges reduce therapeutic effectiveness and patient adherence. By improving retention and release control, drug-eluting inserts or lenses can overcome many of these limitations—highlighting that the delivery method, rather than the drug, is often the key barrier in current treatment strategies. These challenges highlight the need for fabrication strategies that ensure both long-term drug stability and patient-specific customization.

Another important consideration is that the storage conditions of drug-eluting contact lenses can impact drug stability, potentially altering the release profile and therapeutic performance. This may result in variability in both the amount and rate of drug released, depending on the time elapsed since manufacturing. To address this, a fabrication method that enables patient-specific, on-demand production—inspired by the concept of "just-in-time" manufacturing—would be advantageous. In this regard, additive manufacturing (3D printing) offers a superior alternative for producing customized and smart contact lenses, with the flexibility to adjust both physical and pharmacological properties at the point of care.[81] This method used computer aided design (CAD) and offers high accuracy and facile control object dimensions. As an added benefit, 3D printing can also be leveraged to incorporate spatial design elements such as drug reservoirs and microfluidic channels to enhance drug delivery. This method allows printing of multiple objects simultaneously, fast prototyping, and customization (*Figure* 10).

Current treatments, particularly eye drops, suffer from rapid clearance, low ocular bioavailability (<5%), and frequent dosing requirements, which often lead to poor patient compliance. These limitations hinder the therapeutic effectiveness of even well-established drugs. By contrast, our system aims to enhance drug retention and controlled release, indicating that it is the delivery method, not the drug itself, that remains the key limiting factor in current therapies.

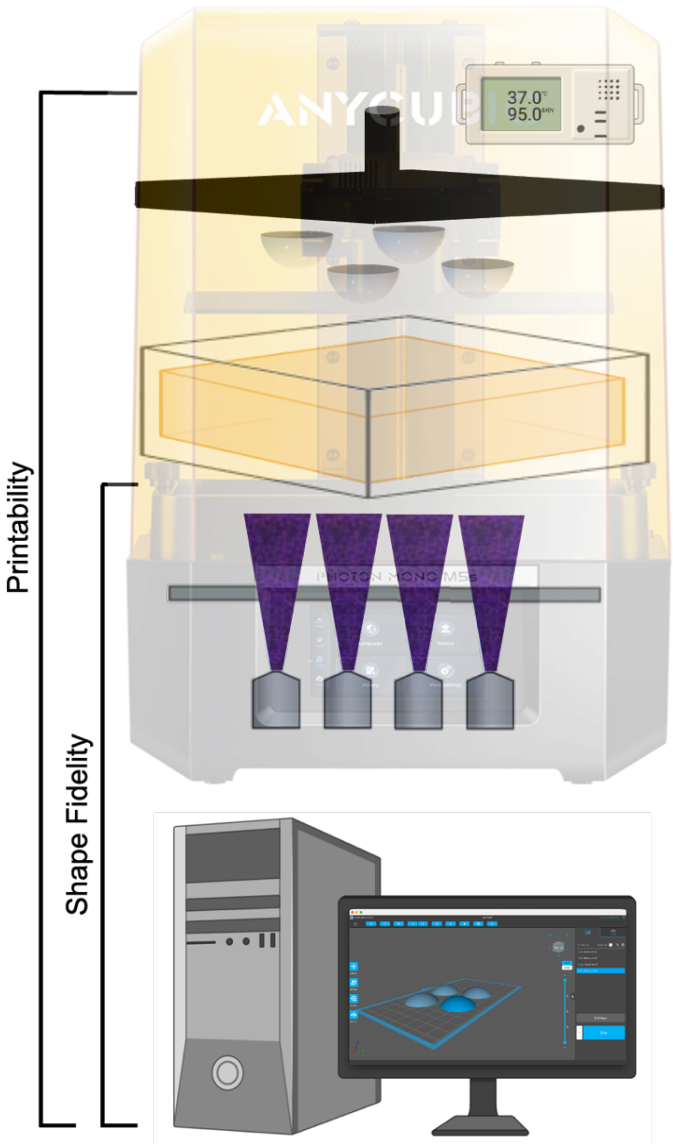


***Figure* 10.** Scheme for fabrication of CLs from stereolithography-based 3D printing.

2.4 3D printing

There have been tremendous advancements in 3D printing since the introduction of early stereolithography (SLA) fabrication systems in the 1980s by Charles Hull.[82] Presently, inkjet and extrusion printers are the most used 3D printers. These printers build a structure in layer-by-layer fashion using rasterized direct-write format. The innovations in 3D printing have opened new avenues in biomedical engineering and drug delivery. The interdependent relationship between the type of 3D printing method and the ink used governs the successful printing of the intended 3D structures. An important consideration in the fabrication of ink for these light-based printing platforms is the incorporation of photoreactive

moieties such as acrylate and methacrylate to facilitate its selective solidification.[83] In the process of photopolymerization, UV or visible light interacts with light sensitive compounds, photoinitiator, and produce free radicals that initiate the polymerization process, resulting in the formation of covalently cross-linked hydrogel.[83] With 3D printing using photopolymerization-based methods, it is easier to tailor the optical, chemical, and mechanical properties of printed materials.[84]

2.4.1 3D printing in biomedicine

3D bioprinting involves utilizing 3D printing-like techniques to fabricate biomedical devices consisting of cells, growth factors and biomaterials to emulate the natural tissue characteristics. However, 3D bioprinting of living constructs has many challenges in transitioning from synthetic materials to biologically functional materials while gaining a precisely controlling the mechanical properties at the microscale and macroscale.[85,86] Interestingly, various cell types and biomaterials can be combined and patterned into constructs that can revolutionize the presently existing clinical therapies. For instance, 3D printed tissues such as skin, bone, and cartilage demonstrate the potential of this technology.[87-89]

2.4.2 Considerations for 3D printing

While designing a bioink for 3D printing of ocular drug delivery systems such as a CL or conjunctival inserts, the following factors should be considered: (a) biodegradability (b) biocompatibility (c) homogeneity (d) optical properties (*Figure* 11). Many commercially available printers in the market claim to print at resolutions as low as 50 μm nominal resolution, however real-world performance does not reach this level of accuracy.[90] However, to 3D print delicate structures and complex geometries such as a CL with fine details, higher resolution is needed. This also leads to greater the chances for errors and deviation in the 3D printed object.[91,92] Also, for biomedical applications the print quality of the 3D printed objects must meet a certain threshold requirement. Without appropriate tuning of the print settings or material composition, the overall print quality tends to be poor.[86,93,94] Owing to their biocompatible nature, both synthetic and naturally occurring biodegradable polymers have been used for a plethora of biomedical applications, including tissue engineering,[43] regenerative medicine,[44] drug delivery,[47] and 3D bioprinting.[45,46]

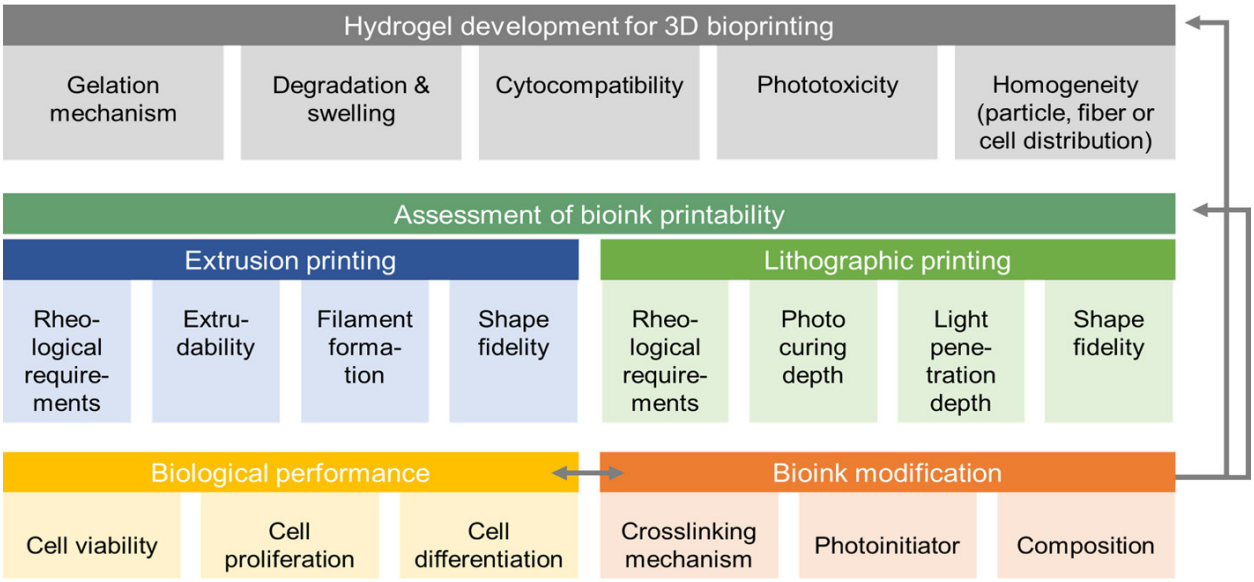


***Figure* 11.** Summary of key properties to be considered during bioink development for 3D printing, including printability assessment.[95]

2.5 Concluding remarks: Thesis directions and plan

This leads to the hypothesis:

A biodegradable contact lens fabricated through an on-demand 3D printing technique, utilizing a physically crosslinked polyvinyl alcohol (PVA) matrix, will enable controlled PVA release while mitigating the challenges of material degradation and premature drug release during storage. This approach will demonstrate a proof-of-concept for the development of customizable ocular drug delivery systems, including contact lenses and conjunctival inserts, using commercial 3D printing technology.

To this end, the aims of this thesis are as follows:

1. 3D Printing of a prototype biodegradable contact lens using GelMA.
2. 3D printing of a contact lens to release PVA as a therapeutic agent.
3. Controlling the burst release of PVA from GelMA via a physical crosslinking method.
4. 3D printing of biodegradable conjunctival inserts for the treatment of dry eyes

Chapter 3

3D Printing of a prototype biodegradable contact lens using Gelatin Methacrylate

*An article was extracted from this chapter and is published in Elsevier's International Journal of Pharmaceutics (DOI: 10.1016/j.ijpharm.2024.124999Z)

This chapter has been published as follows:

Shokrollahi P, Garg P, Wulff D, Hui A, Phan CM, Jones L. Vat photopolymerization 3D printing optimization: Analysis of print conditions and print quality for complex geometries and ocular applications. Int J Pharm 2025; 668: 124999.

Author	Concept/Design	Data Acquisition	Analysis	Write Up/ Publication
Parvin Shokrollahi	Y	Y	Y	Y
Piyush Garg	Y	Y	Y	Y
David Wulff	Y	Y		
Chau-Minh Phan	Y			Y
Lyndon Jones	Y			Y

3.1 Abstract

Purpose: To optimize the printing conditions for biodegradable contact lenses using gelatin methacrylate (GelMA) hydrogel biomaterial ink using a low-cost masked-stereolithography-based commercial 3D printer.

Method: In this work, GelMA biomaterial ink was selected as a base material owing to its biocompatibility and demonstrated high levels of controllability. The GelMA-based ink was used to study the effects of dye concentration and exposure time on print quality. The photocrosslinking process and the 3D printing process was described in detail with respect to soft hydrogel biomaterials. Further evaluation of the optimized printing conditions was achieved by successfully printing high resolution structures such as a contact lens, substantially expanding the scope of this optimized method in producing high-quality prints with intricate details.

Results: The results demonstrates that by tuning the print conditions and ink parameters, soft biomaterials from GelMA ink of higher shape fidelity and accuracy can be efficiently printed even on a low-cost 3D printer. The parameters standardized include 10% (w/v) concentration of GelMA bioink, 3% photo-absorber concentration and 120s exposure time to 3D print a contact lens based on GelMA. Moreover, a fine interplay between the dye concentration (C_{Dye}) and exposure time is key to effective polymerization and resolution, ensuring successful printing of the hydrogel biomaterials with higher structural integrity.

Conclusion: The optimized properties showed that a contact lens of nearly perfect shape was formed with the current set up. Overall, the results highlight the practical potential of this method in optimizing the 3D printing processes involving complex geometries using a low-cost commercial 3D printer.

Keywords: VAT Polymerization 3D Printing, Shape Fidelity, Print Resolution, Contact Lenses

3.2 Introduction

In recent years, there has been explosive growth in the development of bioinks, hydrogels, and biomaterials for 3D printing/bioprinting applications in tissue engineering.[1-4] Unlike conventional materials, these new materials are more transparent, less viscous, and contain water which makes them less compatible with extrusion-based 3D printing setups.[5, 6] Naturally derived photocurable bioinks like chitosan methacrylate and gelatin methacrylate (GelMA) enable fabrication of intricate tissue constructs, showcasing the broad spectrum of materials utilized in 3D printing for biomedical purposes.[7] Researchers have shown significant interest in GelMA due to its exceptional biocompatibility, biodegradability, and moldability.[8, 9] GelMA hydrogel have been utilized to create various structures, including 3D (bio)printed scaffolds, injectable gels, and electrospun fibrous membranes, using techniques such as photo-crosslinking, extrusion-based 3D printing, or electrospinning.[10-13]. An important aspect of 3D printing of GelMA that determines its usefulness for a specific application is the quality of the 3D printed component.[14] However, without appropriate tuning of the print settings or material composition, the overall print quality tends to be poor.[13, 15, 16] Moreover, evaluating the print quality for hydrogel materials in 3D printing is challenging due to its soft and transparent characteristics.[17]

There are many parameters that can affect the photocuring process, and hence the final print quality. These include ink parameters such as photoinitiator concentration, monomer composition, and presence of additives, as well as print parameters such as UV light intensity wavelength, exposure time, temperature and humidity (*Table* 1). In addition to these parameters, the geometry and thickness of the part being cured can also affect the curing process. For example, thicker parts will require longer curing times or higher light intensities to achieve complete cure.

***Table* 1**. Various ink and process parameters affecting the print quality in 3D printing.

Ink Parameters	***Print Parameters***
Photoinitiator type and concentration: The photoinitiator absorbs light and generates free radicals or cations that initiate polymerization. Hence, the type and concentration of photoinitiator affects the curing speed and depth.	*Light intensity and wavelength:* The intensity and wavelength of the light source will affect the curing speed and depth. Higher intensities and shorter wavelengths generally lead to faster curing.

Monomer and oligomer composition: The type and ratio of monomers and oligomers in the ink affects the viscosity, mechanical properties, and cure kinetics of the final biomaterial.	*Exposure time:* The exposure time also affects the curing depth and the degree of crosslinking. Longer exposure times can lead to a higher degree of crosslinking.
Presence of additives: Additives such as pigments, fillers, and stabilizers can affect the curing process and the properties of the cured material. For example, pigments can absorb light and reduce the cure depth.	*Temperature and humidity:* The temperature and humidity of the environment can affect the curing process, particularly for soft hydrogel materials that are sensitive to moisture.

Print quality can be broadly described as a combination of print fidelity and print resolution. Print quality of a 3D printed object is influenced by various factors including, but not limited to, the type of printing technology employed,[18, 19] the printer's actuation accuracy in the x-y-z directions, composition of the ink material,[20, 21] and the print settings used.[22] With an exponential increase in the development of various formulations for 3D printing with biomaterial inks and hydrogels, different chemical compositions and properties of the ink can affect final print quality. For circular structures, the precision of shape is assessed using a parameter called 'circularity.' The circularities (CR) of enclosed circles are determined using *equation* 1.

$$CR = \frac{4\pi A}{L^2} \qquad \textit{Equation 1}$$

where L represents perimeter/circumference and A denotes area. A perfect circle exhibits the maximum circularity of 1.[23]

Print fidelity assesses how closely the 3D-printed object replicates the original Computer Aided Design (CAD), while the print resolution specifies the level of details retained in the print.[24] Many commercially available printers in the market claim to print at resolutions as low as 50 μm nominal resolution, however real-world performance does not reach this level of accuracy.[24] The smaller the details in the object, the higher resolution that is required. This also leads to greater chances for errors and deviation in the 3D printed object.[18, 25] It is typically expected that as the cost of the printer increases (from a few hundred dollars to several hundred thousand dollars), the quality of the prints it produces will improve. However, increased cost lowers the accessibility and practicality, reaching a threshold where 3D printing ceases to be a viable and practical tool. Of note, there has been a concerted effort to investigate different ways to enhance print quality, while concurrently lowering the overall cost of 3D printing.[26]

In this work, we attempted to 3D print a biodegradable contact lens based on a gelatin methacrylate hydrogel material. Given the budget constraints which leads to lower accessibility of 3D printing, the printing conditions for GelMA-based soft hydrogel materials were optimized for a low-cost vat-based commercial 3D printer. As the photocuring process is influenced by different parameters, herein, we studied the effect of two different ink parameters (dye concentration) and print parameters (UV exposure time) on the 3D printing of GelMA hydrogels. A set of 3D objects that included solid cubes with and without a hollow conduit in the centre (descending side lengths) and an object with radial spokes were printed and studied by varying photo-absorber dye concentrations and exposure time. The printer was retrofitted with a humidity and temperature control kit to enable printing at ~60-70% relative humidity and 37 °C. Further validation of the optimized 3D printing conditions was performed by printing delicate structure like a contact lens, to understand the scope of this optimized method in producing high-quality prints with complex geometries and intricate details for gelatin methacrylate hydrogel biomaterial ink.

3.3 Materials and methods

3.3.1 GelMA synthesis

GelMA was synthesized using standard literature procedures to achieve a high degree of substitution (>85%). [27] Briefly, gelatin from porcine skin (10% w/v, Sigma-Aldrich, St. Louis, MO, USA) was reacted with methacrylic anhydride (1% v/v, Sigma-Aldrich, St. Louis, MO, USA) in a carbonate bicarbonate buffer (CB, 12.5 mM sodium bicarbonate, 87.5 mM sodium carbonate anhydrous, pH 9.4) at 50°C for 1h. The reaction was stopped by adding acetic acid to a final concentration of 0.15% (v/v). The resulting product was dialyzed in 12–14 kDa dialysis tubes (Sigma-Aldrich, St. Louis, MO, USA) in deionized water for 24 h. The purified solution was freeze-dried and stored at -80°C prior to use.

3.3.2 Biomaterial ink preparation

For the preparation of the biomaterial-ink, GelMA (10% w/v) was added to lithium phenyl-2,4,6-trimethylbenzoylphosphinate (0.6% w/v, LAP, Sigma, St. Louis, MO, USA) solution made in phosphate buffered saline (PBS, Fisher Scientific, Waltham, MA, USA) at 37°C, 50 rpm until complete dissolution. Next, a yellow dye (Tartrazine, Sigma, St. Louis, MO, USA) was added and the biomaterial ink was used for 3D printing. All the stereolithography (SLA) printing experiments were performed in atmospheric air conditions. The ink composition is reported in *Table* 2

***Table* 2**. Parameters used for 3D printing using GelMA

GelMA (w/v)	LAP (w/v)	C_{Dye} (v/v)	t_{Exp} (s)	T_{Layer} (µm)
10%	0.6%	1% 3% 5%	30 50	100

3.3.3 Designing of CAD models

3D printing of biomaterials for various biomedical applications requires precise print fabrication and reproducibility of the process. Therefore, to ensure consistency in assessing the structural accuracy of 3D printed objects, a set of standard 3D shapes were created with the predefined details using CAD software (FreeCAD 0.19). The set of standard 3D shapes consisted of solid cubes with and without a hollow conduit in the centre (descending side lengths), an object with radial spokes, and a contact lens. The contact lens was designed with diameter 14.98 mm. While not the most common in daily wear lenses,14.98 mm diameter represents the upper bound of some commercially available soft lenses, offering greater ocular coverage, stability, and design flexibility—making it a practical choice for advanced therapeutic and research applications. These CAD models are illustrated in *Figure* 1. The designed models were printed, imaged, and subjected to analysis to evaluate their accuracy and adherence to the CAD specifications.

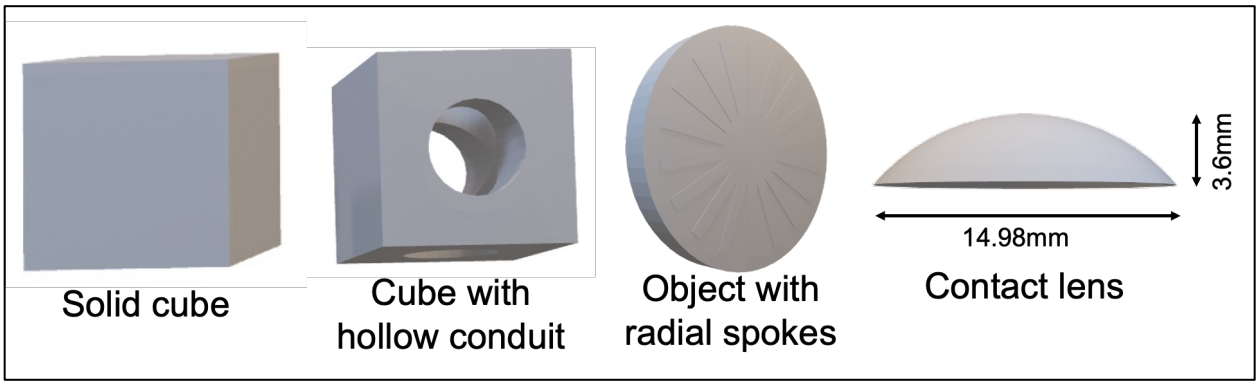


***Figure* 1.** The CAD designs of solid cubes with and without a hollow conduit in the centre, an object with radial spokes, and a contact lens.

3.3.4 3D printing process

The CAD models - comprising complex geometries such as solid cubes (with and without holes) of descending side lengths, an object containing radial spokes and a contact lens - were designed using

FreeCAD software (Version 0.19) and exported as STL files. Using CHITUBOX software (v 1.9.5), the STL files were sliced with 100 μm layer thickness and 3D printed on a low-cost 3D printer (Photon Mono X, Shenzhen, Guangdong, China) with a nominal XY resolution of 50 μm, Z resolution of 10μm, and LCD resolution 3840x2400 pixels. The printer was retrofitted with a humidity and temperature control kit to enable printing at ~60-70% relative humidity and 37 °C. The GelMA ink was incubated at 37 °C for 1 hr and mixed gently before use. The 3D printing photopolymerization process was carried out using UV light of wavelength 405 nm. After printing, the printed objects were washed by sonicating in PBS using a bath sonicator (50D Aquasonic, VWR International, Radnor, PA, USA) for 10 min to remove any unreacted biomaterial-ink components on the surface.

Prior to experimentation, zero position of the print plate (in the Z axis) was set according to the manufacturer's instruction, to ensure accurate layer thickness while printing. Next, the ink tank (vat), featuring a stick-free transparent base, was filled with 35-45ml GelMA ink, depending on the dimensions of the objects to be printed. As the printing commenced, the print plate descended into the tank (the approach step) while maintaining a single-layer gap (Layer thickness, T_{Layer}). A projector projected UV light (405nm) pattern onto the LCD screen and the crosslinking of the GelMA ink occurred at the interface, forming a solid hydrogel structure. As each layer gets crosslinked, the platform retracts in the Z-axis to separate the interface of the printed layer from the vat while simultaneously creating space for GelMA ink to flow and take the empty space. Subsequently, the next layer's pattern is projected, and the layer-by-layer printing process repeats until the complete printed object is obtained (*Figure* 2).

Based on a series of preliminary experiments, a printing window for GelMA concentration (10% w/v), exposure time (t_{Exp}>30s), dye concentration (C_{Dye}>1% v/v), and LAP concentration (C_{LAP}, fixed at 0.6% w/v) were chosen for this study (*Table* 2). The 3D printing parameters were selected according to previous reports confirming that the increase of initiator concentration and light intensity can overcome the oxygen inhibition of photo-polymerisation reactions.[28]

3.3.5 Shape fidelity evaluation

The effects of the dye concentration, exposure time and printing direction were studied on various models (*Figure* 1) based on circularity (*Equation* 1). The images of solid cubes with and without a hollow conduit in the centre and the contact lenses were taken using an iPhone 10 (Apple Inc., Cupertino, CA, USA). The optical images of the printed object with radial spokes were taken on an Imaging Multimode Plate Reader (Cytation 5, Agilent BioTek Instruments, Winooski, VT, USA) using a 4X lens. To minimize subjectivity in the image analysis due to manual measurements, Fiji software was used.

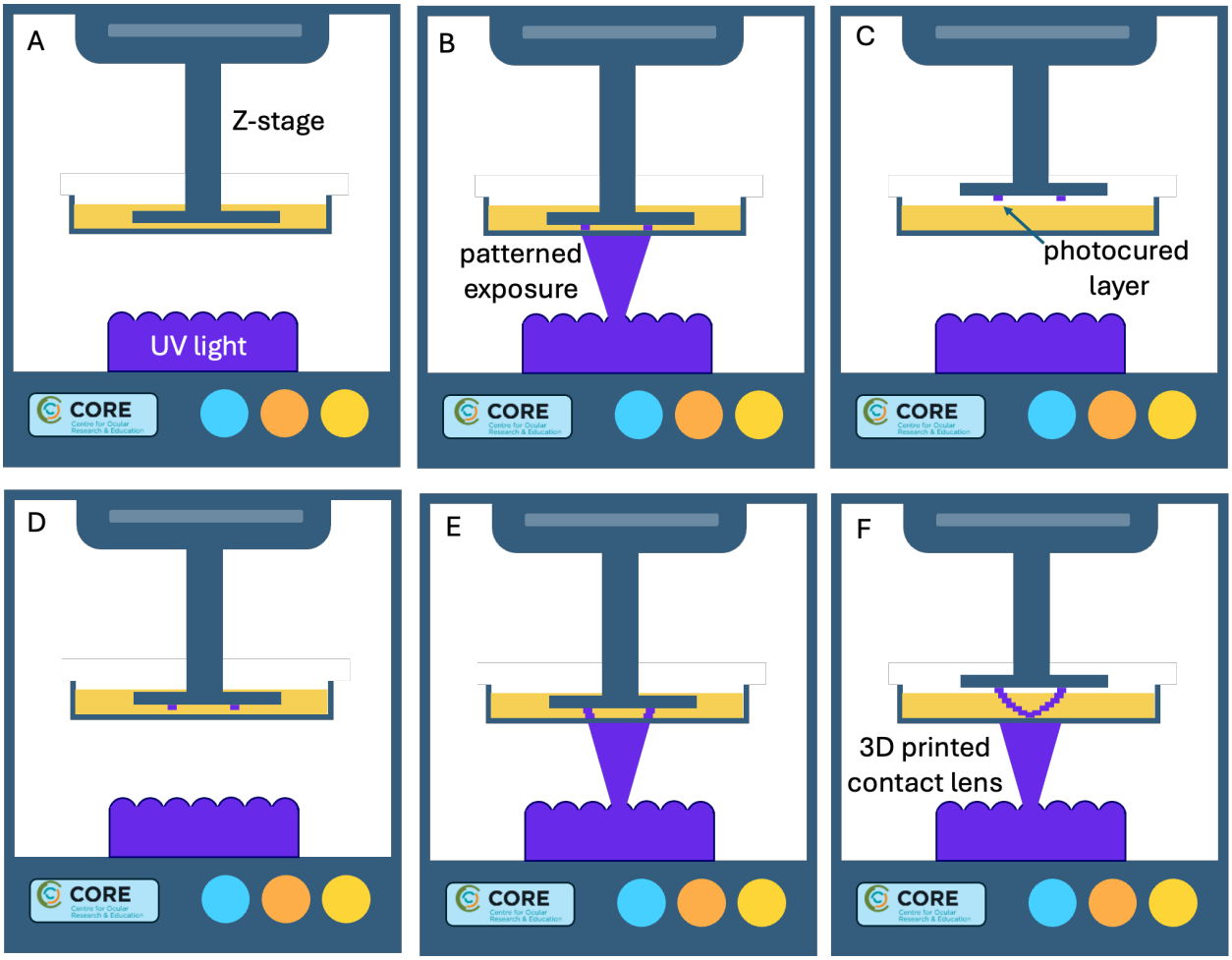


***Figure* 2.** 3D printing process for fabricating a contact lens. A) The stage approaches the vat filled with the biomaterial ink. B) UV light is exposed in a pattern to be 3D printed using the concept of masked-stereolithography. C) The platform retracts, separating the first printed layer from the vat and creating space for GelMA ink to flow and take the empty space. D) The stage or print plate again approaches the vat filled with biomaterial ink. F) UV light is exposed to form the next layers. F) The process repeats itself until the contact lens is completely printed.

3.4 Results and discussions

3.4.1 3D printing process

When 3D printing of soft hydrogel materials it is important to note that the physical and mechanical properties of the printed structures depend on environmental conditions, including temperature and humidity. Both parameters are crucial to ensure printability and print reproducibility. Since gelatin and its derivatives form a physical hydrogel with limited flow properties below 30°C, and that the printed objects will eventually be tested at a physiologically relevant temperature of 37°C, the 3D printer was retrofitted with a temperature controller that enabled printing at 37°C. As the process of photopolymerization is exothermic in nature, to achieve high structural quality of GelMA-based formulations, the evaporation of water during the exothermic photopolymerization also needs to be addressed. This can cause an increase in viscosity of the ink formulation and a gradual change in the uniformity of the printed object. To overcome this challenge, an atomization humidifier was used to maintain about 60-70% relative humidity in the printing chamber (*Figure* 3).

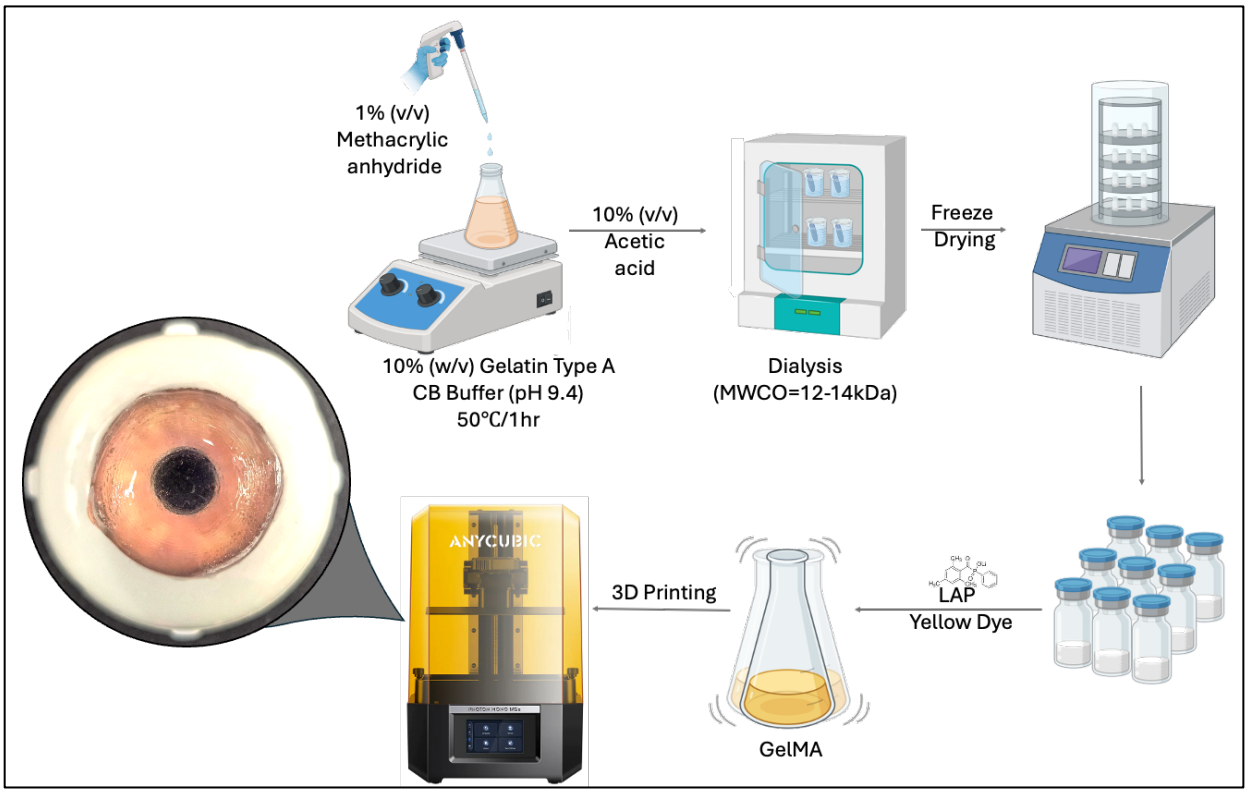


***Figure* 3.** Scheme of preparation of GelMA prepolymer solution for 3D printing of CLs.

3.4.2 Effect of dye concentration on print quality

In vat photopolymerization 3D printing of hydrogels, dyes are used as photosensitizers to enhance the reactivity of the ink to light and improve the resolution of the printed object by reducing light scattering.[29] Occasionally, the dye adds to the mechanical stability by acting as fillers or crosslinkers within the hydrogel matrix.[30] Therefore, careful adjustment of the dye concentration (C_{Dye}) is key for effective polymerization and resolution, ensuring successful printing of the hydrogel biomaterials with fine details and higher structural integrity.[29] *Figure* 4 describes the impact of varying dye concentrations (1%, 3%, and 5% v/v) on the printability of GelMA biomaterial ink print quality with the help of different 3D models (solid cubes of descending side lengths as well as cubes featuring a central hollow conduit with descending diameters).

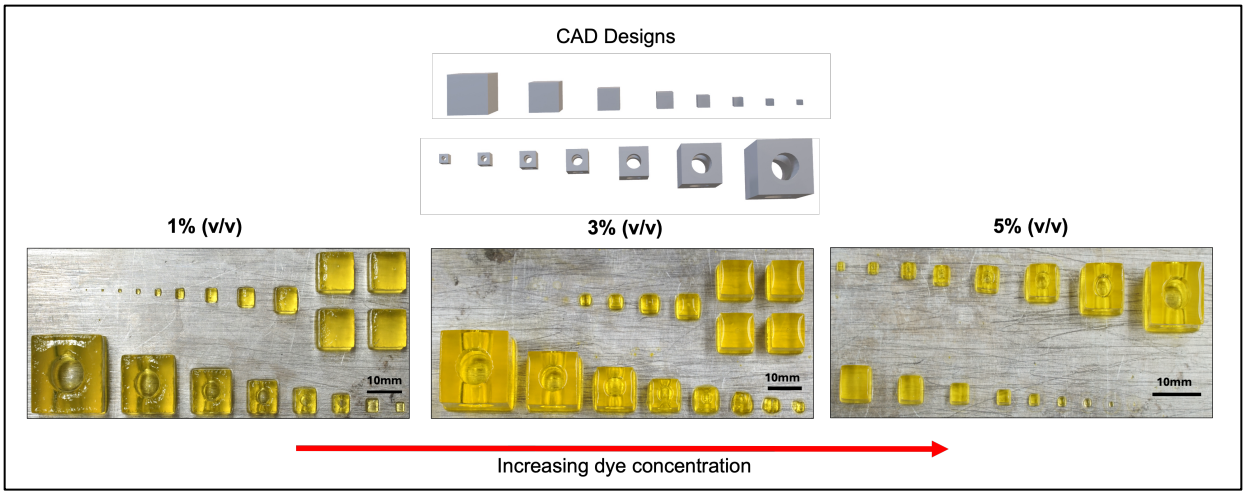


***Figure* 4**. Effect of Tartrazine dye concentration (C_{Dye}) print quality. Scale bars represent 10mm.

***Table* 3.** Circularity values for different dye concentrations (v/v)

Side length	1%	3%	5%
20mm	0.86	0.89	0.88
15mm	0.86	0.88	0.89
10mm	0.89	0.90	0.89
7.5mm	0.87	0.89	0.85
5mm	0.88	0.91	0.85

To evaluate the shape fidelity of 3D printed hydrogels, circularity and printability are the most used measures. While both circularity and printability metrics offer valuable insights into the shape fidelity of 3D printed objects, their applications differ based on the geometry of the printed features. Circularity excels in assessing the fidelity of circular shapes, providing a direct measure of how closely the printed outcome matches a perfect circle. Additionally, printability incorporates both perimeter and area measurements, offers a more comprehensive assessment of shape fidelity for a wider range of shapes, particularly those with corners, such as squares. Therefore, when evaluating the accuracy of a square or rectangular print, usually printability is used.[31] The CRs of the central conduits (top view) in the printed objects were determined according to *equation 1*, and the results are summarized in *Table* 3. As mentioned before, a perfect circle exhibits a circularity of 1. When concentration of Tartrazine was increased from 3 to 5% in the ink, slight decrease in print quality was recorded based on the CR values. This is in agreement with increased dye concentration, decreased light intensity and thus, decreased crosslinking of the ink at the same exposure time. Therefore, a dye concentration of 3% was selected for the next steps (*Table* 4).

***Table* 4**. Effect of dye concentration on print quality.

Model	**T_{Layer} (µm)**	**C_{Dye} (v/v)**	**Observations**
Cubes with hollow conduits	100	1%	Round corners, irregular central conduits
		3%	Perfect corners, better central conduits
		5%	Perfect corners, good central conduits

3.4.3 Effect of exposure time on print quality

Exposure time in vat photopolymerization is another critical parameter for ensuring proper curing, higher resolution, robust mechanical properties, optimal print speed, better surface quality, and desired product performance.[32] To study the effect of exposure time on the print quality, a model object with 18 radial spokes of width 600µm and height 100µm (*Figure* 5) was printed at two different exposure times (*Table* 5).

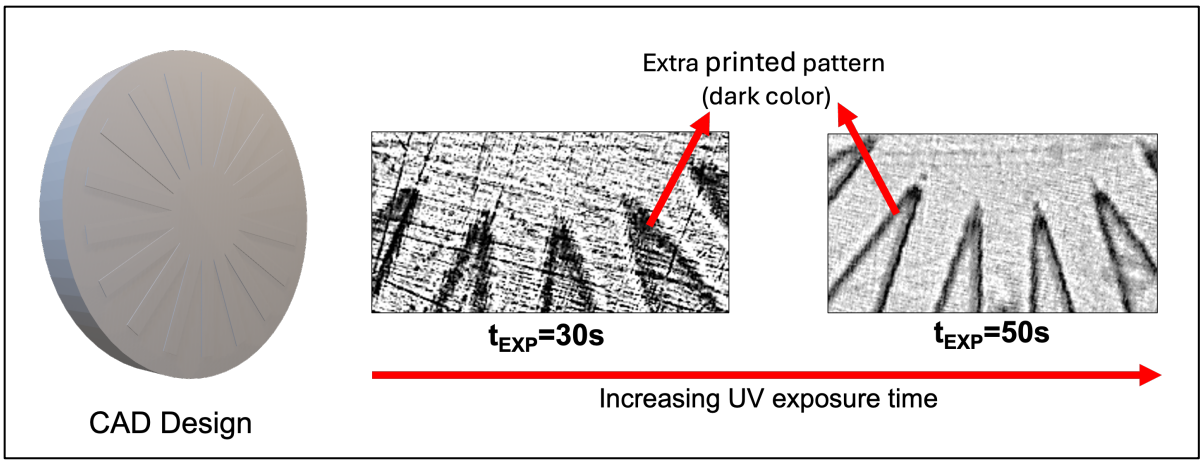


***Figure* 5**. Effect of exposure time (t_{EXP}) on the print quality. The spokes model comprises of 18 radial lines of 600µm width and 100µm height.

The object with radial spokes was printed at t_{Exp}=30s and a layer thickness of 100µm depicted the emergence of an extra pattern (as a dark area) in addition to the radial lines. This dark pattern was more pronounced where the radial lines crossed the boundary of the central circle, as depicted by the arrows in *Figure* 5. However, when the same sample was printed at a higher UV exposure time (t_{Exp}=50s), the dark pattern reduced significantly, and well-defined boundaries were observed, with the corners becoming remarkably sharper (*Figure* 5). This demonstrates that by increasing t_{Exp} , higher shape fidelity for the radial lines can be achieved. In the field of 3D printing, structures composed of one or two layers are commonly used in most qualitative and quantitative shape fidelity experiments. Therefore, in this study, the print/object thickness of the spokes in our initially printed design were sliced into a single layer (T_{Layer}=100).

***Table* 5**. Effect of exposure time on print quality.

Model	T_{Layer} (µm)	t_{Exp} (s)	Observations
Object with radial spokes	100	30	Emergence of extra pattern (dark area)
		50	Better resolution, reduced extra pattern

3.4.4 Putting it all together: 3D printed contact lenses

For multi-layer prints, it has been shown that penetration depth of UV light in GelMA biomaterial ink is remarkably greater than the layer thickness.[33] Slight extra curing is required to guarantee a good bonding between the layers as printing process advances. This means a depth greater than the set layer thickness needs to be exposed to UV light and cured with each curing step to ensure layer stitching between the layers.[34] Utilizing the optimized parameters and conditions from above, next, we attempted to 3D print a GelMA-based contact lens from this ink. Since the overall thickness of the lens was 300µm and owing to the curved structure of the lens, the overall exposure time of each layer was rather limited, therefore a t_{Exp} of 120s was used to 3D print a contact lens. The images in *Figure* 6 depicts that a contact lens of nearly perfect shape was formed. A key parameter for ocular applications is transparency. The transmittance curves for GelMA hydrogels were plotted in the visible range of light (400-800 nm) and the mean light transmittance of GelMA was about 91.4% from 400-800nm, which was greater than the threshold percentage (~85%) to be defined as a transparent substance along all the visible spectrum (Figure 4b, *Chapter* 4).[35] Contact lenses are gaining significant interest as potential ocular drug delivery devices for the treatment of various ocular conditions. Interestingly, for manufacturing of patient-specific drug delivery lenses on a small scale in terms of fitting, therapeutic load, and ocular condition, 3D printing could be an alternative method for fabricating personalized lenses. Of note, GelMA has been used in a variety of biomedical applications as a potential carrier for delivering different therapeutic of interests including dry eye.[36]

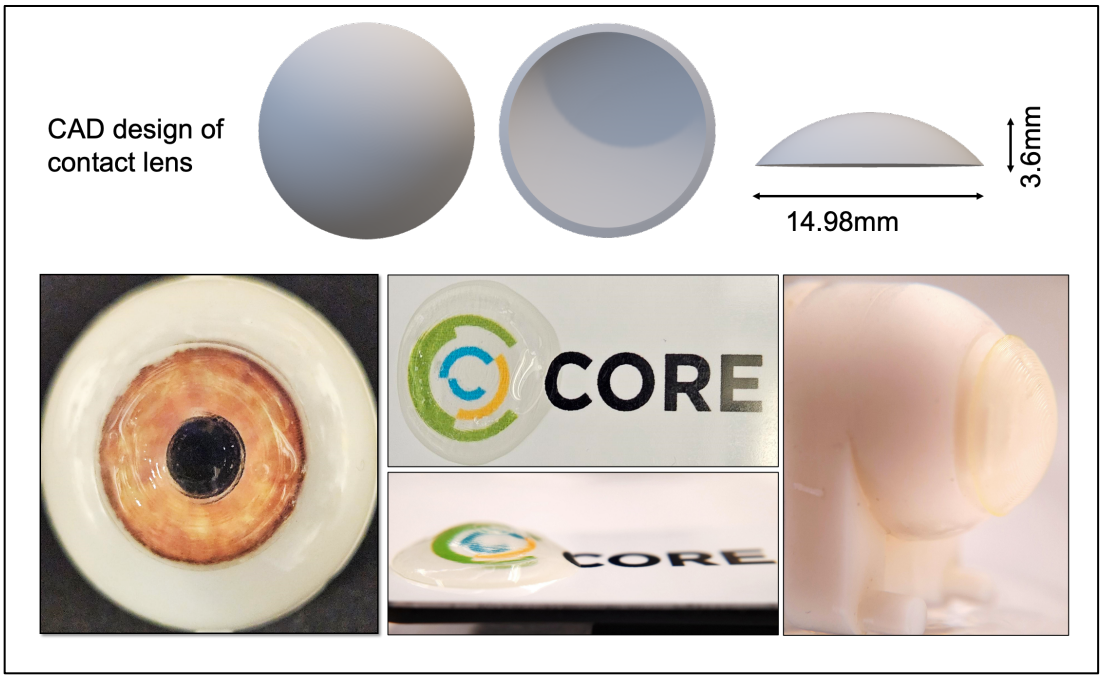


***Figure* 6.** 3D printed contact lens and CAD design.

3.5 Conclusion

An appropriate photocurable biomaterial ink for light-based printing techniques such as SLA printing should meet three requirements of rapid photo-crosslinking rate, dense crosslinking structure, and excellent fluidity for rapid filling of gaps and spaces. In this work, GelMA biomaterial ink was selected as a base material owing to its biocompatibility and demonstrated high levels of controllability. This study developed a method for determining optimal printing conditions for geometries including solid cubes, hollow conduits, and radial spokes using a low-cost commercial 3D printer with exposure time of 50s. As the photocuring process is influenced by different parameters, herein, the effect of two different ink parameters (dye concentration) and print parameters (UV exposure time) was further described on 3D printing of soft hydrogels materials. The effectiveness of our optimized parameters was confirmed by the successful printing a soft contact lens (exposure time 120s), showing excellent shape fidelity. Overall, these results demonstrate that by tuning the print conditions and ink parameters, soft biomaterials from GelMA ink of better shape fidelity and accuracy can be efficiently printed even on a low-cost 3D printer.

Chapter 4

3D Printed Contact Lenses to Release PVA as a Therapeutic Agent for the Treatment of Dry Eyes

*An article was extracted from this chapter and is published in Special Issue on Pharmaceutical Applications of 3D printing, MDPI's Pharmaceutics (DOI: 10.3390/pharmaceutics17020219)

This chapter has been published as follows:

Garg P, Shokrollahi P, Darge HF, Phan CM, Jones L. 3D-printed contact lenses to release polyvinyl alcohol as a therapeutic agent for the treatment of dry eyes. Pharmaceutics 2025; 17(2): 219.

Author	Concept/Design	Data Acquisition	Analysis	Write Up/ Publication
Piyush Garg	Y	Y	Y	Y
Parvin Shokrollahi	Y	Y	Y	Y
Haile Darge		Y		
Chau-Minh Phan	Y			Y
Lyndon Jones	Y			Y

4.1 Abstract:

Purpose: Dry eye disease is highly prevalent and the most common treatment, lubricating eye drops, only remain effective for a very short period of time. This project aims to 3D print a proof-of-concept, custom-fit, polyvinyl alcohol (PVA)-eluting contact lens (CL) for the treatment of dry eye disease.

Method: In this work, a low cost stereolithography-based 3D printer was retrofitted with a humidity and temperature control kit to 3D print PVA-loaded custom-fit CL. To evaluate the print quality of the 3D printed CL, circularity is used to evaluate the shape fidelity in 3D printing. The PVA release from these lenses was assessed along with its role to act as a viscosity enhancer. The effect of PVA was further analysed by a dry eye disease (desiccation stress) cell model and its role to stabilize the tear film was studied by using the non-invasive keratograph break-up time measurements on a 3D printed eyeball model.

Results: The shape fidelity evaluation of the 3D printed CL displayed excellent circularity. The diameter, sagittal depth, and base curve of the 3D printed lenses were measured to be 14.27±0.06 mm, 3.77±0.16 mm, and 6.4±0.24 mm, respectively. The PVA release curves showed that approximately 1300 µg of PVA was released over the study duration of 24 hrs. The viscosity measurements demonstrate that viscosity is a function of PVA concentration and PVA can protect human corneal epithelial cells (HCEC) against desiccation stress at concentrations above 1.4% (w/v).

Conclusion: PVA is a commonly used viscosity enhancer in eye drops, with the capability of reducing symptoms of dry eye by stabilizing the tear film and reducing tear evaporation. The protective effects of PVA could be attributed to its water retaining ability, which provides moisturization and prevents the loss of water. Overall, this work demonstrates that 3D printing of a PVA-eluting CL is possible by tuning the material properties and 3D printing parameters and can be used as a promising approach for the treatment of dry eye.

Keywords: 3D printed contact lenses, Dry eye disease, Polyvinyl alcohol, Shape fidelity, Desiccation stress, Tear break-up time.

4.2 Introduction

There has been significant interest in using contact lenses (CL) as drug delivery devices due to their hypothesized ability to increase residence time of drugs on the ocular surface. However, CL wearers frequently complain of CL discomfort, often associated with dry eye disease, which sometimes results in discontinuation of lens wear.[1] Placement of a CL onto the ocular surface disrupts the structure and stability of the tear film by dividing it into the pre-lens and post-lens tear film.[2] A strategy to treat dry eyes associated with CL discomfort involves topical delivery of various ocular lubricants such as polyvinylpyrrolidone, hyaluronic acid, hydroxypropyl methylcellulose, and polyvinyl alcohol (PVA) via a CL.[2] However, to-date only one PVA releasing CL material is commercially available, nelfilcon A (Alcon, Ft Worth, TX), which has been shown to stabilize the tear film while improving comfort.[3] Additionally, the blister pack solution of this lens contains other moisturizing agents including hydroxypropyl methylcellulose, polyethylene glycol and PVA, which get released from the lens when in-situ due to the natural blinking action of the eye.[3,4] The concept of releasing lubricating agents onto the ocular surface using a CL offers several advantages, including protecting the surface of the eyes by keeping them moist and enhanced patient compliance compared with frequent instillation of ocular lubricants.

The majority of CLs are fabricated using relatively cost-effective moulding methods, which produce CL on a large scale. However, this makes these methods unsuitable for customization to meet the needs of an individual patient, an approach towards so-called “personalized medicine”. This customization could relate to patient-specific fitting factors (especially related to diameter or base curve radius), as well as factors related to various drug concentrations, depending on the ocular condition being treated for an individual. Another issue is that the storage conditions of drug eluting CL may have an impact on drug stability, and hence the release profiles of drugs and therapeutic molecules from these lenses. This could lead to differences in the amount and rate of drug released, depending on when the drug-eluting CL was manufactured. Therefore, a method to fabricate personalized CL for an individual patient as they are needed (inspired by so-called “just-in-time” concepts) would be helpful. This work explores an on-demand 3D printing or additive manufacturing technique as an alternate method for fabricating custom-fit CL on a small scale.[5] Moreover, 3D printing offers several advantages, such as precise control over object dimensions using computer aided design models, custom-fit, manufacturing of multiple lenses at the same time for an individual patient, and minimal post-processing.[6]

Owing to the precision and high resolution required for the 3D printing of medical devices, stereolithography (SLA)-based techniques may prove to be superior compared to other extrusion-based printing methods, which are limited by low viscosity materials.[7] SLA-based 3D printing makes it possible

to use different photopolymerizable materials loaded with therapeutics of interest to fabricate CL with desired functionalities. Moreover, this technique offers freedom of design fabrication, higher resolution, and improved shape fidelity.[5] The print quality and shape fidelity of these 3D printed CL can be described using circularity. Shape fidelity refers to the accuracy with which the 3D-printed object matches the intended original computer aided design (CAD) or model and circularity refers to the precision of the shape printed.[8] Although, the process of 3D printing can lead to a staircase effect (concentric rings) on the surface, there are techniques available in the literature to improve the surface smoothness to address the staircase effect such as decreasing the layer thickness while 3D printing. An ideal post-processing method should have lower labor and material costs along with higher consistency; however, such methods lead to higher fabrication time and equipment costs. Recently, a post processing method was proposed by Xue *et al.* where the printed structure was soaked in a resin tank after the print was completed, following which the print plate was rotated vertically upwards for the extrusion printing mode and the liquid resin formed on the surface was cured with the help of UV light. These 'additive' methods, where a layer of resin is formed on the surface owing to the surface tension, could be useful to address the issue of the staircase effect on 3D printed GelMA-based soft materials. [26]

In terms of mechanism of action, lubricating agents released from 3D printed custom fit lenses can act as viscosity building macromolecules to form a protective layer over the ocular surface, thereby reducing the desiccation stress experienced by the cornea in a dry eye situation. PVA is a commonly used viscosity enhancer in eye drops,[9] with the capability of reducing symptoms of dry eye by stabilizing the tear film and reducing evaporation. Ocular lubricants to treat moderate dry eye that contain PVA include Blink™ (Johnson & Johnson, Jacksonville, FL, USA), Refresh Classic™ (Allergan, Dublin, Ireland), and Liquifilm™ (Allergan, Dublin Ireland). These lubricating eye drops all contain approximately 1.4% PVA.[10]

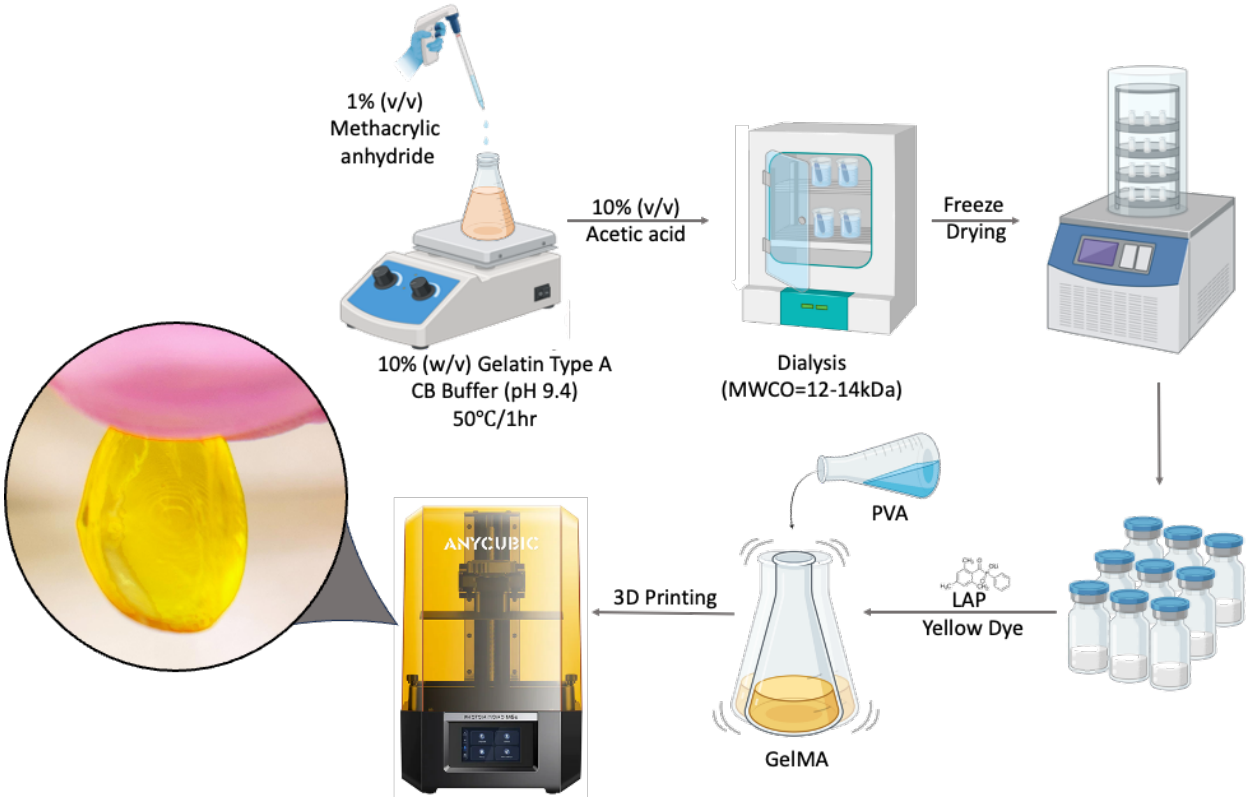
In this work, a stereolithography based technique was used to 3D print a custom-fit CL which can release PVA as a viscosity enhancing agent for potential applications in dry eye. This work shows that the printing parameters can be optimized to achieve successful 3D printing using a low-cost commercially available 3D printer. To evaluate how closely a 3D printed CL resembles the computer-aided design model, circularity was used to evaluate the shape fidelity in 3D printing. Next, the PVA release was studied from these lenses along with its ability to prevent the ocular surface against desiccation stress using a dry eye disease model.

4.3 Materials and Methods

4.3.1 Synthesis of GelMA

GelMA was prepared by the direct reaction of 40 g Type A gelatin with methacrylic anhydride (1% v/v, Sigma, St. Louis, MO, USA) in 400mL carbonate bicarbonate buffer (12.5 mM sodium bicarbonate, 87.5 mM sodium carbonate anhydrous, pH 9.4) buffer at 50°C for 1 hr. The substitution reaction was stopped by adding 6ml of 10% acetic acid and the resulting product was dialyzed in 12-14 kDa dialysis tubes (Sigma, St. Louis, MO, USA) in deionized water for 24 hrs to remove low molecular weight impurities. After dialysis, the GelMA solution was freeze dried and stored at -80°C until further use.

4.3.2 Preparation of GelMA and P-Gel inks



***Scheme* 1.** Scheme of preparation of P-Gel prepolymer solution for 3D printing of CL

To prepare the GelMA prepolymer solution (ink), GelMA (10% w/v) was added to lithium phenyl-2,4,6-trimethylbenzoylphosphinate (0.6% w/v, LAP, Sigma, St. Louis, MO, USA) solution made in phosphate buffered saline (PBS, Fisher Scientific, Waltham, MA, USA). To make PVA/GelMA (P-Gel-3%) ink, GelMA (20% w/v) was added to LAP (1.2% w/v) solution dissolved in PBS. PVA (6% w/v)

solution was made separately in PBS and heated up to 90°C until completely dissolved. The two solutions were added in 1:1 ratio to make the P-Gel-3% ink comprising of GelMA (10% w/v), PVA (3% w/v), and LAP (0.6% w/v). A similar method was used to make P-Gel-1.5% ink. These solutions were incubated at 37 °C for 1 hr before use (Scheme 1).

4.3.3 3D printing of Contact Lenses

Contact lenses of base diameter 14.98 mm and height 3.6 mm were designed using a computer-aided design software (FreeCAD 0.19) and then 3D-printed using a commercial masked-stereolithography (mSLA) 3D printer (AnyCubic Photon Mono M5, Shenzhen, Guangdong, China). The printer was retrofitted with a humidity and temperature control kit to enable printing at ~70% humidity and 37 °C. The GelMA and P-Gel ink solutions were incubated at 37 °C for 1 hr and mixed gently before use. The 3D printing photopolymerization process was carried out using UV light of wavelength 405 nm. The exposure time for the layers was set to 80 s while the first 3 base layers were exposed to 120 s of UV light. The layer thickness while printing was set to 100 µm. These 3D printed lenses were washed with warm PBS to remove any uncured polymer solution and post-cured with UV light (405 nm). Ensuring repeatability of printing parameters—such as temperature, extrusion rate, and print speed—is critical for consistent fabrication of drug-loaded lenses, as even slight variations can affect structural integrity, drug distribution, and overall device performance.

4.3.4 Print Quantification

The 3D printed CLs were imaged using a mobile phone (Galaxy S23, Samsung Electronics, Suwon, South Korea) and were analyzed using Fiji Software (n=3).[11] Using 2D top view, the images were analysed and two key parameters of 3D printing, shape fidelity and circularity, were calculated. The shape fidelity was assessed by determining the ratio between the theoretical area (A_t) vs the actual printed area (A_p) and the theoretical circumference (C_t) vs the actual printed circumference (C_p). For a perfect circle, the shape fidelity scores should be equal to 1. For circular structures, the precision of shape is assessed using a parameter called 'circularity'.[8] The circularity was calculated using the equation described in *Table* 1. For a perfect circle, the circularity value would be 1.

***Table* 1.** *Calculations for Shape Fidelity and Circularity of the 3D printed CL.*

Shape Fidelity		
$Area\ Ratio = \frac{A_p}{A_t}$	$Circumference\ ratio = \frac{C_p}{C_t}$	$Circularity = \frac{4\pi A_p}{(C_p)^2}$

where A_p and C_p are the printed area and circumference of the 3D printed CL, respectively (calculated from the 2D top view)

Lens metrology measurements (total diameter and sagittal depth) were determined using the Chiltern Optimec (Optimec Limited, Malvern, United Kingdom), and the base curve was calculated with the assumption of a spherical lens design. The sagittal height (sag) and diameter (d) measurements were used to calculate the base curve (bc) using the following formula: $bc=[sag^2+(d/2)^2]/(sag\times2)$. Before measurement, the lens chamber was filled with PBS and the lens was placed on the mantle, and the contours of the magnified lens images were sketched. Each lens was measured twice, with the lens rotated approximately 90° on the mantle for the second measurement. The true lens dimensions were calculated under consideration of the magnification factor of the Chiltern (×0.05896), and the average of both measurements was used for analysis.

4.3.5 Light Transmittance

The optical transparency of the samples was determined from their light transmittance (%T) using a UV-Vis spectrometer (SpectraMax M5e, Molecular Devices, San Jose, CA, USA). The hydrogels samples were prepared on a small glass coverslip and placed inside a cuvette with the help of a mold. The absorbance of the samples was measured in the wavelength range of 400-800 nm. For the blank measurement, the absorbance of the glass coverslip was measured from 400-800 nm. The formula $\%T = 100 * 10^{\wedge(-absorbance)}$, derived from the Beer-Lambert Law, was used to calculate the light transmitted. Here, %T represents the percentage of light that passes through the hydrogel sample and reaches the detector on the other side.

4.3.6 PVA release from 3D printed CL

To study the PVA release from these CL, they were incubated in glass vials with gentle agitation with 8 ml PBS at 35 °C. At each indicated time point, 300 µl of the solution was removed for detection of PVA and replaced with fresh PBS. For detection of PVA, a solution of iodine (150 mM potassium iodide, 50 mM diiodine in deionized water, Sigma, St. Louis, MO, USA) and borate (64.7 mM boric acid in deionized water, Sigma, St. Louis, MO, USA) was mixed in a 1:5 ratio of iodine solution:borate solution

to generate the PVA detection solution. The solution was gently inverted 4-6 times in a conical tube to ensure even mixing. To measure PVA in solution, 163.6 ml of PVA detection solution was added to 36.4 ml of samples of interest in a 96-well plate and incubated at room temperature for 20 min with gentle shaking. Absorbances were read at 630 nm using an Imaging Multimode Plate Reader (Cytation 5, Agilent BioTek Instruments, Winooski, VT, USA).[12]

4.3.7 Drug Release Kinetics via Mathematical Modeling

To evaluate release kinetic profiles of the samples over the studied time duration, different mathematical models were studied.[13] These included zero- and first-order release model, Higuchi release model, and Korsmeyer-Peppas model. The graphs were plotted as mentioned in *Table* 2 and the coefficient of determination (R^2) was calculated for each model.[14, 15]

(a) Zero order model: In this model, the drug release is represented by:

$C_t = C_o + K_o t$

where C_t is the amount of drug released at time t, C_o is the initial concentration of drug in solution (at t=0), and K_o is the zero-order rate constant. The graph is plotted between cumulative drug release *vs.* time and the coefficient of determination (R^2) was calculated.

(b) First order model: In this model, the drug release is represented by:

$dC/dt = -K_1 C$

where K_1 is the first order rate constant

After rearranging and taking integral,

$\log C_t = \log C_o - (K_1/2.303)t$

where C_t is the amount of drug remaining at time t and C_o is the initial concentration of the drug. The graph is plotted between log cumulative % drug remaining *vs.* time and the coefficient of determination (R^2) was calculated.

(c) Higuchi model: In this model, the drug release is represented by:

$M_t/M_\infty = K_h t^{1/2}$

where M_t/M_∞ is the fraction of drug released at each time point, M_t is the amount of drug released in time t, M_∞ is the amount of drug released after infinite time, and K_h represents the Higuchi release kinetic constant. The graph is plotted between cumulative % drug release *vs.* square root of time and the coefficient of determination (R^2) was calculated.

(d) Korsmeyer-Peppas model: In this model, the drug release is represented by:

$M_t/ M_\infty = K_{kp} t^n$

$\log (M_t/M_\infty) = \log K_{kp} + n \log t$

where M_t/M_∞ is the fraction of drug released at time t, M_t is the amount of drug released in time t, M_∞ is the amount of drug released after infinite time. n is the diffusional exponent or drug release exponent and K_{kp} is the Korsmeyer-Peppas release rate constant. The graph is plotted between log cumulative % drug release vs. log t and the coefficient of determination (R^2) was calculated.

The graphs were plotted as mentioned in *Table* 1 and the coefficient of determination (R^2) was calculated for each model.[47, 48]

***Table* 2.** Curve fitting of various models for drug release kinetics

	Zero Order	**First Order**	**Higuchi model**	**Korsmeyer-Peppas model**
Equation	$C_t = C_o + K_o t$	$\log C_t = \log C_o - (K_1/2.303)t$	$M_t/M_\infty = K_h t^{1/2}$	$\log (M_t/M_\infty) = \log K_{kp} + n \log t$
Graph	cumulative drug release vs. time	log cumulative % drug remaining vs. time	cumulative % drug release vs. $\sqrt{t}$	log (cumulative % drug release) vs. log t

4.3.8 Viscosity Measurements

The viscosity measurements for different concentrations of PVA solutions (ranging from 0.5%, 0.7%, 1.0%, 1.4%, and 2% w/v) were carried out on a Viscometer L2.16 (Cambridge Applied System, Boston, MA, USA) which uses the concept of the variation on the falling-body. In brief, a piston (0.25-5 cP) was suspended in an elongated cavity. The electromagnets in the wall force the piston to move in a reciprocating up and down motion. The movement of the piston is inversely related with the viscosity of the fluid. The instrument calculates the viscosity of the sample by measuring the speed at which the piston moves.[16]

4.3.9 *Non-Invasive Keratograph Break-up Time (NIKBUT)*

The NIKBUT measurements[17,18] were conducted using PBS to avoid the variabilities that may be caused by interactions of PVA with artificial tear solution components. A CL (Biotrue, Bausch & Lomb, Vaughan, ON, Canada) was removed from the blister pack, rinsed with the three respective formulations (a PBS control, 1.4% PVA or Refresh eye drop), and placed on a 3D printed eye model (Ocublink, Waterloo, ON, Canada). A 10 µl of sample volume was pipetted on the lens and the drop was spread on the lens surface after two to three blinks. NIKBUT analysis was performed (n=5) using a Keratograph 5M (Oculus Optikgeräte GmbH, Wetzlar, Germany). The rings from the keratograph were projected onto the lens surface and the images of the reflected rings were captured for 25 s. The NIKBUT was measured as the time from the last complete blink to the first appearance of a distortion of the lines.

4.3.10 Simulating Dry Eye Conditions via Desiccation Stress on Human Corneal Epithelial Cells

HPV-immortalized HCEC were maintained between passages 3-15 and cultured in DMEM/F12 medium (Sigma, St. Louis, MO, USA) containing 1% FBS and 1% penicillin/streptomycin (pen/strep) at 37°C, 5% CO_2, and high humidity (> 95%). Media was replaced every 2-3 days until confluency. HCEC were maintained as described above, and $15x10^4$ cells were seeded into 96-well plates (ThermoFisher, Waltham, MA, USA), then incubated overnight at 37 °C with high humidity and 5% CO_2. After 24 hrs of incubation, the culture media was removed from the plate. The cells were immediately treated with 150 µL of the test formulations and the culture medium control solution. The cells were incubated at 37 °C and 5% CO_2 for 30 min. The test solutions from the cells were removed and the cells placed in the chamber at 37 °C and 45% RH for 2 min to desiccate the cells. The cell viability was assessed using the MTT assay and the absorbance values were measured at 570 nm using a multimode plate reader (Cytation 5, Agilent BioTek Instruments, Winooski, VT, USA).[19]

4.3.11 Statistical Analysis

Statistical analysis was performed using GraphPad Prism Version 10.0 (GraphPad Software, La Jolla, CA, USA). All data are reported as mean and standard deviation, unless otherwise stated. Two-way ANOVA was performed to determine differences across testing groups wherever applicable. Tukey's multiple comparison tests were used when necessary. In all cases, statistical significance was considered significant for a p-value of <0.05, unless otherwise stated.

4.4 Results and Discussion

4.4.1 3D printing of Contact Lenses

Figure 1 shows the 3D printed CLs with P-Gel-1.5% and P-Gel-3% inks compared to a commercially available CL (Dailies Aqua Comfort Plus™; Alcon, Ft Worth, TX, USA). The CL were printed in about an hour and the minimum thickness for the lenses that was reliably printed each time using the current 3D printing setup was 400 µm. It should be noted that despite the high water contect in these lenses, the contact lenses were successfully 3D printed with high shape fidelity. These lenses demonstrated clean and sharp edges and could be printed without any support structures. Reports indicate that an effective photocurable biomaterial ink suitable for projection-based printing methods, such as SLA LCD printing, should possess three key characteristics: a fast photo-crosslinking rate, a tightly crosslinked structure, and exceptional fluidity to ensure swift filling of gaps and spaces.[20] In this work, GelMA was used as a base material owing to its biocompatibility and demonstrated high levels of controllability.[21, 22]

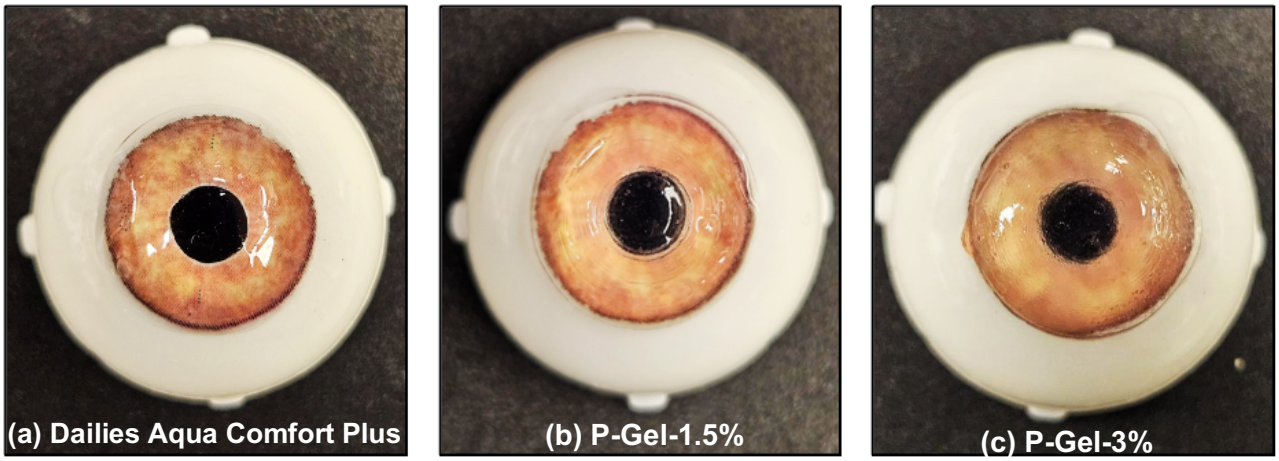


***Figure* 1.** Comparative optical clarity of (a) commercially available Dailies Aqua Comfort Plus™ CL and (b,c) 3D printed PVA-loaded CL (P-Gel-1.5% and P-Gel-3%). The images were taken on a 3D printed eye model mimicking the human eye to show the fitting of these lenses and their optical clarity.

Another crucial aspect in vat-polymerization is to avoid the evaporation of water during the exothermic polymerization reaction. Consequently, this could lead to the increased viscosity of the printable ink related to the gradual increase of the polymer concentration at the interface and interferes with the layer separation/approach step.[23] To overcome these challenges, the 3D printing conditions such as the dye concentration and UV exposure time were selected along with proper environment conditions including temperature (~ 37 °C) and humidity (~70% RH). The results showed that it is possible to 3D print a structure as delicate as a CL with remarkable shape fidelity and accuracy on a low-cost commercial printer.

Based on a series of preliminary experiments, the printing window for GelMA concentration (10%), exposure time (80s), dye concentration (3%), and LAP concentration (0.6%) were optimized and used. The printing window parameters were selected regarding previous reports confirming that an increase of initiator concentration and light intensity can overcome the oxygen inhibition of photo-polymerisation reactions.[24] The 3D printed lenses were carefully removed from the print plate and washed in warm PBS to remove any uncured polymer on the surface. Reports suggest that mechanical characteristics such as elasticity, hardness, and compressibility of GelMA are governed by the kinetics of cross-linking during the photocross-linking process.[22] Therefore, to improve the base mechanical strength of GelMA, several methods are used, such as increasing the prepolymer concentration, higher degree of substitution, and functionalization, or higher UV exposure time.[25] Besides increasing the mechanical strength, the post curing also ensures consistency in the final print. Therefore, once the CL were washed, they were post cured using a 405 nm UV light. This post curing step is important to improve the mechanical strength of 3D printed lenses. Without proper post-curing, the 3D printed object will be weaker in certain areas, compromising its long-term structural stability. The post curing step, also helps to photobleach the excess yellow dye in these lenses, as shown in *Figure* 2.

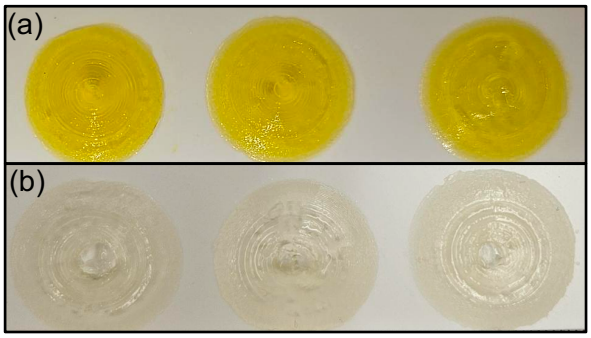


***Figure* 2.** 3D printed contact lenses (a) before and (b) after washing and post curing

4.4.2 Print Quantification Analysis

The 3D printed lenses were analyzed for their shape fidelity (area ratio, circumference ratio, and circularity) where the ideal scores would be equal to 1. The area ratio, circumference ratio, and circularity was calculated based on the formulas described in *Table* 1.

The area ratios of GelMA, P-Gel-1.5% and P-Gel-3% were 0.8180, 0.8893, and 0.8585 respectively. The ideal value for area ratio would be equal to 1 and a value of <1 denotes that the printed CL is smaller than the theoretical area and vice versa. Compared to GelMA, the higher area ratios in case of P-Gels could be attributed to the presence of PVA, which makes the structure more robust and mechanically stronger.[27-30] The circumference ratios of GelMA, P-Gel-1.5% and P-Gel-3% were 1.1446, 1.0564, and 0.9921 respectively. The ideal value for circumference ratio would also be equal to 1 and value of >1 or <1 denotes that the printed CL has an irregular boundary. The printed circumference (C_p) calculated from this method was highly variable because even slight irregularities in the periphery of the lenses would contribute largely

to the circumference ratio. Hence, an irregularity in the boundary could give a higher false value of printed circumference, even if the print is smaller in area.

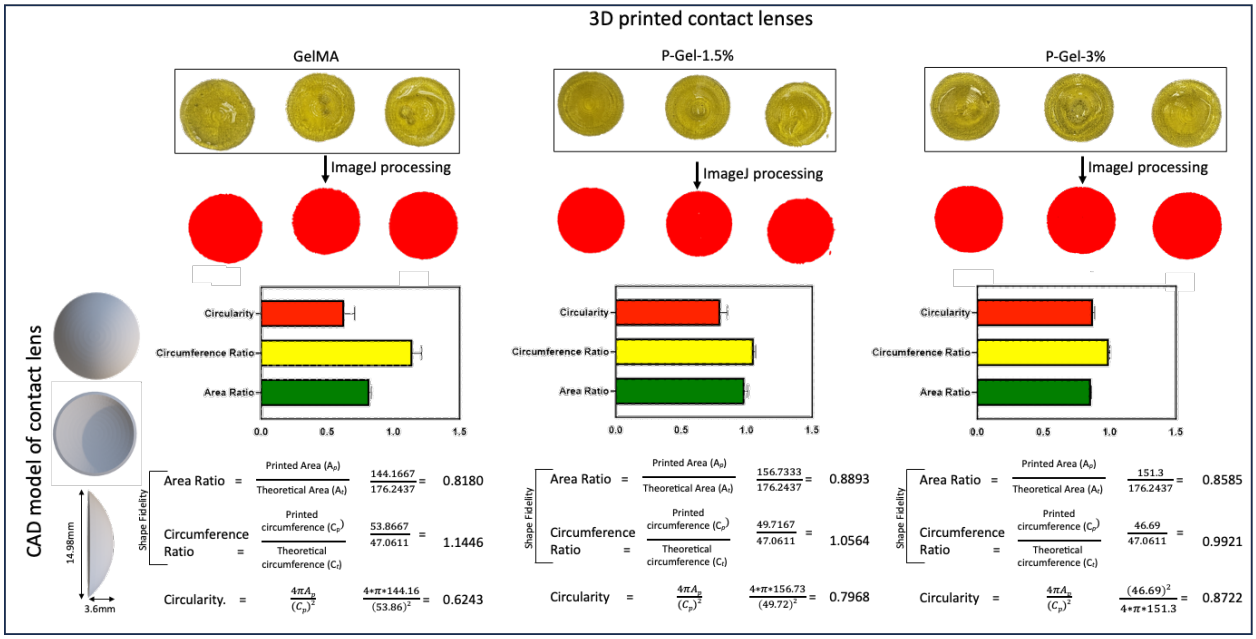


***Figure* 3.** Analysis of Shape Fidelity and Circularity of the 3D printed contact lenses (calculations based on 2D top view).

The diameter and sagittal depth of the 3D printed contact lenses were measured to be 14.27±0.06 mm and 3.77±0.16 mm. The base curve was calculated with the assumption of a spherical lens design. The sagittal depth (sag) and diameter (d) measurements were used to calculate the base curve (bc) using the following formula: $bc=[sag^2+(d/2)^2]/(sag\times2)$ and calculated to be 6.4±0.24 mm. For circular structures, the precision of the shape is assessed using a parameter called 'circularity'. The circularity of GelMA, P-Gel-1.5% and P-Gel-3% lenses were 1.6016, 1.2549, and 1.1465 respectively. The ideal values for circularity should be equal to 1. Two lenses based on GelMA or P-Gel inks with the similar perimeter can have different areas if one or both have irregular boundaries, resulting in differing areas. Variations in printing conditions (temperature and humidity), water content, and handling could lead to such changes and therefore, deviation in circularity values. Interestingly, a higher variability (standard deviation) in the circularity was observed with the lenses printed with GelMA, which could be attributed to the relatively weaker mechanical properties of GelMA compared to P-Gel. A reduction in variability was observed with the P-Gel contact lenses owing to their robust and mechanically stronger structures.[31, 32]

4.4.3 Light Transmittance and Optical Transparency

Figure 4a shows the optical clarity of a CL 3D printed from GelMA and P-Gels containing 1.5% and 3% PVA on a colored background (Figure 4a). Next, the transmittance curves for GelMA and P-Gel hydrogels were plotted in the visible range of light (400-800 nm). At 450 nm, GelMA gels exhibited about 89.2% transmittance while P-Gel-1.5% and P-Gel-3% displayed around 89.5% and 80.9% transmittance. At 630 nm, the transmittance of GelMA was 92.2% and for P-Gels, it was around 91.5% (P-Gel-1.5%) and 89.0% (P-Gel-3%). The mean light transmittance of GelMA, P-Gel-1.5% and P-Gel-3% was about 91.4%, 90.9%, and 87.2% respectively at 400-800nm, respectively (Figure 4b). The results showed that the transparency decreased with an increase in PVA concentration from 1.5% to 3%, which is likely due to the presence of high polymeric phase compared to GelMA hydrogels. Among the three groups, P-Gel 3% showed the transmittance values under the threshold percentage (~85%) to be defined as a transparent substance along all the visible spectrum.[9]

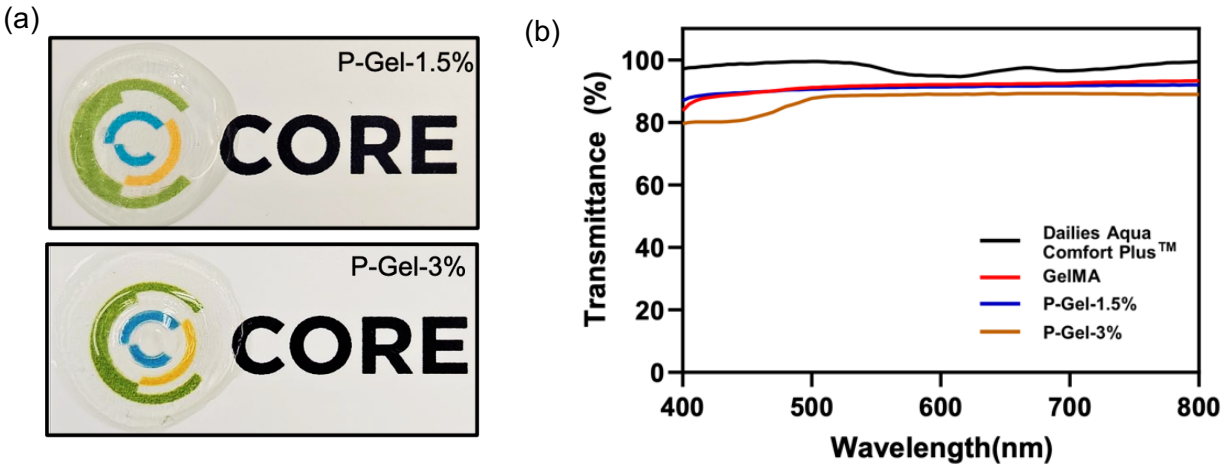


***Figure* 4.** (a) Optical transparency of 3D printed CLs on a colored background (b) Optical transmittance curves of Dailies Aqua Comfort Plus™ (Nelfilcon A), GelMA, P-Gel-1.5% and P-Gel-3%.

4.4.4 PVA release

The PVA release curves depict the PVA released from 3D printed CL with different PVA concentrations (*Figure* 5a). About 1300 µg and 2900 µg of PVA was released from P-Gel-1.5% and P-Gel-3% CL at the end of 24 hrs. The instantaneous release amounts of PVA were calculated (in µg/ml) and plotted as 3D bars with the help of OriginPro 2024 software (*Figure* 5b). The graph shows that about 40-80 µg PVA was released at every successive time points with P-Gel-1.5%, while for the lenses containing 3% PVA, the release was in the range of 140-180 µg.

To study the drug release kinetics and how different factors affect the dissolution rate and behaviors, various mathematical equations describing the release dependence on time were used. The drug release was evaluated though four main release kinetic models: zero-order, first-order, the Higuchi model, and the Korsmeyer-Peppas model. To evaluate the best fit model for the release profiles in our study, the goodness of fit for each model or the coefficient of determination (R^2) was calculated using GraphPad Prism (*Table* 2 and 3). The release profiles of the PVA containing hydrogels showed highest linearity (*Figure* 5c) with the Korsmeyer-Peppas model (R^2=0.9806 and R^2=0.9864 for P-Gel-1.5% and P-Gel-3% respectively). The release exponent (n) for P-Gel-1.5% and P-Gel-3% samples were 0.3464 and 0.3476, indicating that these systems follow Fickian diffusion (*Table* 3). In the Fickian

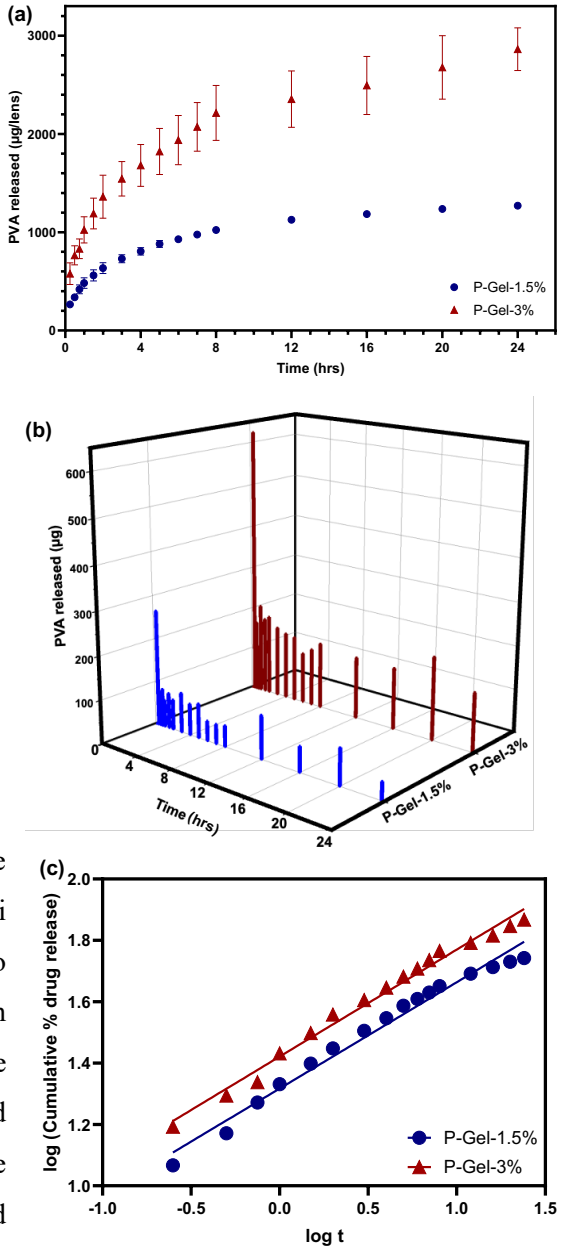


***Figure* 5.** (a) Cumulative PVA release curves of P-Gel-1.5% and P-Gel-3% (b) Instantaneous release of PVA (µg/ml) from P-Gel-1.5% and P-Gel-3% (c) Modelling of the PVA release data using the Korsmeyer-Peppas model (R^2=0.9806 and R^2=0.9864 for P-Gel-1.5% and P-Gel-3% respectively)

model (Case I), the drug release is governed by diffusion. The release exponent (n) values below 0.5 confirm the diffusion-controlled behavior rather than swelling or erosion-driven release. This finding has important practical implications: it suggests that the rate and duration of drug release can be effectively tuned by modifying polymer composition, crosslink density, or device geometry, without the need for complex reservoir systems. Moreover, understanding that diffusion is the dominant mechanism enables predictive modeling of release kinetics for different drug, providing a robust framework for rational design of next-generation inserts with controlled and sustained drug delivery profiles.[33]

***Table* 3.** The coefficient of determination (R^2) values of P-Gel-1.5% and P-Gel-3% calculated using different kinetic models.

Kinetic Model	P-Gel-1.5%	P-Gel-3%
Zero-order	0.7824	0.8131
First order	0.8487	0.9181
Higuchi	0.9364	0.9532
Korsmeyer-Peppas	0.9806	0.9864
Diffusion exponent (n-value)*	0.3464	0.3476

*Calculated by the linear regression of the Korsmeyer-Peppas equation of $\log(M_t/M_\infty)$ versus $\log t$

4.4.5 NIKBUT measurements

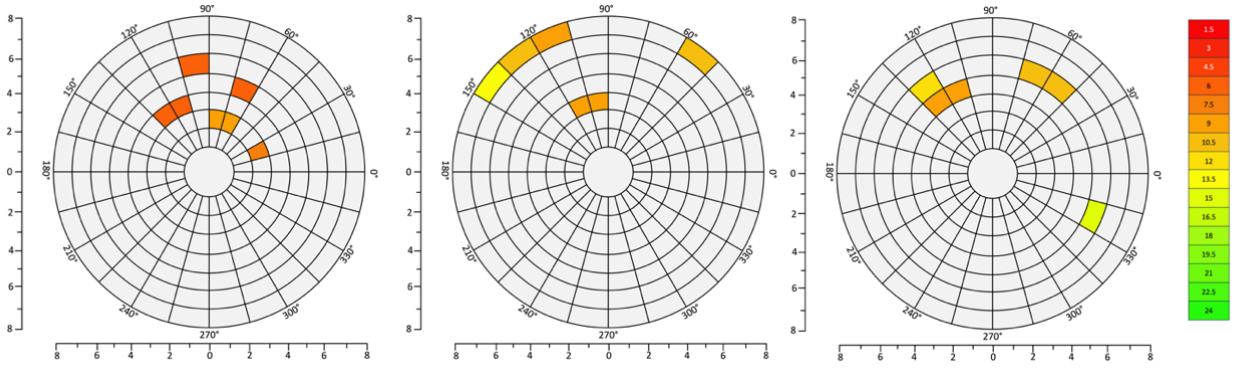


***Figure* 6.** Assessments of non-invasive keratograph break-up time (NIKBUT) of PBS, 1.4% (w/v) PVA and Refresh Classic eye drops on a 3D printed eye model (n=5).

The results from the NIKBUT analysis for the CL containing 1.4% (w/v) PVA were similar to a commercially available Refresh Classic eye drop. These results were plotted manually on a modified version of the Oculus grid after subjective review of the true tear break-ups. The first breakups for PBS solution were around 6.6±1.2s. However, for the 1.4% PVA solution and Refresh solution, the first tear break up times were 10.3±1.7s and 11±2.2s (*Table* 4). These significantly higher NIKBUT values ($p<0.05$) for 1.4% PVA solution and Refresh Classic eye drop supports the concept of 3D printed custom-fit PVA-eluting CL being potentially useful to treat dry eyes (*Figure* 7). This PVA solution used was made separately in PBS to assess the effect of PVA on tear-breakup times and avoid interactions from GelMA components at this stage.

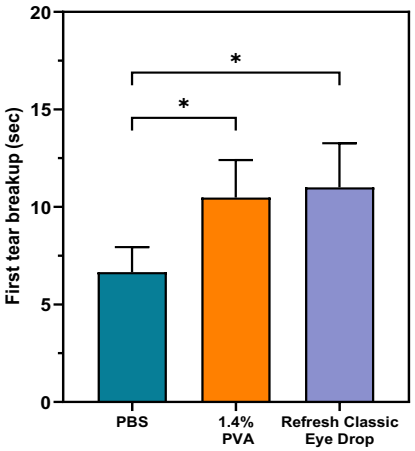


***Figure* 7**. Statistical analysis for the tear break up times.

***Table* 4.** First tear break up time (in seconds)

PBS	1.4% (w/v) PVA	Refresh Classic
6.6±1.2s	10.3±1.7s	11 ±2.2s

4.4.6 Viscosity Measurements

The viscosities of different concentrations of PVA solutions were calculated using a Viscometer and the graph between viscosity and concentration was plotted (*Figure* 8). The results demonstrate that viscosity increases with an increase in the amount of PVA and is a function of polymer concentration.[34] The viscosity of 1.4% PVA solution was about 1.72 cP, whereas the Refresh Classic eye drop was around 3.65 cP. The active ingredients in Refresh Classic eye drops are 1.4% PVA and 0.6% povidone. Therefore, the higher viscosity of Refresh Classic eye drops at a similar PVA concentration could be due the different composition of PVA in terms of molecular weight (chain number and chain length)[9] and presence of other agents such as povidone in Refresh Classic eye drops. Viscosity enhancing agents such as PVA comprise the bulk of artificial tears and have been used in patients with dry eye disease.[35] An ideal viscosity enhancer should possess sufficient viscosity and adequate rheological behavior to lubricate the ocular surface and have sufficient ocular surface residence time. Also referred to as

demulcents or lubricants, the US FDA recognizes six categories of these agents that can be used in over-the-counter formulations, which include cellulose derivatives, dextran, gelatin, liquid polyols, polyvinyl alcohol and povidone.[36] These viscosity enhancing compounds have hygroscopic properties (water retaining ability on the ocular surface), allowing them to prevent the loss of water and moisturize the ocular surface.[37] This is supported by the NIKBUT analysis results (*Table* 4), where the 1.4% PVA solution demonstrates higher break up time compared to PBS alone. Of note, the compatibility of PVA with the eye compartment is widely known[38] and is a commonly used viscosity enhancer in eye drops.[9] Therefore, 3D printed custom-fit PVA-eluting CL could be used as a potential strategy to treat dry eyes.

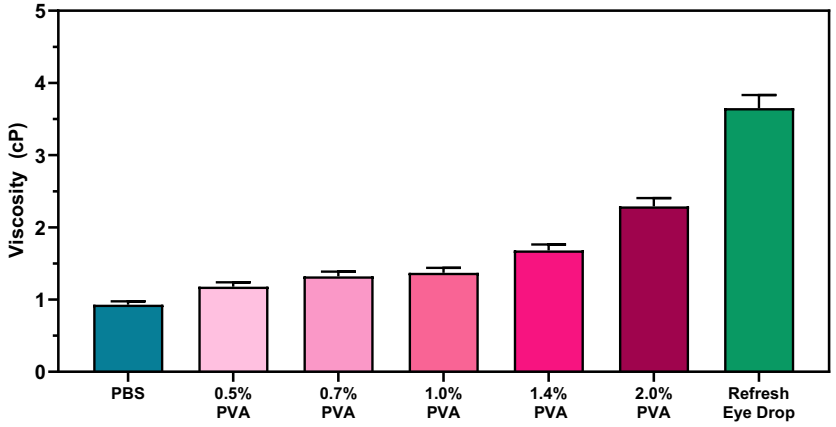


***Figure* 8.** Graph representing viscosity as a function of PVA concentration.

4.4.7 Ability of PVA to protect HCEC against desiccation stress

Dry eye disease (DED) is a multifactorial disease with numerous patient symptoms that ultimately lead to discomfort and potential damage to the eye.[1] Although there are several methods to address the various pathophysiological mechanisms behind DED (ranging from stabilizing the tear film to reducing pro-inflammatory responses on the ocular surface),[1] PVA releasing contact lenses could be attractive method. To study the ability of PVA to protect corneal cells against desiccation stress, a previously established protocol was followed.[19] This protocol helps to assess the overall impact of the dry eye formulation on the viability of corneal epithelial cells.

Figure 9 demonstrates that PVA at concentrations around 2%, showed significantly higher cell viability ($p<0.05$) compared to the control. Similar results were observed with the Refresh Classic eye drops ($p<0.05$). Importantly, after the formulation was removed from the culture wells, the chemical interaction between the remaining molecules in contact with the cells impacted the desiccation and provided protection. These results confirm the feasibility of PVA to be loaded in the 3D printed CL and protect the HCEC against desiccation stress. As indicated from the package contents, Refresh Classic eye drops contain two active ingredients, 1.4% PVA and 0.6% povidone. As previously indicated, the presence of two different active ingredients as well as different composition of PVA in terms of molecular weight (chain number and chain length)[9] in Refresh Classic eye drops could be the reason for their higher protection.

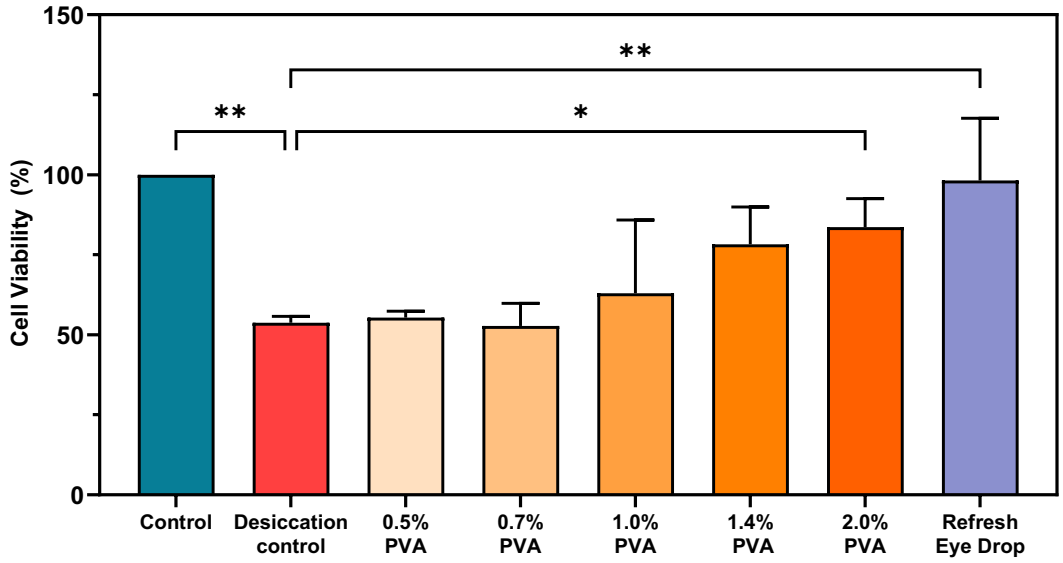


***Figure* 9.** Effect of PVA and Refresh Classic eye drops on HCEC and resistance against desiccation stress.

4.5 Conclusion

In summary, this work attempts to 3D print a proof-of-concept PVA-eluting contact lens based on GelMA for potential application in dry eye disease. The PVA-eluting 3D printed lenses displayed better shape fidelity than GelMA as indicated by the circularity scores of 0.6243, 0.7968, and 0.8722 for GelMA, P-Gel, 1.5%, and P-Gel-3% respectively. Measurements of the P-Gel-1.5% lenses indicated a diameter of 14.27±0.06 mm, a sagittal depth of 3.77±0.16 mm, and a base curve of 6.4±0.24 mm which is similar to commercially available contact lenses. Interestingly, stereolithography-based 3D printing makes it possible to use different photopolymerizable materials loaded with therapeutics of interest, such as PVA, and to fabricate CL with desired functionalities. PVA release profiles suggest that approximately 1300 μg of PVA was released over 24 hours. PVA is a commonly used viscosity enhancer in eye drops, with the capability of reducing symptoms of dry eye by stabilizing the tear film and reducing evaporation. This was further validated by its ability to protect HCEC against desiccation stress. The mean light transmittance of GelMA, P-Gel-1.5% and P-Gel-3% was about 91.4%, 90.9%, and 87.2% respectively at 400-800nm, respectively, which is close to a commercially available PVA-containing contact lens (97.5%). The results from this study suggest that 3D printing of a delicate structure such as a contact lens is possible by tuning the material properties and 3D printing parameters. Looking forward, we will focus on optimizing the release kinetics and taking control over the release of PVA from gelatin methacrylate-based biomaterials.

Chapter 5

Controlled PVA Release from Chemical-Physical Interpenetrating Networks to Treat Dry Eyes

*An article was extracted from this chapter and is published in American Chemical Society's Omega Journal (DOI: 10.1021/acsomega.4c08667)

This chapter has been published as follows:

Garg P, Shokrollahi P, Darge HF, Phan CM, Jones L. Controlled PVA release from chemical–physical interpenetrating networks to treat dry eyes. ACS Omega 2024; 10(1): 1249–1260.

Author	Concept/Design	Data Acquisition	Analysis	Write Up/ Publication
Piyush Garg	Y	Y	Y	Y
Parvin Shokrollahi	Y	Y	Y	Y
Haile Darge		Y		
Chau-Minh Phan	Y			Y
Lyndon Jones	Y			Y

5.1 Abstract

Purpose: To fabricate a chemical-physical double interpenetrating network to take control over the release of polyvinyl alcohol (PVA), a well-known therapeutic agent used to stabilize tear film, from gelatin methacrylate (GelMA) hydrogels.

Method: In this chapter, PVA was specifically used as part of a GelMA-based polymeric hydrogel owing to its physical crosslinking ability via a simple freeze thaw method. The interpenetrating polymer network was fabricated in a sequential manner where GelMA was chemically crosslinked by photocrosslinking, followed by physical crosslinking of PVA using a relatively short freeze thaw cycle. With the help of a suite of characterizations, we further delineate the mechanism behind formation of these freeze thaw induced crystalline domains and their role in taking control over the release of PVA.

Results: The appearance of endothermic peaks at 48 ℃ and 60 ℃ in differential scanning calorimetry (DSC) thermograms and 20°-2θ peaks in X-ray diffraction (XRD) patterns suggest the presence of these crystalline domains. The release profiles of the PVA containing hydrogels showed highest linearity with the Korsmeyer-Peppas model ($0.9944<R^2<0.9952$), indicating that these systems follow non-Fickian or anomalous transport.

Conclusion: The results from this study highlight that upon applying only one short freeze thaw cycle (of 1 or 2 hr), a crystalline domain formation of PVA was induced in the interpenetrating network.

Keywords: Dye eye disease, polyvinyl alcohol, hydrogels, interpenetrating network, controlled release

5.2 Introduction

The human eye is one of the most complex organs in the human body and can be divided into anterior (consisting of cornea, conjunctiva, aqueous humor, iris ciliary body and crystalline lens) and posterior (consisting of sclera, choroid and retinal pigment epithelium) segments.[1] Globally, a number of individuals are impacted by different ocular conditions which directly compromise their vision and overall quality of life. Although eye drops have been used to administer about 90% of medications to the eye,[2] they have a low bioavailability due to dilution by the tears and rapid drainage from the ocular surface.[3] As a result, development of long-lasting ophthalmic formulations for a wide variety of eye diseases is of great interest to both researchers and eyecare practitioners. Soft, hydrophilic contact lenses have often been discussed as a potential option to deliver drugs to the ocular surface.[4, 5] One potential application of soft hydrogels is in the treatment of dry eye[6], a common ocular surface disorder that affects a substantial segment of the population.[7, 8]

Hydrogels are three dimensional, highly hydrophilic, soft polymeric materials that are used in a broad range of biomedical applications, including contact lenses[9] and *in vitro* and *in vivo* as drug delivery platforms.[10, 11] Hydrogels are of great interest for ocular drug delivery as they can increase the therapeutic efficacy of ophthalmic drugs by increasing the drug residence time at the site of administration, and can facilitate co-delivery of multiple drugs.[12-14] Gelatin derivatives, in particular, gelatin methacrylate (GelMA) hydrogels, are attractive candidates for biomedical use due to their outstanding biocompatibility[15] and can easily form a 3D network via physical or chemical crosslinking.[16] The photo crosslinking method used to crosslink GelMA can be performed in mild crosslinking conditions (room temperature, neutral pH, in aqueous environments, etc.), with a short reaction time and low cytotoxicity.[15, 17] Gelatin methacrylate materials are highly biocompatible, versatile and can be used for a variety of ocular applications such as their use as bioinks for fabricating biodegradable drug delivery systems,[18] sustained drug release systems to be potentially used as ocular inserts,[19] injectable hydrogels for delivery of ocular drugs,[20] MMP-triggered controlled release vehicle for hyaluronic acid and model drugs for the potential treatment of corneal epithelial wound healing,[21] cell loaded interpenetrating hydrogel networks as corneal stroma substitutes,[22] controlled release of vitamins for the treatment of the ocular surface, corneal healing, and acceleration of epithelial growth, while concurrently preventing potential inflammation.[23] Gelatin backbone could also be grafted with simple chemical modifications with glycidyl methacrylate to obtain an elastic protein-based hydrogel

with biomimetic properties. Such properties allow to tune their viscoelastic and mechanical properties to facilitate their ocular applications.[24] Moreover, to understand the process of mass transport of a therapeutic agent through a hydrogel, it is important to gain insights into its macroscopic properties, such as porosity and crosslink density. Increasing the composition of the polymer phase in a hydrogel network and therefore the crosslink density is one strategy to modulate the drug release from GelMA hydrogels.[25] One method to potentially increase the crosslink density of GelMA could be obtained by forming GelMA-based interpenetrating networks.

Interpenetrating polymer networks are made up of two or more distinct polymer networks where the macromolecular chains of each network permeate through one another without being covalently bound to each other. Compared to hydrogels with a single network, interpenetrating networks have a partial interlacing on the molecular scale and are reported to provide improved mechanical and dynamic properties.[26-28] Polyvinyl alcohol (PVA) is a commonly used viscosity enhancer in eye drops[29] with the capability of reducing symptoms of dry eye by stabilizing the tear film and reducing evaporation.[30] It can be crosslinked using physical methods such as freeze thaw cycles without the addition of reactive chemicals, which is inherently more biocompatible.[31]

PVA hydrogels have been used for fabricating drug delivery systems for wound healing,[32] as antibacterial agents,[33, 34] anti-inflammatory agents,[35] anticancer agents,[36] and for targeted release.[37] It is anticipated that a GelMA-PVA interpenetrating network would display properties of both polymers and demonstrate enhanced biocompatibility and mechanical properties.[38] Upon freeze thawing of PVA, the crystalline domain formation is increased and this concept could potentially be used as a strategy to modify the release rate of therapeutic molecules from drug delivery platforms.[39, 40]

The release profiles of PVA from commercially available hydrogel contact lens materials exhibits rapid initial release.[41, 42] To overcome this limitation, we report a PVA-releasing interpenetrating network of GelMA and PVA fabricated in a sequential manner (chemical-physical double network) for therapeutically promising outcomes. In the first step, ice crystal formation occurs during the freezing cycle. The subsequent thawing leads to the formation of hydrogen bonds between the PVA chains, creating ‘physical crosslinks’ without the need for any additional chemical crosslinkers. In this study, relatively short freeze thaw (FT) cycles were applied to physically crosslink PVA and precisely tune crystallization, hydrogen bonding and final network properties to take control over the rate of PVA release by leveraging its physical crosslinking abilities.

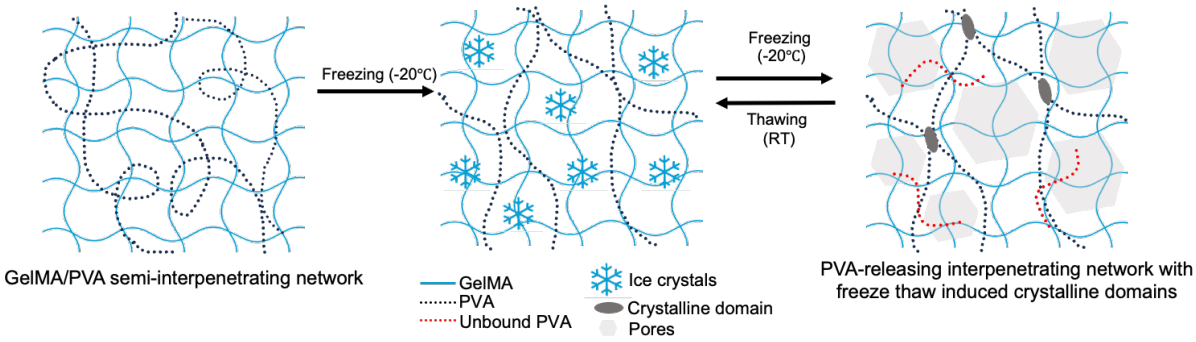
5.3 Materials and methods

5.3.1 Synthesis of GelMA

GelMA was prepared by direct reaction of Type A gelatin (40 g, 300 Bloom, Sigma, St. Louis, MO, USA) with methacrylic anhydride (1% v/v, Sigma, St. Louis, MO, USA) in carbonate bicarbonate buffer (12.5 mM sodium bicarbonate, 87.5 mM sodium carbonate anhydrous, pH 9.4, 400mL) buffer at 50°C for 1 hr. The substitution reaction was stopped by adding acetic acid (6mL, 10%) and the resulting product was dialyzed in 12-14 kDa dialysis tubes (Sigma, St. Louis, MO, USA) in deionized water for 24 hr to remove low molecular weight impurities. After dialysis, the GelMA solution was freeze dried and stored at -80°C until further use.[43]

5.3.2 Preparation of GelMA and GelMA/PVA Hydrogel Discs

To prepare the GelMA prepolymer solution, GelMA (10% w/v) was added to lithium phenyl-2,4,6-trimethylbenzoylphosphinate (0.6% w/v, LAP, Sigma, St. Louis, MO, USA) solution made in phosphate buffered saline (PBS, Fisher Scientific, Waltham, MA, USA). To make PVA/GelMA (P-Gel) prepolymer solution, GelMA (20% w/v) was added to LAP solution dissolved in PBS (1.2% w/v). PVA (10% w/v, molecular weight 89-98 kDa, 99+% hydrolyzed, Sigma, St. Louis, MO, USA) solution was made separately in PBS and heated up to 90°C until completely dissolved. The two solutions were added in 1:1 ratio to make the P-Gel prepolymer solution comprising of GelMA (10%), PVA (5%), and LAP (0.6%). These solutions were incubated at 37 °C for 1 hr before use. The GelMA and P-Gel prepolymer solutions were photopolymerized using a UV lamp fitted into a custom-made box (wavelength 405 nm, 60 W output, and 10 cm distance from the light source) to fabricate discs of 10 mm in diameter and 4 mm in thickness. The discs were crosslinked for 2 min on both sides to ensure complete crosslinking. The P-Gel hydrogel discs then underwent a single freeze thaw cycle at -20 °C for 1 hr (P-Gel-1FT), and 2 hr (P-Gel-2FT).[44]



Scheme 1. Schematic illustration for the formation of PVA/GelMA hydrogel networks.

5.3.3 Morphological Characterization

To gain insights into the hydrogels, the samples were first swollen in PBS (pH 7.4), followed by freezing at -80 °C overnight and then freeze dried (Labconco Freeze Dry System Freezone 2.5 Liter, 7670000, Kansas City, MO, USA) for 24 h. The freeze-dried samples were fixed on an aluminium stub by using double-sided adhesive conducting carbon tape and then imaged using environmental scanning electron microscopy (ESEM, Quanta FEG 250, FEI Company, Hillsboro, OR, USA). The SEM images were used to calculate the pore sizes using ImageJ software and the pore size distributions were plotted in OriginPro 2024 software.

5.3.4 Chemical Characterization

Fourier Transform Infrared (FTIR) measurements were made with Bruker Tensor 27 (Karlsruhe, Germany) in attenuated reflectance mode (ATR, PIKE Technologies, Fitchburg, WI, USA) between 600 to 4000 cm^{-1} at a fixed resolution of 4 cm^{-1}. Nuclear Magnetic Resonance (NMR) spectra were obtained using the Bruker Ascend 300 MHz spectrometer using D_2O as solvent at 14 mg/ml at room temperature. Powder X-Ray Diffraction (XRD) patterns for the samples were recorded in the 2θ range 10–50° using a Cu Kα radiation Bruker D8 (Karlsruhe, Germany).

5.3.5 Thermal Analysis

Differential scanning calorimetry (DSC) analysis was carried out using Q-2000 (TA instruments, New Castle, DE, USA). The sample (8 to 12 mg) was taken and weighed in an Aluminium pan with a lid and underwent cyclic DSC of heating cycles of 10 °C/min up to 200 °C in the first cycle and a cooling cycle of 10 °C/min under nitrogen purge (50 ml/min). In the second heating cycle, the sample was heated from 25 to 250 °C. The data from the two heating cycles were recorded for analysis.

5.3.6 Swelling Behaviour

Swelling ratios of the hydrogels were measured using a gravimetric method. The hydrogel discs were freeze dried initially and their weights were noted. These discs were incubated in 4 mL PBS at 35 °C and 50 rpm and allowed to swell for 24 hr. At fixed time intervals, the samples were removed from PBS; the surface water was soaked gently, and the weight at time *t* was noted until equilibrium swelling was reached. At any given time, t, the swelling ratio was calculated using the following equation:

$$\text{Swelling ratio} = (W_t - W_i)/W_i * 100$$

Where W_i represents the initial dry weight of the hydrogels, whereas W_t is defined as the weight of the swollen hydrogels at time *t*. The swelling kinetics were studied using power law and a graph was plotted between $\log(M_t/M_\infty)$ *versus* log *t* with the help of GraphPad Prism. Here, M_t represents the weight of hydrogel at time *t* and M_∞ represents the weight at equilibrium swelling. Slope of the curves were calculated to determine the diffusional exponent *n.*

5.3.7 Mechanical Properties

Hydrogel samples (12mm height and 10mm diameter) were swollen for 24 h at room temperature in a PBS buffer at pH 7.4 prior to mechanical measurements. The compression tests were performed on Texture Analyser (Hamilton, MA, USA) universal testing machine (UTM) model XT plus using Texture Exponent software. The swollen hydrogel samples were dabbed gently with tissue paper to discard surface water prior to performing the compressive test. Each sample was positioned in the middle of the stage and the load cell of 5 kg was used.

5.3.8 Release and Detection of PVA

The P-Gel, P-Gel-1FT and P-Gel-2FT hydrogel discs were incubated in glass vials with 10 mL of PBS solution at 35°C and 50 rpm. At each indicated time point, 300 µL of the solution was removed for detection of PVA and replaced with fresh PBS. For detection of PVA, the method reported by Procházková, et al., was used with slight modifications. Briefly, a solution of iodine (150 mM potassium iodide, 50 mM diiodine in deionized water, Sigma 221945 and 207772, St. Louis, MO, USA) was mixed with borate (64.7 mM boric acid in deionized water, Sigma B0394, St. Louis, MO, USA) in a 1:5 ratio of iodine solution:borate solution to generate the PVA detection solution. The solution was gently inverted 4-6 times in a conical tube to ensure even mixing. To measure PVA in solution, 163.6 µL of PVA detection solution was added to 36.4 µL of samples of interest in a 96-well plate and incubated at room temperature for 20 minutes with gentle shaking. Absorbances were read at 630 nm using an Imaging Multimode Plate Reader (Cytation 5, Agilent BioTek Instruments, Winooski, VT, USA).[45]

5.3.9 Drug Release Kinetics via Mathematical Modeling

To evaluate release kinetic profiles of the samples over the studied time duration, different mathematical models were studied.[46] These included zero- and first-order release model, Higuchi release model, and Korsmeyer-Peppas model.

(e) Zero order model: In this model, the drug release is represented by:

$C_t = C_o + K_o t$

where C_t is the amount of drug released at time t, C_o is the initial concentration of drug in solution (at $t=0$), and K_o is the zero-order rate constant. The graph is plotted between cumulative drug release *vs.* time and the coefficient of determination (R^2) was calculated.

(f) First order model: In this model, the drug release is represented by:

$dC/dt = -K_1 C$

where K_1 is the first order rate constant

After rearranging and taking integral,

$\log C_t = \log C_o - (K_1/2.303)t$

where C_t is the amount of drug remaining at time t and C_o is the initial concentration of the drug. The graph is plotted between log cumulative % drug remaining *vs.* time and the coefficient of determination (R^2) was calculated.

(g) Higuchi model: In this model, the drug release is represented by:

$M_t/M_\infty = K_h t^{1/2}$

where M_t/M_∞ is the fraction of drug released at each time point, M_t is the amount of drug released in time t, M_∞ is the amount of drug released after infinite time, and K_h represents the Higuchi release kinetic constant. The graph is plotted between cumulative % drug release *vs.* square root of time and the coefficient of determination (R^2) was calculated.

(h) Korsmeyer-Peppas model: In this model, the drug release is represented by:

$M_t / M_\infty = K_{kp} t^n$

$\log (M_t/M_\infty) = \log K_{kp} + n \log t$

where M_t/M_∞ is the fraction of drug released at time t, M_t is the amount of drug released in time t, M_∞ is the amount of drug released after infinite time. n is the diffusional exponent or drug release exponent and K_{kp} is the Korsmeyer-Peppas release rate constant. The graph is plotted between log cumulative % drug release vs. log t and the coefficient of determination (R^2) was calculated.

The graphs were plotted as mentioned in *Table* 1 and the coefficient of determination (R^2) was calculated for each model.[47, 48]

***Table* 1.** Curve fitting of various models for drug release kinetics

	Zero Order	**First Order**	**Higuchi model**	**Korsmeyer-Peppas model**
Equation	$C_t = C_o + K_o t$	$\log C_t = \log C_o - (K_1/2.303)t$	$M_t/M_\infty = K_h t^{1/2}$	$\log (M_t/M_\infty) = \log K_{kp} + n \log t$
Graph	cumulative drug release vs. time	log cumulative % drug remaining vs. time	cumulative % drug release vs. $\sqrt{t}$	log (cumulative % drug release) vs. log t

5.3.10 Cytotoxicity Evaluation

The 3-[4,5-dimethylthiazol-2-yl]-2,5-diphenyltetrazolium bromide (MTT) assay was conducted to assess the cytotoxicity of the GelMA and P-Gel hydrogels with HCECs (human corneal epithelial cells). HCECs were routinely cultured in DMEM/F12 medium (Sigma, St. Louis, MO, USA) containing 1% FBS and 1% penicillin/streptomycin (ThermoFisher Scientific, Waltham, MA, US) at 37°C, and 5% CO_2 in a humidified atmosphere.

For the MTT assay, the cells were seeded in a 96-well plate at a density of 1×10^4 cells per well using complete culture medium. The hydrogel discs (weighing about 10 mg) were sterilized by exposing them to ultraviolet light for 30 min before incubation with the cells. A sterilized solution of 0.2% (w/v) PVA was made in culture media and a 200 µL sample was used for the cytocompatibility assay. After incubating the sterilized hydrogels and PVA solutions with cells for 24 hr, the cells were washed with PBS and treated with 1mg/ml MTT solution prepared in culture media. The MTT solution was removed after 4 hr of incubation and 150 µL DMSO was added to each well to dissolve the formazan crystals and the absorbance was measured at 570 nm using microplate reader (Cytation 5, Agilent BioTek Instruments, Winooski, VT, USA). All conditions were taken in triplicates. The viability of HCEC cells was calculated according to the following formula.[49]

$$\text{Cell Viability (\%)} = \frac{\text{absorbance of test} - \text{absorbance of blank}}{\text{absorbance of control} - \text{absorbance of blank}} X100$$

5.3.11 Statistical Analysis

Statistical analysis was performed using GraphPad Prism 10.1.2 (GraphPad Software, La Jolla, CA, USA). All data are reported as mean and standard deviation, unless otherwise stated. Two-way ANOVA was performed to determine differences across testing groups. Tukey's multiple comparison tests were used when necessary. In all cases, statistical significance was considered significant for a p value of <0.05 unless otherwise stated.

5.4 Results and Discussion

5.4.1 Morphological Characterization

SEM images of all the hydrogels displayed a highly interconnected porous architecture (*Figure* 1a-d). GelMA hydrogels had a very broad pore size distribution, with pores sizes ranging from 1 to 90 µm and mean pore size of 23 µm (*Figure* 2a). The pore size distribution for P-Gel samples was in the range of 1 to 60 µm with a mean pore size of 18 µm (*Figure* 2b). The pore size distribution of freeze thawed P-Gel hydrogels (*Figure* 2c and 2d) were observed to be similar to P-Gel samples, where the pore sizes decreased and were more uniform compared to GelMA sample. It is interesting to note a remarkably narrower pore size distribution upon addition of PVA. This smaller and more homogeneous pore architecture along with slightly thicker pore walls suggest a good compatibility between GelMA and PVA.[50, 51]

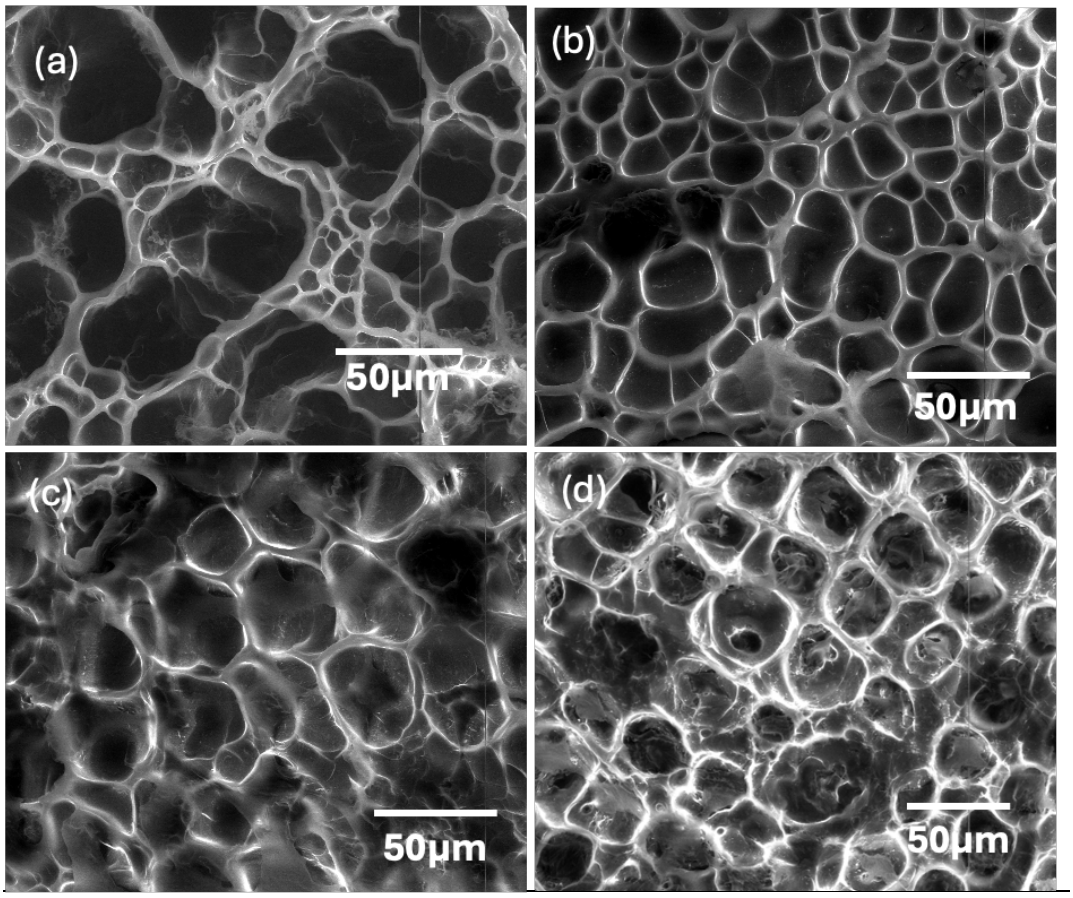


***Figure* 1.** Cross sectional SEM images of the freeze dried (a) GelMA (b) P-Gel (c) P-Gel-1FT, and (d) P-Gel-2FT hydrogels showing a highly interconnected porous structure. The pore architecture becomes more uniform with the addition of PVA.

The morphology of the P-Gel hydrogels in *Figure* 1b could be attributed to formation of a semi-interpenetrating network, where GelMA forms a chemically crosslinked network through photo-crosslinking. During the freezing step in the lyophilization process, thermally induced phase separation occurs between the solvent phase and the polymer phase, creating a polymeric network.[52] The larger pore size of GelMA hydrogels (*Figure* 1a) could be attributed to presence of less polymeric phase in GelMA hydrogels (10% GelMA) compared to the P-Gel samples (10% GelMA and 5% PVA). Thus, GelMA hydrogels hold more water to undergo ice crystal formation during the freezing step, leading to relatively larger pore sizes (*Figure* 1a). Moreover, PVA molecules might penetrate and partially fill the free voids between GelMA chains, thus increasing the crosslinking density and resulting in the formation of smaller sized pores between the crosslinked GelMA chains (*Figure* 1b-d).[53]

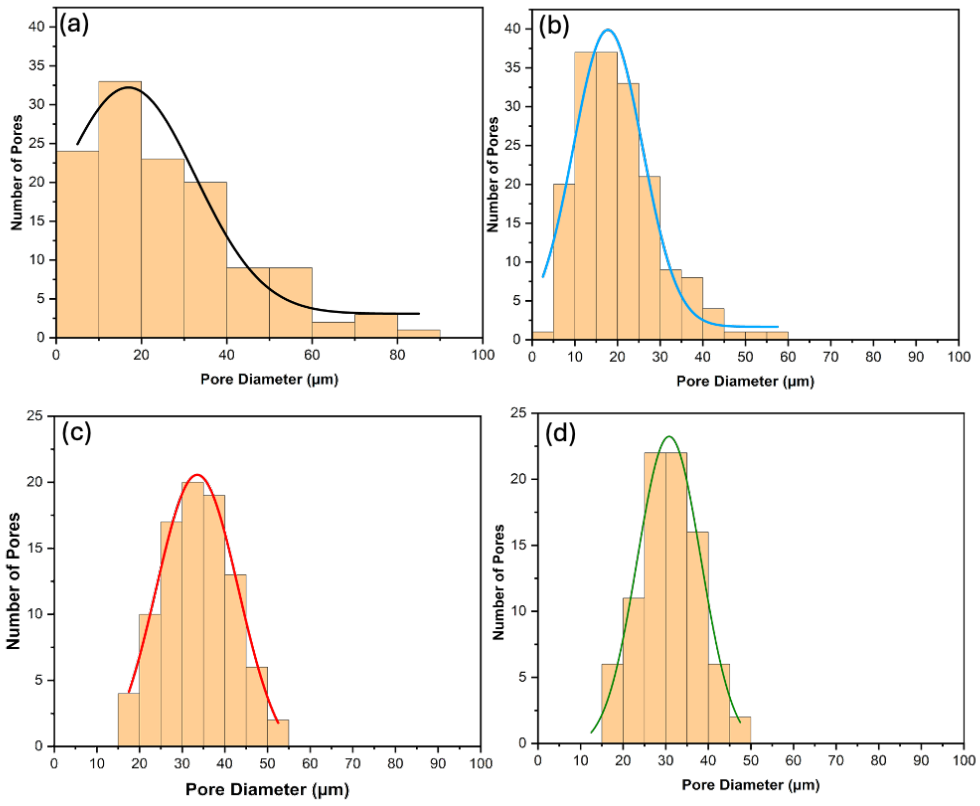


***Figure* 2.** Pore size distribution of (a) GelMA (b) P-Gel (c) P-Gel-1FT, and (d) P-Gel-2FT. GelMA shows a broad pore size distribution with pores sizes ranging from 1 to 90 µm, with most pores ranging from 15-20 µm. The P-Gel samples showed more uniform pore sizes with mean pore size of 10-25 µm.

5.4.2 Chemical Characterization

5.4.2.1 Fourier Transform Infrared (FTIR) Spectroscopy

When gelatin is reacted with methacrylic anhydride, gelatin undergoes amidation to form GelMA. During the reaction, nucleophilic attack of a primary amine to carbonyl carbon of methacrylic anhydride takes place, where an amide linkage is formed following amine deprotonation. In the next step, the photo initiator initiates free radical polymerization upon exposure to UV light (405 nm) and forms crosslinked GelMA hydrogels. Multiple peaks between ~3500-3200 cm^{-1} resemble the O-H stretching and N-H stretching whereas the peak at ~2936 cm^{-1} is attributed to the C-H stretching.[54] The peak at ~1640 cm^{-1} in GelMA represents the C=O stretching (amide I).[55] The peak around 1640 cm^{-1}corresponding to the C=C stretching of the methacrylate groups is close to the C=O stretching peak of the amide I, making it difficult to verify its disappearance after the crosslinking process in GelMA spectrum.[56] The peak at ~1534 cm^{-1} corresponds to N-H bending and stretching vibrations of C-N groups (amide II) and the peaks around ~1445 cm^{-1} and ~1335cm^{-1} are assigned to -CH_2 bending vibrations, C-N stretching vibrations within amide III, respectively.[57-59] In the PVA FTIR spectrum, the

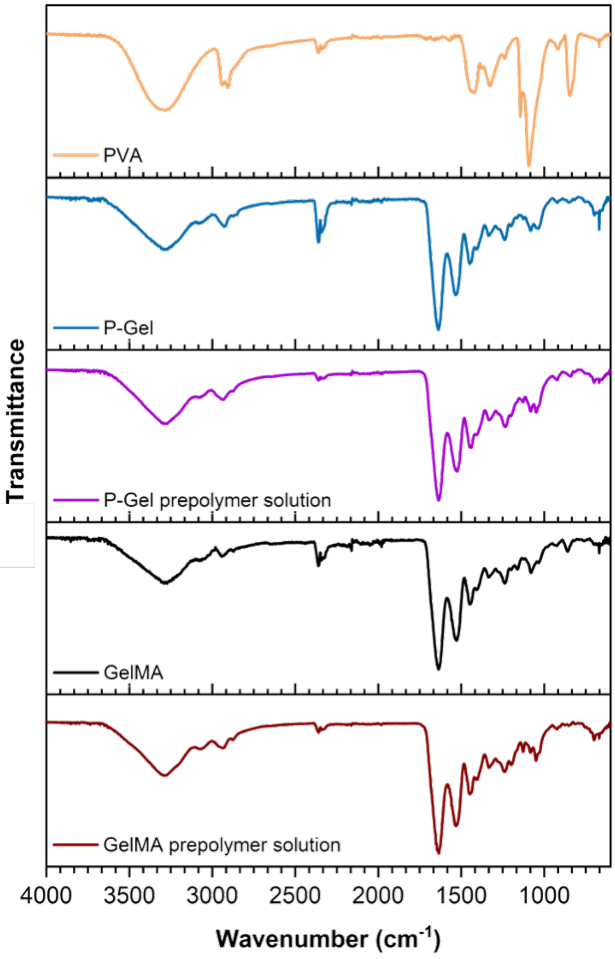


***Figure* 3.** FTIR spectra of GelMA prepolymer solution, GelMA hydrogels, P-Gel prepolymer solution, P-Gel hydrogels and PVA powder.

peak around ~1140 cm^{-1} corresponds to the C-O and C-C stretching, denoting its crystalline regions.[54, 60] This band is observed in the P-Gel prepolymer solution and hydrogels, indicating the presence of PVA. The sharp peak at ~1092 cm^{-1} in PVA spectrum corresponds to the C-O vibration.[58] When PVA is added to the GelMA polymer solution, it might undergo supramolecular interactions (H-bonding) between the -OH/-NH_2 groups of PVA and GelMA. The appearance of a shoulder around ~1088 cm^{-1} in the P-Gel hydrogels interactions may be attributed to these supramolecular interactions (*Figure* 3). These supramolecular interactions may also be the source of the additional transition that appeared around 48 °C in the DSC thermograms of P-Gel-2FT in the first heating cycle (*Figure* 5b).

5.4.2.2 Nuclear Magnetic Resonance (NMR)

The gelatin macromers were functionalized using methacrylic anhydride (4.0 mL per 40 g gelatin) during the reaction. The conjugation of methacryloyl groups to gelatin molecules were monitored and confirmed by ^{1}HNMR spectroscopy (Figure 4). Appearance of the signals at 5.36 and 5.62 ppm (the protons of vinyl group of methacrylic anhydride) and decrease of signal at 2.92 ppm (the protons of methylene of lysine signal) confirmed modification of gelatin with methacrylic anhydride. Since the proton signal of the aromatic amino acid moieties in gelatin remained constant, intensity of these protons was used to normalize the intensity of these protons in gelatin and the synthesized GelMA. Therefore, the degree of substitution (DS) of GelMA was calculated by comparing the proton signal at 2.9 ppm of the unmodified gelatin with that of GelMA. The DS of GelMA was calculated as about 61.8% in this study which is in good agreement with those previously reported for GelMA prepared in a similar condition.[61,62]

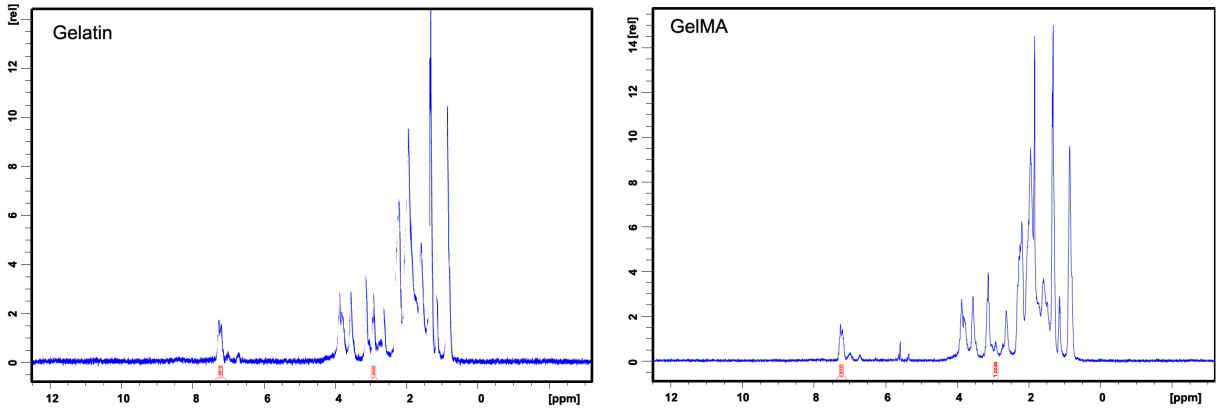


***Figure* 4.** ^{1}HNMR of gelatin and GelMA.

5.4.2.3 X-Ray Diffraction (XRD)

XRD patterns of the PVA powder and GelMA (*Figure* 5a) revealed that the PVA peak was around 22.5°-2θ, while that of GelMA was around 20°-2θ.[63] The peak around 20°-2θ and 41°-2θ in PVA represents the semi-crystalline nature of PVA with both crystalline and amorphous regions.[64, 65] XRD patterns of the P-Gel, P-Gel-1FT, and P-Gel-2FT showed a prominent peak around 20°-2θ. From the GelMA XRD pattern, it is observed that the peak around 20°-2θ was broad, however, the PVA peak at 20°-2θ is relatively sharper and of higher intensity.[65] In the presence of PVA in the P-Gel interpenetrating network, the diffraction pattern shows slight changes. The P-Gel hydrogel possess a diffraction peak at 20°-2θ which is higher, and sharper compared to the diffraction pattern of GelMA. These results suggest that the hydrogen bond intermolecular interactions occur between the PVA and GelMA chains.[66] Similarly, in P-Gel-1FT and P-Gel-2FT samples, the 20°-2θ peak is relatively sharper and higher in intensity, indicating that crystallinity of the interpenetrating network could be mainly due to PVA.[67]

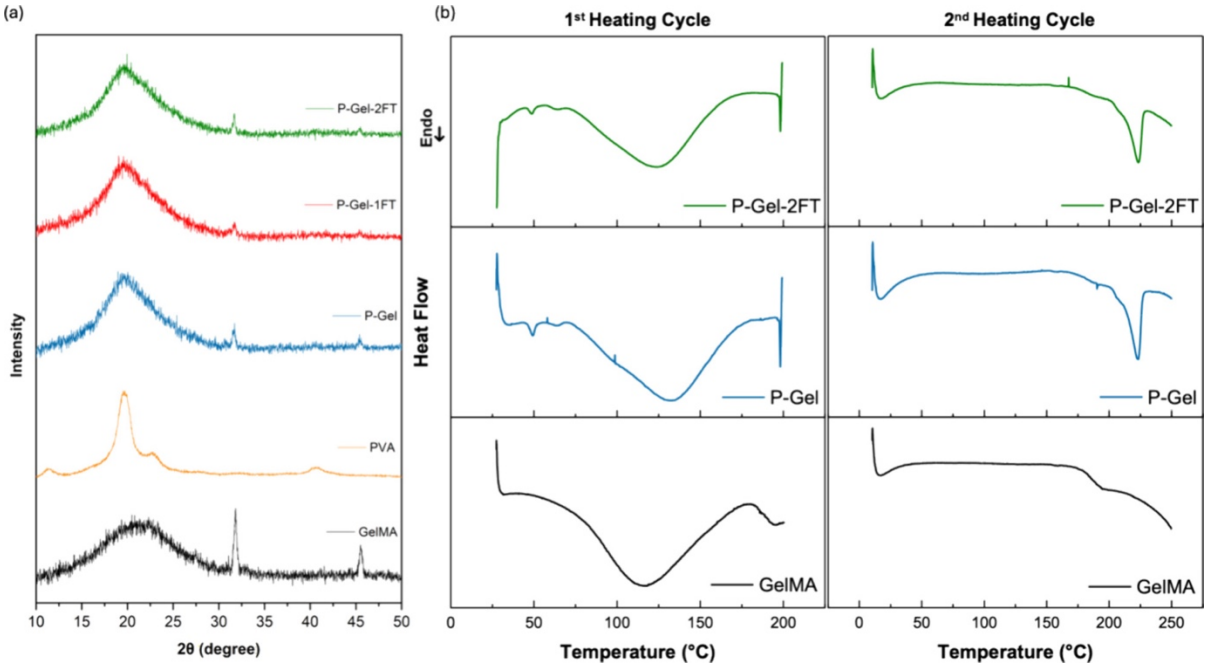


***Figure* 5.** (a) XRD patterns of GelMA, PVA, P-Gel, P-Gel-1FT, and P-Gel-2FT samples. (b) DSC thermogram of GelMA, P-Gel, and P-Gel-2FT samples for the first (~200 °C) and second heating (~ 250 °C) cycle.

5.4.3 Thermal Analysis

Next, a thermal analysis was used to study the microstructure of the hydrogels. The first heating cycle in the DSC thermogram (*Figure* 5b) indicated broad endothermal transitions at around 113 °C for GelMA and 123 °C for P-Gel and P-Gel-2FT that correspond to evaporation of water molecules from the samples. During the second heating cycle, no exothermic or endothermal transition was observed in the GelMA sample, indicating that no further physical/chemical changes took place in this temperature range. Meanwhile, for P-Gel and P-Gel-2FT samples, two endothermal transitions were observed at around 48 and 62 °C in the first heating curve. Similar transitions have been previously reported for freeze-thawed PVA hydrogels at similar temperatures around 60 °C and are attributed to a gel-to-sol transition owing to dissociation of H-bonding and melting of the crystalline phase.[52] The transition around 48 °C in P-Gel and P-Gel-2FT hydrogels could be attributed to the supramolecular interactions (H-bonding) between the −OH/–NH_2 groups of PVA and GelMA and its effect on crystalline domain formation in PVA. The stability (melting temperature) and size (melting enthalpy) of the crystalline domains control mechanical and physical properties of the PVA-containing hydrogels, and these two parameters are influenced by the duration and number of freeze-thaw cycles.[68] The melting enthalpies of the P-Gel and P-Gel 2FT hydrogels were measured using the TA Universal Analysis 2000 v4.5A. An increase in enthalpy of the melting transition from P-Gel to P-Gel-2FT (0.3304 to 0.4104 J/g) in the temperature range of 48–60 °C supports increased crystallinity upon FT cycles and is in line with the literature reports.[68] As the temperature increased to 250 °C in the second heating cycle, an endothermal transition was observed in the P-Gel-2FT thermogram at around 225 °C, which corresponds to the melting of PVA in the samples.[69]

5.4.4 Swelling Behaviour

The swelling behaviour of the freeze dried GelMA, P-Gel, P-Gel-1FT, and P-Gel-2FT hydrogels is shown in *Figure* 6a. A post hoc Tukey test was applied to identify any significant difference between the swelling behaviour of the hydrogel samples. After 1.5 hr, the GelMA hydrogel showed a significant difference in the swelling compared to the P-Gel sample ($p<0.05$). From the swelling curves (*Figure* 6a), it can be inferred that P-Gel, P-Gel-1FT and P-Gel-2FT samples undergo less swelling compared to GelMA. This reduced swelling could help to control the release and support a sustained release of PVA from the interpenetrating network. Moreover, there is a gradual decrease in the degree of swelling with increase in crosslink density owing to the presence of lower polymeric

phase in GelMA hydrogels compared to the P-Gel samples. This is also corroborated by the SEM results (*Figure* 1). Next, log (M_t/M_∞) *versus* log *t* was plotted to understand the swelling kinetics (*Figure* 6b) of the hydrogels. Interestingly, GelMA hydrogel showed the highest linearity (R^2 value=0.9159) with the power law, indicating that the swelling of these gels followed Fickian diffusion (*n* value<0.45). Additionally, P-Gels, P-Gel-1FT and P-Gel-2FT showed slightly smaller R^2 values (0.8884, 0.6764, 0.7206, respectively). *n* values for these hydrogels were also found to be <0.45, indicating diffusion-controlled swelling.[70]

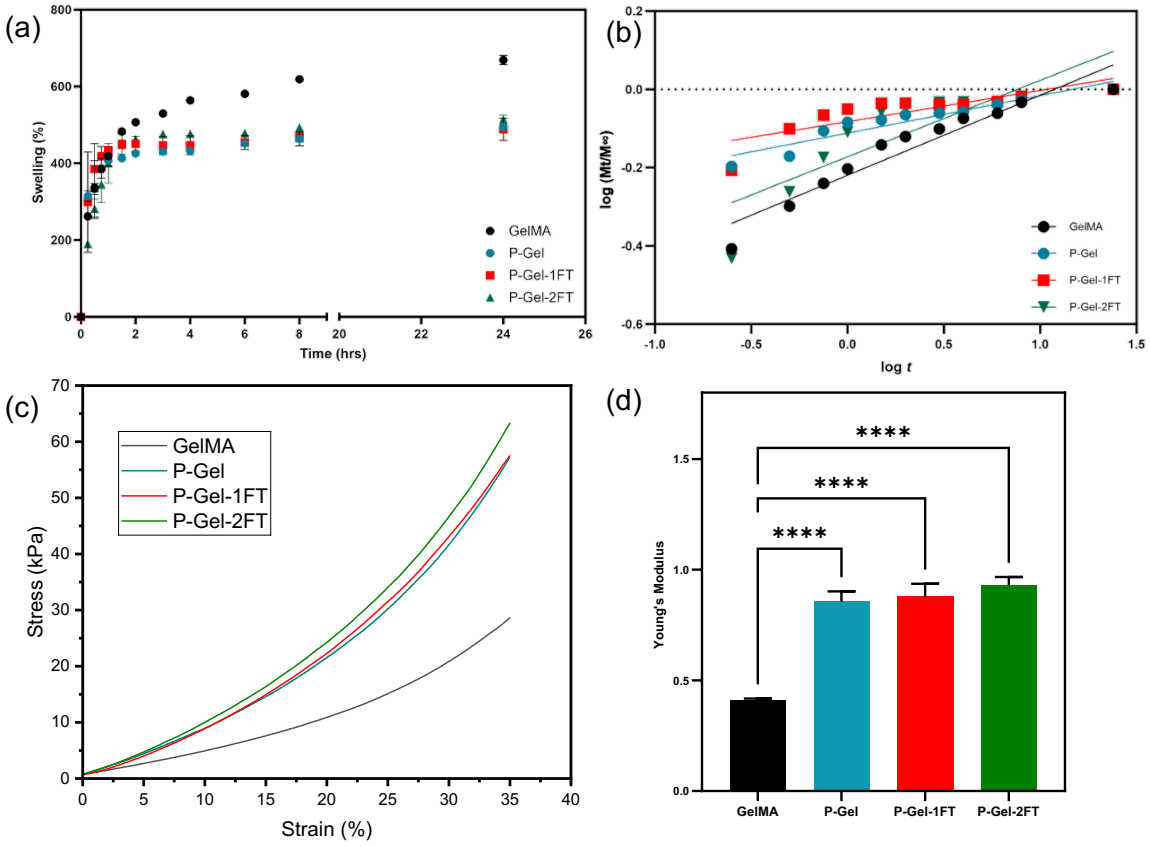


***Figure* 6.** (a) Equilibrium Swelling of GelMA, P-Gel and freeze thawed hydrogels. (b) Swelling kinetics analysis based on power law. (c) Stress Strain curves and (d) Young's modulus for GelMA, P-Gel and freeze thawed hydrogels.

5.4.5 Mechanical Properties

Figure 6c shows the compressive stress-strain curves of GelMA, P-Gel, P-Gel-1FT, and P-Gel-2FT hydrogels. The compression experiments suggest that the double networks containing PVA had a two-fold higher compressive modulus (0.8564±0.0457) than 10% GelMA alone (0.4099±0.00829). The P-Gel hydrogels that underwent 1hr and 2hr freeze thawed also exhibit a remarkable compressive modulus (*Table* 2 and 3). This could be attributed to the freeze thaw and solvent displacement process which results in intensified physical interactions to form a second stiffer and tougher network of PVA.[38] These stronger non-covalent interactions could be the reason for a slight increase in the Young's modulus observed with the 1hr and 2hr freeze thawed samples (0.8766±0.0596, and 0.9302±0.0364 respectively, *Figure* 6d). Reports suggest that there are different gelation parameters (such as the number, temperature and time of FT cycles) and polymer parameters (such as molecular weight, concentration and degree of hydrolysis of PVA) that affect the final mechanical properties of PVA hydrogels.[52] Similarly, the mechanical properties of GelMA-based hydrogels are influenced by various parameters such as concentration and degree of substitution of GelMA, type and concentration of photoinitiator used, and intensity and duration of UV exposure.[71]

***Table* 2.** Young's Modulus

Young's Modulus (kPa)	GelMA	P-Gel	P-Gel-1FT	P-Gel-2FT
Mean	0.4099	0.8564	0.8766	0.9302
SD	0.0082	0.0457	0.0596	0.0364

***Table* 3.** Compressive Strength

Stress (kPa)	GelMA	P-Gel	P-Gel-1FT	P-Gel-2FT
Mean	26.4391	59.0745	62.7813	63.0322
SD	0.4161	1.5958	4.4641	0.7766

5.4.6 Release of PVA

PVA release curves (*Figure* 7) depict the effect of the freeze thaw method in tuning the release of PVA. Interestingly, after the samples experienced a freeze thaw cycle of about 2 hr, there was a lower release of PVA compared to P-Gel. A post-hoc Tukey test was employed, which revealed that after 5 hr, the P-Gel-2FT hydrogel exhibited significantly lower PVA release ($p<0.05$) compared to P-Gels. Furthermore, P-Gel-1FT sample showed significantly lower release of PVA after 7 hr ($p<0.05$)

compared to P-Gels. The observed decrease in release of PVA by altering the freeze thaw parameters is in good agreement with the concept of using freeze thaw to adjust the release rates of PVA. Although release of PVA from P-Gel-2FT is less than P-Gel-1FT samples (*Figure* 7), the difference was not statistically significant (p>0.0 5).

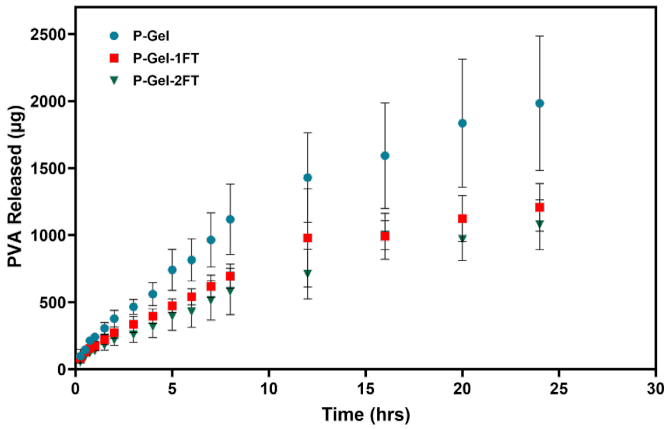


***Figure* 7.** PVA release curves and the effect of freezing times on the release rate of PVA (per 100mg hydrogel). The freeze thawed samples show lower release of PVA than the P-Gel samples, supporting the concept of using freeze thaw cycles to control release rates.

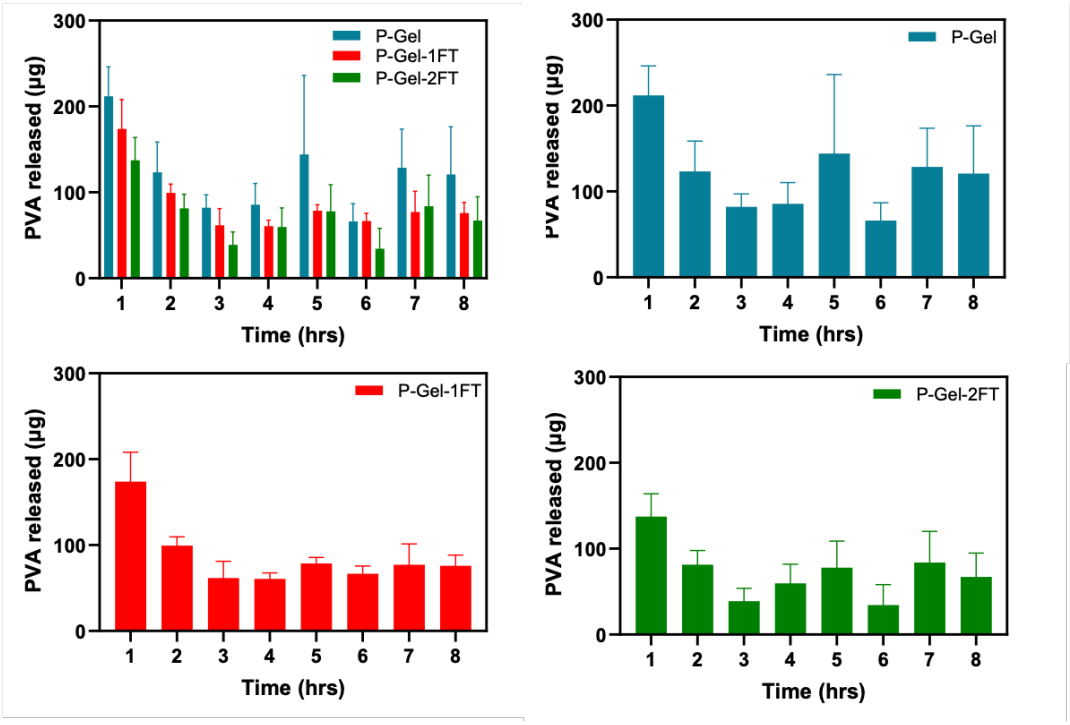


***Figure* 8.** PVA release profiles per time point showing the effect of freezing thaw cycle on the release of PVA.

There are three main processes that explain the effect of freeze thaw cycles on P-Gel semi-interpenetrating network; (a) hydrogen bonding (b) crystalline domain formation, and (c) phase separation. During the freezing step, ice crystals are formed which allow PVA chains to come closer and form PVA rich domains.[52] The close proximity between these PVA chains promotes the formation of crystalline domains through inter- and intra-molecular H-bonds that act as cross-linking sites. Upon thawing, these ice crystals melt, leaving behind pores surrounded by a PVA skeleton.[52] During successive freeze thaw cycles, more PVA chains come into closer contact with each other and new crystalline domains or sites are generated. Theoretically, higher freezing durations cause more H-bonding to occur, increasing crystallinity.[52] Of note, it is important to consider the temperatures at which these hydrogels will be stored or used, because temperatures >60 ℃ could lead to gel-to-sol transition owing to dissociation of H-bonding and melting of the crystalline phase.[52] In our case, the desired application of these PVA-containing hydrogels would be to release this therapeutic agent on the ocular surface, which has a temperature of about 35 ℃. There are various factors which influence crystallinity and water uptake of PVA containing hydrogels, such as concentration of PVA, number of freeze thaw cycles, molecular weight of PVA, temperature and duration of freeze thaw cycles[52], suggesting that carefully designing these parameters for freeze thaw cycles can help achieve tunable release rates.

5.4.7 Drug Release Kinetics via Mathematical Modeling

To study the drug release kinetics and how different factors affect the dissolution velocity and behaviors, various mathematical equations describing the release dependence on time are used. In this study, drug release was evaluated though four main release kinetic models: zero- (*Figure* 9a) and a first-order release model (*Figure* 9b), a Higuchi release model (*Figure* 9c) and a Korsmeyer-Peppas model (*Figure* 9d). In the context of drug release, zero-order release kinetics implies that the drug is released at a constant rate over time, regardless of its initial concentration. This can be desirable for certain medications as it provides a constant and predictable therapeutic effect. The first order release kinetics describes the rate of drug release as directly proportional to the initial concentration of the drug. This means that as concentration of the drug decreases, the rate of release also decreases. Higuchi's model is based on Fickian diffusion and is specifically derived for drugs dispersed in solid or

semi-solid matrices, typically without considering the effect of swelling or dissolution of the matrix. According to this model, the graph between the concentration of the drug and square root of time would be a linear function. [72] Korsmeyer-Peppas is a semi-empirical model that describes several release mechanisms, including Fickian diffusion, Case II transport, or a combination of both (anomalous transport).[73]

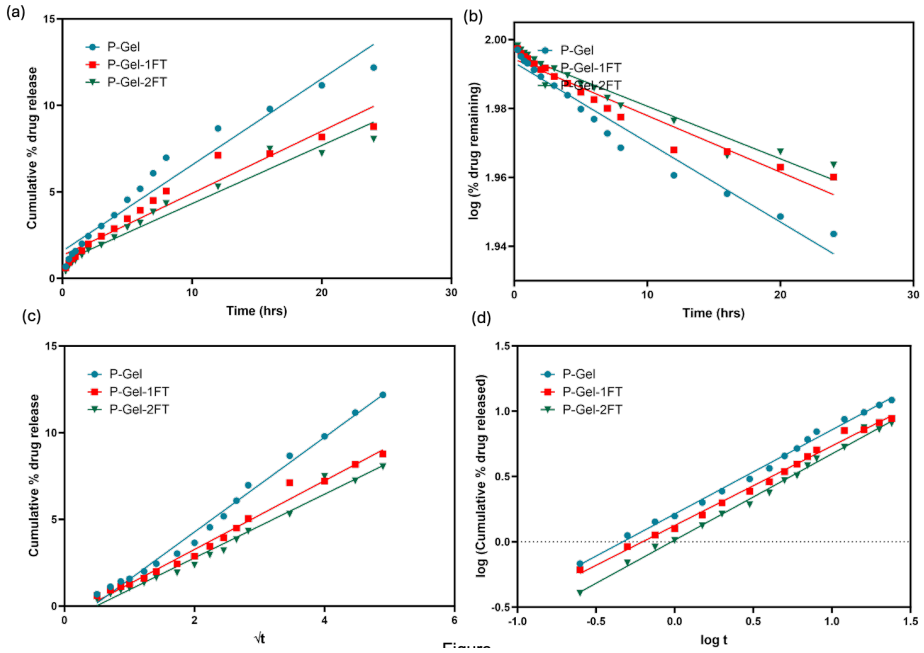


***Figure* 9.** Modelling of the PVA release data on well-known mathematical models: (a) zero order, (b) first order, (c) Higuchi's model, and (d) Korsmeyer-Peppas model.

To evaluate the best fit model for the release profiles in our study, the goodness of fit for each model or the coefficient of determination (R^2) was calculated using GraphPad Prism. The release profiles of the PVA containing hydrogels showed highest linearity with the Korsmeyer-Peppas model ($0.9944<R^2<0.9952$). The release exponent (n) for P-Gel, P-Gel-1FT and P-Gel-2FT samples were 0.6442, 0.6090, and 0.6601, respectively, indicating that these systems follow non-Fickian or anomalous transport (*Table* 4). This mechanism is governed by rate of time dependent solute diffusion and swelling of the polymer matrix ($0.45<n<0.89$ and $n\neq0.5$).[74] Moreover, the formation of crystalline domains upon freeze thawing can hinder the mobility of polymeric chains,[52] thus slowing their rearrangement. This along with the diffusion process occurring simultaneously causes time-dependent anomalous effects, thus explaining a better fit to the Korsmeyer-Peppas model.[73]

***Table* 4.** The coefficient of determination (R^2) values of P-Gel, P-Gel-1FT, and P-Gel-2FT calculated by using different kinetic models.

Kinetic Model	P-Gel	P-Gel-1FT	P-Gel-2FT
Zero-order	0.9568	0.9407	0.9560
First Order	0.9629	0.9449	0.9588
Higuchi	0.9914	0.9863	0.9798
Korsmeyer-Peppas	0.9954	0.9944	0.9952
Diffusion exponent (n value)*	0.6442	0.6090	0.6601

*Calculated by the linear regression of Korsmeyer-Peppas equation of $\log(M_t/M_\infty)$ versus $\log t$.

5.4.8 Cytotoxicity evaluation

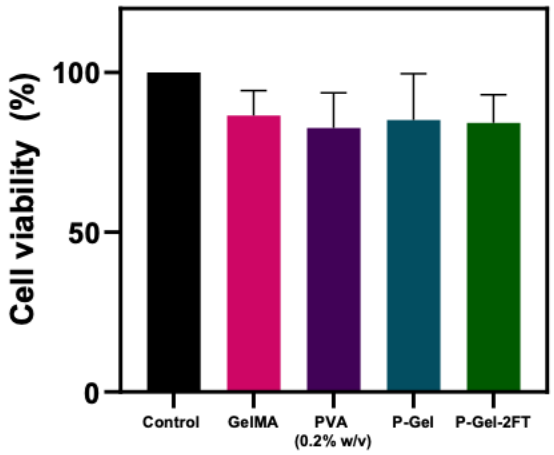


***Figure* 10.** MTT assay for GelMA, PVA, P-Gel and P-Gel-2FT

Cytotoxicity of biomaterials is an essential aspect for ocular applications. The efficacy and safety of a drug delivery vehicle depends on its ability to deliver the therapeutic agent specifically to the ocular surface while exhibiting no cytotoxicity. To realize this, we first investigated and compared the cytotoxicity of GelMA, P-Gel, P-Gel-2FT and 0.2% (w/v) PVA solution using the MTT assay (*Figure* 10). The cell viabilities in the presence of GelMA and P-Gel-5% samples were about 86.5% and 85.1% respectively after 24 hr of incubation, indicating they were not cytotoxic to the cells. Similarly, freeze thaw cycles did not induce any adverse effects on the cells. Moreover, 0.2% (w/v) PVA showed >80% cell viability, suggesting its non-toxic nature. This concentration was selected based on the PVA

concentration released per time point (*Figure* 8). These findings support the use of these hydrogels as suitable vehicles for applications in controlled drug release of PVA. While these results confirm that the materials are not overtly cytotoxic, cell viability alone does not fully capture cellular health or immunogenicity. To further validate biocompatibility, future studies should consider assessing apoptotic markers and inflammatory cytokine expression, which would provide deeper insight into potential sublethal stress or immune activation induced by the materials.

5.5 Conclusion

In summary, freeze thaw induced crystalline domains were formed inside a chemical-physical interpenetrating network to tune the release rate of PVA, which is a commonly used therapeutic agent to treat dry eyes. The results from this study suggest that this method could potentially be easier to translate into application given the purported safety associated with utilizing a physical crosslinking method to create desired release profiles, as opposed to employing additional harsh chemical crosslinking agents. Of note, there are various factors such as concentration and molecular weight of PVA, number, temperature, and duration of freeze thaw cycles which influence the physical and chemical properties of PVA containing hydrogels, suggesting that engineering these parameters is crucial to take control over the release rate of PVA. Furthermore, the macroscopic properties of these hydrogels are determined by the relative amount of crystalline and amorphous phases of PVA present. Looking ahead, we envisage that the physical barriers created with freeze thaw cycles may also be explored to take control over the release of other molecules of interest from these gels. Interestingly, the versatile properties of GelMA could be explored to fabricate drug-eluting contact lenses or drug-loaded ocular inserts to be placed in cul-de-sac in the lower eye lid providing prolonged release of molecules of interests.

Chapter 6

Biodegradable 3D printed conjunctival inserts for the treatment of dry eyes

*An article was extracted from this chapter and is published in Special Issue on Advanced Biodegradable Polymers for Drug Delivery, MDPI's Polymers (DOI: 10.3390/polym17050623)

This chapter has been published as follows:

Garg P, Shokrollahi P, Phan CM, Jones L. Biodegradable 3D-printed conjunctival inserts for the treatment of dry eyes. Polymers 2025; 17(5): 623.

Author	Concept/Design	Data Acquisition	Analysis	Write Up/ Publication
Piyush Garg	Y	Y	Y	Y
Parvin Shokrollahi	Y		Y	Y
Chau-Minh Phan	Y			Y
Lyndon Jones	Y			Y

6.1 Abstract

Purpose: To fabricate biodegradable conjunctival gelatin methacrylate (GelMA) inserts for release of PVA using 3D printing.

Method: In this work, biodegradable conjunctival inserts were 3D printed using stereolithography-based technique. The release of PVA from these inserts (containing 10% GelMA and 5% PVA, P-Gel-5%) was assessed along with different mathematical models of drug release. The biodegradation rates of these inserts were studied in the presence of matrix metalloproteinase-9 (MMP9) enzyme, also found on the ocular surface. The morphology of the inserts before and after enzymatic degradation was monitored using scanning electron microscopy.

Results: The 3D printed P-Gel-5% inserts formed a semi-interpenetrating network which was mechanically stronger than GelMA inserts. The PVA release graphs demonstrate that at the end of 24 hrs, about 222.7±20.3 µg, 265.5±27.1 µg 242.7±30.4 µg of PVA was released when 25 µg/ml, 50 µg/ml and 100 µg/ml MMP9 enzyme concentration was used, respectively. The release profiles of the P-Gel-5% containing hydrogels in the presence of different concentrations of MMP9 showed highest linearity with the Korsmeyer-Peppas model. The degradation study was performed for 24 hrs and the results suggest that degradation rate is a function of MMP9 enzyme concentration. Over 80% of P-Gel-5% inserts were degradaded at the end of 8 hrs, 12 hrs, and 24 hrs in the presence of 100 µg/ml, 50 µg/ml, and 25µg/ml MMP9 enzyme solutions respectively.

Conclusion: The results from this study highlight the 3D printing abilities of GelMA to design conjunctival inserts. These inserts could be used to deliver PVA, which is well known therapeutic agent for dry eye disease. Overall, this study describes that PVA release is influenced by multiple mechanisms such as diffusion and enzymatic degradation, which is supported by the morphological studies and biodegradation results.

Keywords: Biodegradable polymers, 3D printing, conjunctival inserts, matrix metalloproteinase-9.

6.2 Introduction

Dry eye disease (DED) is a multifaceted condition marked by tear film instability, inflammation, and sensory dysfunction. It is often associated with other eye health issues, including meibomian gland dysfunction, autoimmune disorders like Sjögren's syndrome, and post-surgical effects from procedures such as LASIK. DED is categorized into aqueous-deficient and evaporative types, stemming from either insufficient tear production or excessive evaporation. Various factors, including environmental conditions, systemic diseases, medication use, and prolonged screen exposure, can worsen symptoms.[1] It is often characterized by high osmolarity of the tear film, with diagnostic threshold levels ranging from 305 to 316 mOsm/L,[2] and inflammation of the ocular surface.[3] As the condition progresses, there is a noted escalation in both tear osmolarity levels and inter-eye variability which is potentially useful in diagnosis and effective disease management.[4,5] This increased osmolarity initiates an inflammatory response, leading to cellular distress among epithelial cells and increased production of cytokines and matrix metalloproteinase-9 (MMP-9), an enzymatic protein involved in proteolysis.[6] Many studies have demonstrated elevated MMP-9 levels in the tears of individuals suffering from dry eye, which correlate closely with clinical examination findings.[7-9] The activity of MMP-9 increases with the severity of DED, contributing to compromised corneal epithelial barrier function, increased shedding of corneal epithelial cells, and irregularities in the corneal surface.[10,11]

Eye drops are a common treatment for DED, but they have limited effectiveness and require frequent application. Other reasons contributing to the inefficiencies of the ophthalmic drops include low bioavailability, largely due to lacrimal secretion, rapid tear turnover, and efficient nasolacrimal drainage pathways. Thus, it would be helpful in the clinical management of DED to have a more efficient method to deliver products to the ocular surface that require less frequent dosing and remain on the ocular surface for an extended period.

An ideal ocular delivery system should possess properties such as biocompatibility, high drug residence time, low systemic absorption, and sustained drug release. Among the various strategies explored, integrating drug-loaded materials into ocular devices, such as contact lenses, shows the greatest potential for maximizing drug retention and bioavailability. Although contact lens based drug delivery systems[12] can be used to prolong the ocular surface residence time, the burst release of drugs still remains an unresolved issue.[13-15] Moreover, loading sufficient amount of drugs and achieving drug concentrations at target sites equal to or above minimum effective levels remain a challenge.[16] To this

end, conjunctival inserts, placed in the lower conjunctival sac beneath the lower eyelid, offer potential as alternatives to conventional ocular drug delivery systems. Depending on the typical day time wearing period, the release needs to be in the range of a few hours. Conjunctival inserts offer benefits such as precise dosing, reduced systemic absorption, minimal side effects, and sustained drug release. Recently, Duman et al. reported that a 3D-printed ocular insert based on polycaprolactone (PCL) combined with a liposomal strategy could support and enhance delivery of moxifloxacin to the eye. The inserts were fabricated using a melt-extrusion 3D printing technique with a PCL filament. Moxifloxacin was loaded into liposomes which were then incorporated into the PCL matrix during the printing process. A key finding of this work was the successful sustained release of moxifloxacin from the inserts over a period of 7 days *in vitro*. The *ex vivo* corneal permeation studies demonstrated significantly higher moxifloxacin penetration compared to conventional eye drops. The loading amount of moxifloxacin in the inserts was optimized, and the results showed a high encapsulation efficiency of the liposomal drug within the PCL matrix.[17] However, while supporting a relatively long term release of Moxifloxacin for up to 7 days, the mechanical properties of PCL may compromise patient comfort. In addition, PCL holds a slow biodegradation profile of up to two years and therefore, insert removal after the release period would be another concern. In another study, hot melt extrusion printing was coupled with fused deposition modelling for 3D-printing of a hydroxypropyl cellulose insert loaded with ciprofloxacin and it was shown that the insert was capable of sustained ciprofloxacin release *in vitro* for over 24 hrs. The *ex vivo* studies using porcine corneas showed enhanced drug permeation compared to conventional eye drops.[16] Ocular inserts have been previously commercialised and Ocusert™ was the first controlled-release polymer drug delivery system that exemplified this approach. Placed beneath the lower eyelid, this device administered the active ingredient pilocarpine to treat glaucoma. The device delivered the drug at a consistent rate over the course of one week, offering superior efficacy compared to pilocarpine eye drops, resulting in reduced incidence of side effects.[18] Ultimately it was discontinued due to low uptake and the release of more effective drugs to treat glaucoma.

In addition, degradation is a necessity in biomedical applications.[19] Of note, biodegradable polymers have been used for fabricating drug delivery systems and are known to improve the drug efficacy by controlling the release rate.[20] These polymers could also be moulded in any shape or size and polymerized using photo-crosslinking. According to the International Union of Pure and Applied Chemistry (IUPAC), ‘degradable polymers’ undergo in vivo degradation resulting solely from hydrolysis by the water present in tissues and organs, referred to as hydrolysis or hydrolytic

degradation.[21] Depending on the intended use, different products may require different stability or degradation properties.[22] For instance, in the case of chronic implantable biomedical devices, the polymers must be stable in biological environments for the device to perform their optimal function for a specified time period. which could last for a few years. Contrary to this, the degradation time for the polymers used to design tissue engineering scaffolds should be comparable to the tissue healing process, which could last from a few weeks to months. Similarly, the optimal degradation time frame for polymers used in drug delivery applications may range from few hours to months. Several factors can control the rate of degradation of polymeric biomaterials, including crosslink density, degree of substitution, and the presence or absence of pendant groups. One such biodegradable material that could be used for this purpose is gelatin methacrylate (GelMA). GelMA is a biodegradable and biocompatible material, used for a variety of biomedical applications, and can be physically, chemically, or enzymatically crosslinked.[23,24] Of note, the photo crosslinking method used to make GelMA offers several advantages such as mild crosslinking conditions and low cytotoxicity.[25] Moreover, the biocompatible and biodegradable properties of GelMA could also make it possible to explore a new avenue to release incorporated drugs during passive exposures to various ocular enzymes.[26]

Despite considerable advancements in the fabrication techniques of GelMA hydrogels and their extensive utilization across diverse biomedical disciplines, various challenges exist, such as control over pore size and distribution and reproducibility of mechanical properties, necessitating further investigation and development. Owing to the precision and high resolution required for the fabrication of biomedical devices from soft hydrogel-based biomaterials, in this work, a stereolithography (SLA)-based 3D printing technique was employed to fabricate these conjunctival inserts from GelMA-based polymeric ink. Interestingly, SLA-based 3D printing makes it possible to use different photopolymerizable materials loaded with therapeutics of interest.[27] One such therapeutic molecule of interest is polyvinyl alcohol (PVA), which is a commonly used viscosity enhancer in eye drops,[28] with the capability of reducing symptoms of dry eye by stabilizing the tear film and reducing evaporation. Many ocular lubricants to treat moderate dry eye contain PVA.[29]

In this work, we planned to combine the favourable properties of GelMA and PVA to design prototype biodegradable conjunctival inserts which could potentially be used for treatment of dry eyes. Interestingly, GelMA degrades in the presence of collagenases or MMPs and these enzymes are also found on the ocular surface. Additionally, in various ocular conditions, including moderate to severe dry eyes, the levels of MMP9 enzymes are elevated.[7,30] The MMP9 enzyme cleaves collagen/gelatin

chains,[31,32] thereby providing a stimulus for enzymatic degradation of GelMA. As the GelMA chains are cleaved, the PVA molecules from the network structure are released, helping to protect the ocular surface against the negative impact of the DED process.

6.3 Materials and Methods

6.3.1 Synthesis of GelMA

GelMA was prepared by the direct reaction of 40 g Type A gelatin with methacrylic anhydride (1% v/v, Sigma, St. Louis, MO, USA) in 400mL carbonate bicarbonate buffer (12.5 mM sodium bicarbonate, 87.5 mM sodium carbonate anhydrous, pH 9.4) buffer at 50°C for 1 hr. The substitution reaction was stopped by adding by 6mL of 10% acetic acid and the resulting product was dialyzed in 12-14 kDa dialysis tubes (Sigma, St. Louis, MO, USA) in deionized water for 24 hr to remove low molecular weight impurities. After dialysis, the GelMA solution was freeze dried and stored at -80°C until further use.

6.3.2 Preparation GelMA and P-Gel-5% ink

To prepare the P-Gel-5% prepolymer solution, GelMA (20% w/v) was dissolved in LAP solution (1.2% w/v, Sigma 900889, St. Louis, MO, USA) in phosphate-buffered saline (PBS, Fisher Scientific, Waltham, MA, USA). Separately, a PVA solution (10% w/v, molecular weight 89-98 kDa, 99+% hydrolyzed, Sigma, St. Louis, MO, USA) was prepared in PBS and heated at 90°C until fully dissolved. The two solutions were combined in a 1:1 ratio, resulting in the P-Gel-5% prepolymer solution containing GelMA (10% w/v), PVA (5% w/v), and LAP (0.6% w/v). For the preparation of GelMA ink, GelMA (10 % w/v) was dissolved in LAP solution (0.6 % w/v) made in PBS at 37 °C. Tartrazine was added (photo-absorber, 0.3% w/v) to GelMA and P-Gel-5% inks and incubated at 37°C for 1 hour prior to use.

6.3.3 3D printing of P-Gel-5% Conjunctival Inserts

Ocular inserts of 4 mm diameter and 1000 μm thickness were designed using computer-aided design software (FreeCAD 0.19) and then 3D-printed using a commercial masked-stereolithography (mSLA) 3D printer (AnyCubic Photon Mono M5, Shenzhen, China). The printer was retrofitted with a

humidity and temperature control kit to enable printing at ~95% humidity and 37 °C (Figure 1). The GelMA and P2-Gel-5% prepolymer ink solutions were mixed gently before use. The 3D-printing photopolymerization process was performed with UV light of wavelength 405 nm. The overall thickness of the insert was 1000 µm, and they were printed with a layer thickness of 100 µm and exposure time of 120 s.[33] The choice of a 1000 µm insert thickness was primarily due to the physical limitations of the SLA 3D printer, including resolution constraints and layer accuracy at smaller dimensions. Printing at 100 µm posed challenges in structural integrity, handling, and post-processing, increasing the risk of deformation. Additionally, the thicker inserts allowed for sufficient drug loading and measurable, sustained release profiles, which would have been difficult to achieve and quantify reliably with ultra-thin constructs. The 1000 µm thickness thus provided a balance between printability, mechanical stability, and experimental reproducibility.

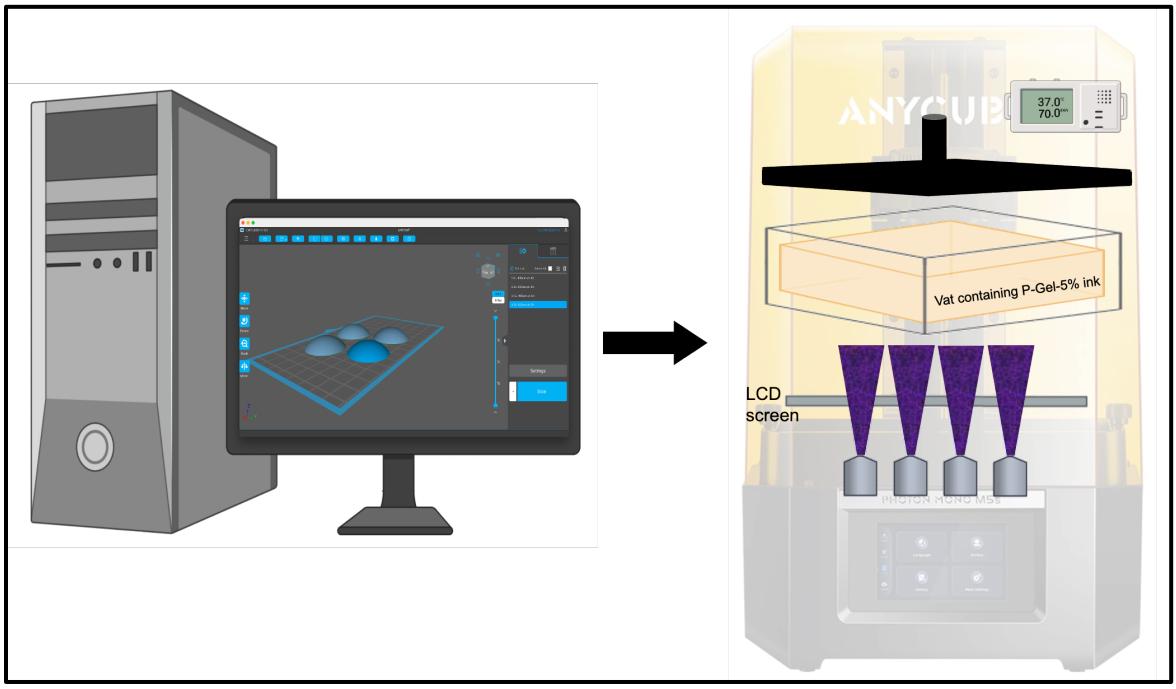


Figure 1. Fabrication of GelMA and P-Gel-5% conjunctival inserts using 3D printing

6.3.4 Mechanical Testing

Mechanical properties of the GelMA and P-Gel-5% hydrogel samples were measured in compression mode using a universal testing machine (UTM, Texture Analyser XT Plus, Hamilton, MA, USA). The test was conducted on hydrogel samples (12 mm height and 10 mm diameter) that were

swollen for 24 h in PBS buffer at pH 7.4. The samples were gently dabbed and placed in the middle of the stage, and a load cell of 5 kg was applied. Each measurement was repeated three times.

6.3.5 Equilibrium Swelling

Swelling ratios of the hydrogels were determined using a gravimetric approach. Initially, the hydrogel discs were freeze-dried (at −80 °C and 133 × 10^{-3} mbar), and their weights were recorded. They were then immersed in 4 mL of PBS at 35 °C with gentle agitation at 50 rpm, allowing them to swell for 24 h. At specific time intervals, the samples were taken out of the PBS; excess surface water was carefully blotted off, and their weights were measured at specific time intervals until equilibrium swelling was achieved. The swelling ratio at any given time *t* was calculated using the following equation:

$$\text{Swelling ratio} = (W_t - W_i)/W_i * 100$$

where W_i represents the initial dry weight of the hydrogels, whereas W_t is defined as the weight of the swollen hydrogels at time *t*.

6.3.6 Water Contact Angle

To evaluate hydrophilicity of the hydrogels, water contact angles of the GelMA and P-Gel-5% samples were measured using an Optical Contact Analyzer (DataPhysics Instruments GmbH, Filderstadt, Germany), via sessile drop technique. In brief, 8 µl of high-performance liquid chromatography grade water was deposited on the surface at a rate of 2 μls^{-1} and imaged once the droplet was settled. Water contact angles of the resulting images were analysed using SCA 20 software (version 2.04, Build 4). For each hydrogel, three separate droplets were quantified across the surface and the reported values are an average of these independent measurements.

6.3.7 Biodegradation of P-Gel-5% inserts by MMP9

P-Gel-5% inserts (4 mm diameter and 1 mm thickness) were 3D printed. These inserts were gently washed with warm PBS and briefly dried using a Kimwipe™ (Kimberly-Clark Professional 34155, Irving, TX, USA) and their weights were measured on a scale and recorded. Next, inserts were added to 1.7 ml microcentrifuge tubes with 1mL of enzyme solution containing varying MMP9 (Gibco, Billings, MT, USA) concentrations dissolved in 1X PBS. Samples were incubated, with gentle

agitation, at 37 °C. At each indicated time point, samples were briefly vortexed, and 50 ml of the solution was removed for detection of PVA.

6.3.8 Scanning Electron Microscopy

To investigate the biodegradation mechanism of the conjunctival inserts, the 3D-printed samples were incubated in a 50 μg/mL MMP9 enzyme solution for 24 h. Following degradation, the inserts were frozen at −80 °C overnight and subsequently freeze-dried for 24 h using a Labconco Freeze Dry System Freezone 2.5 Liter (7670000, Kansas City, MO, USA). The freeze-dried samples were then mounted on an aluminum stub using double-sided adhesive conductive carbon tape and analyzed using environmental scanning electron microscopy (ESEM, Quanta FEG 250, FEI Company, Hillsboro, OR, USA).

6.3.9 Release and Detection of PVA

The ocular inserts containing 5% (w/v) PVA (P-Gel-5%) were incubated in glass vials with 1 mL of PBS solution at 37 °C and 50 rpm. At each indicated time point, 200 μL of the solution was removed for detection of PVA and replaced with fresh PBS. For detection of PVA, a solution of iodine (150 mM potassium iodide, 50 mM diiodine in deionized water, Sigma 221945 and 207772, St. Louis, MO, USA) and borate (64.7 mM boric acid in deionized water, Sigma B0394, St. Louis, MO, USA) was mixed in 1:5 ratio of iodine solution:borate solution to generate the PVA detection solution. The solution was gently inverted 4–6 times in a conical tube to ensure even mixing. To measure PVA in solution, 163.6 μL of PVA detection solution was added to 36.4 μL of samples of interest in a 96-well plate and incubated at room temperature for 20 min with gentle shaking. The absorbance of the unknown samples, in addition to a set of standard samples of known PVA concentrations prepared in 1X PBS, was read at 630 nm using an Imaging Multimode Plate Reader (Cytation 5, Agilent BioTek Instruments, Winooski, VT, USA).[34] The PVA release was quantified using a calibration curve method.

This curve was plotted for standard solutions ranging from 10–250 µg/mL. The R^2 value for the calibration curve was 0.9997.

6.3.10 Drug Release Kinetics via Mathematical Modeling

To evaluate the release kinetic profiles of the samples over the studied time duration, different mathematical models were studied [35]. These included the zero- and first-order release model, Higuchi release model, and Korsmeyer–Peppas model. The graphs were plotted as mentioned in Table 2, and the coefficient of determination (R2) was calculated for each model.[36]

(a) Zero order model: In this model, the drug release is represented by:

$C_t = C_o + K_o t$

where C_t is the amount of drug released at time t, C_o is the initial concentration of drug in solution (at t=0), and K_o is the zero-order rate constant. The graph is plotted between cumulative drug release *vs.* time and the coefficient of determination (R^2) was calculated.

(b) First order model: In this model, the drug release is represented by:

$dC/dt = -K_1 C$

where K_1 is the first order rate constant

After rearranging and taking integral,

$\log C_t = \log C_o - (K_1/2.303)t$

where C_t is the amount of drug remaining at time t and C_o is the initial concentration of the drug. The graph is plotted between log cumulative % drug remaining *vs.* time and the coefficient of determination (R^2) was calculated.

(c) Higuchi model: In this model, the drug release is represented by:

$M_t/M_\infty = K_h t^{1/2}$

where M_t/M_∞ is the fraction of drug released at each time point, M_t is the amount of drug released in time t, M_∞ is the amount of drug released after infinite time, and K_h represents the Higuchi release kinetic constant. The graph is plotted between cumulative % drug release *vs.* square root of time and the coefficient of determination (R^2) was calculated.

(d) Korsmeyer-Peppas model: In this model, the drug release is represented by:

$M_t / M_\infty = K_{kp} t^n$

$\log (M_t/M_\infty) = \log K_{kp} + n \log t$

where M_t/M_∞ is the fraction of drug released at time t, M_t is the amount of drug released in time t, M_∞ is the amount of drug released after infinite time. n is the diffusional exponent or drug release exponent and K_{kp} is the Korsmeyer-Peppas release rate constant. The graph is plotted between log cumulative % drug release vs. log t and the coefficient of determination (R^2) was calculated.

The graphs were plotted as mentioned in *Table* 1 and the coefficient of determination (R^2) was calculated for each model.

***Table* 1.** Curve fitting of various models for drug release kinetics

	Zero Order	**First Order**	**Higuchi model**	**Korsmeyer-Peppas model**
Equation	$C_t = C_o + K_o t$	$\log C_t = \log C_o - (K_1/2.303)t$	$M_t/M_\infty = K_h t^{1/2}$	$\log (M_t/M_\infty) = \log K_{kp} + n \log t$
Graph	cumulative drug release vs. time	log cumulative % drug remaining vs. time	cumulative % drug release vs. $\sqrt{t}$	log (cumulative % drug release) vs. log t

6.3.11 Statistical Analysis

Statistical analysis was performed using GraphPad Prism Version 10.0 (GraphPad Software, La Jolla, CA, USA). All data are reported as mean and standard deviation unless otherwise stated. Two-way ANOVA was performed to determine differences across testing groups wherever applicable. Tukey's multiple comparison tests were used when necessary. In all cases, statistical significance was considered significant for a p-value of <0.05 unless otherwise stated.

6.4 Results and Discussion

6.4.1 3D printing of Ocular Inserts

Figure 2 shows the 3D-printed P-Gel-5% conjunctival inserts. The discs were 4 mm in diameter and 1000 µm in height and were printed in about 30 min. Multiple conjunctival inserts could be fabricated at once, as shown on the print plate of the 3D printer. Notably, 3D printing offers precise control over dimensions, ensuring reproducibility. Previous studies indicate that a good photocurable biomaterial ink for projection-based printing techniques such as SLA LCD printing should meet three major requirements: (a) rapid photo-crosslinking rate, (b) dense crosslinking structure, and (c) excellent fluidity (for rapid filling of gaps and spaces) [37]. In this work, GelMA was selected as a base material owing to its biocompatibility and demonstrated high levels of controllability as well as consistency across batches [38, 39].

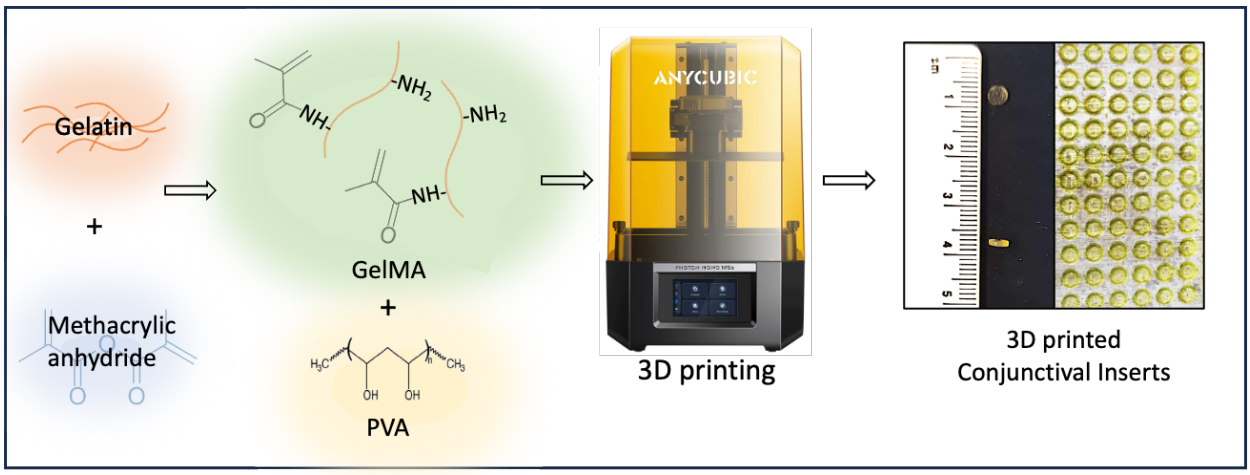


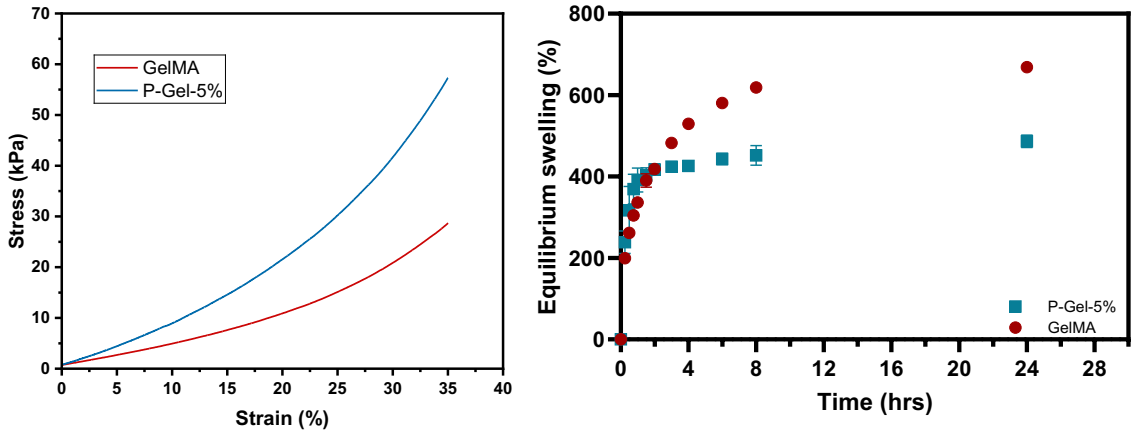
***Figure* 2.** 3D printing of PVA-loaded conjunctival inserts.

The P-Gel-5% inserts formed a semi-interpenetrating network in this case where only one polymer phase, GelMA, was chemically crosslinked, and PVA was dispersed inside the GelMA matrix. Interestingly, PVA can also undergo supramolecular interactions (H-bonding) with GelMA chains, which contributes to the higher structural stability of the P-Gel-5% inserts. Reports suggest that the interpenetrating network hydrogels align with the requirements of extrusion-based 3D printing. [40-42] However, vat polymerization-based techniques offer higher geometrical complexity and higher shape

fidelity [27]. While 3D printing involves a semi-interpenetrating network, it should be noted that the presence of PVA should not interfere with crosslinking of the acrylate species; thus, in this work, PVA was kept at a lower concentration of 5% *w/v* [43]. Also, the 3D printing conditions, such as the dye concentration and UV exposure time, were aptly selected, along with appropriate environmental conditions, including temperature (~37 °C) and humidity (~70% RH). It should be noted that despite the high water content of these inserts, they could be 3D-printed with a high shape fidelity characterized by flat surfaces and clean and sharp edges.

6.4.2. Mechanical Testing, Equilibrium Water Content (EWC), and Water Contact Angle

The data from mechanical testing in compression mode (Figure 3a) indicate the physically stronger nature of the P-Gel-5% hydrogels compared to GelMA hydrogels. This could be attributed to the presence of PVA crystalline domains in the P-Gel-5% semi-interpenetrating network [44]. The addition of PVA to GelMA leads to the formation of hydrogen bonds and small ordered regions called crystalline domains dispersed inside the GelMA matrix. The PVA crystalline domains can be described as a layered structure held together by hydroxyl bonds along with weak van der Waals forces operating between two layers [45]. Higher amounts of PVA chains lead to the formation of more hydrogen bonds and crystalline regions, forming a relatively stiffer network [46].



(**a**) (**b**)

Figure 3. (**a**) Mechanical strength and (**b**) equilibrium swelling graphs for GelMA and P-Gel-5% samples.

Additionally, the supramolecular interactions (H-bonding) between the -OH/-NH_2 groups of PVA and GelMA, respectively, also contribute to the higher mechanical strength and lower equilibrium swelling of the P-Gel-5% hydrogels. These supramolecular interactions as inferred from the scanning electron microscopy images of P-Gel-5% hydrogels, where P-Gel-5% forms a semi-interpenetrating network [36]. As previously mentioned, during the freezing step in the lyophilization process, thermally induced phase separation occurs between the solvent phase and the polymer phase, creating a polymeric network [47]. GelMA hydrogels display a larger pore size due to the presence of a lower polymeric phase in GelMA hydrogels (10% GelMA) compared to the P-Gel-5% hydrogels (10% GelMA and 5% PVA). Thus, the presence of a lower polymeric phase in GelMA hydrogels allows it to hold more water to undergo ice crystal formation during the freezing step of lyophilization. The PVA molecules might penetrate and partially fill the free voids between GelMA chains, thus forming smaller-sized pores between the crosslinked GelMA chains, thus increasing the crosslinking density. The increased crosslinked polymer fraction gives more resistance to the compressive force and, hence, higher mechanical strength to the P-Gel-5% hydrogels [48].

Reportedly, the molecular chains of gelatin can extend more easily compared to the PVA polymer chains [49]. This is further corroborated by the results from the equilibrium swelling curves for GelMA and P-Gel-5% hydrogels, as shown in Figure 3b. From the swelling curves, it can be inferred that there is a decrease in the degree of swelling in P-Gel-5% samples compared to GelMA hydrogels. Previous studies suggest that higher swelling leads to higher degradation and lower mechanical strength, which also aligns with our results [49]. The interplay between degradation rate and mechanical properties of GelMA/PVA hydrogels could be used to fabricate conjunctival inserts with desired functionalities. For instance, if the degradation rate is too fast, it would lead to the mechanical failure of these inserts, impacting the drug release profiles. Moreover, the relative amount of crystalline and amorphous phases of PVA present is a key determinant of the macroscopic properties of the P-Gel-5% hydrogels. An increase in the crystalline fraction of PVA can cause a decrease in the water permeability of the P-Gel hydrogels compared to GelMA [46, 47, 50, 51].

Figure 4 shows the water contact angles of the GelMA and P-Gel-5% samples. The water contact angle of GelMA samples was 60.6°, and the P-Gel-5% sample's angle was 61.5°, indicating their hydrophilic nature. These results were not significantly different from each other ($p = 0.1268$). A measured contact angle of 61° indicates moderate hydrophilicity, suggesting that the surface is wettable

but not highly so. In the context of contact lenses, this value is acceptable but falls short when compared to commercial soft lenses, which typically exhibit lower contact angles in the range of 20° to 40° to ensure better wettability and wearer comfort. For instance, Etafilcon A lenses (e.g., Acuvue) demonstrate angles as low as 22°–30°, while silicone hydrogel lenses (Senofilcon A and Lotrafilcon B), after surface treatment, achieve 24°–45°. These lower angles contribute to enhanced tear film stability and ocular surface interaction, which are critical for long-term comfort. While a 61° angle may be less favourable for daily-wear lenses, it remains within a usable range for short-term therapeutic applications or drug-eluting inserts, where comfort is secondary to functionality. Nonetheless, further surface optimization, such as blending with hydrophilic polymers or employing post-processing modifications, could improve wettability and better align the material properties with those of commercially available lenses.

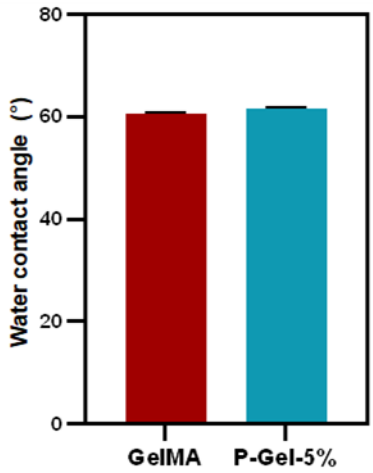


***Figure* 4.** Water contact angle for GelMA and P-Gel-5% conjunctival inserts.

6.4.3. PVA Release from P-Gel-5% Inserts in the Presence of MMP9

The PVA release curves depict the PVA released from the 3D-printed ocular inserts (Figure 5) in the presence of different concentrations of MMP9 enzymes (25 µg/mL, 50 µg/mL, and 100 µg/mL). About 119.5 ± 9.4 µg of PVA was released from P-Gel-5% inserts at the end of 24 h without the presence of MMP9. In the presence of the MMP9 enzyme, about 222.7 ± 20.3 µg, 265.5 ± 27.1 µg, and 242.7 ± 30.4 µg of PVA were released when exposed to 25 µg/mL, 50 µg/mL, and 100 µg/mL of MMP9 at the end of 24 h (Figure 5). This increased amount of PVA release can be attributed to faster

disintegration of the semi-interpenetrating network in the presence of elevated enzyme concentrations, thus favoring higher release of PVA.

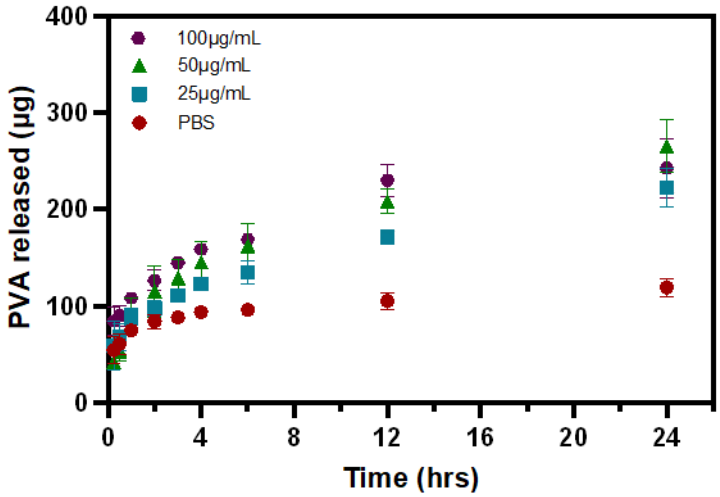


***Figure* 5.** PVA release curves of 3D-printed P-Gel-5% conjunctival inserts in the presence of varying concentrations of MMP9 enzyme.

The 24-hour drug release profile demonstrated in this study was primarily selected to allow for direct observation of material behaviour and drug elution over a manageable experimental timescale. However, whether this release duration is sufficient depends on the clinical context. For chronic ocular conditions such as dry eye disease, longer release durations—ranging from several days to a few weeks—would be more desirable to reduce dosing frequency and improve patient compliance.

6.4.4. Biodegradation of P-Gel-5% Inserts in the Presence of MMP9

Figure 6 shows the biodegradation profile of the P-Gel-5% conjunctival inserts in the presence of MMP9 enzyme. About 96.02%, 83.36%, and 81.72% of the P-Gel-5% inserts were degraded at the end of 8 h, 12 h, and 24 h in the presence of 100, 50, and 25 µg/mL of MMP9, respectively. These results suggest that enzyme concentration play a significant role in MMP-mediated degradation of GelMA hydrogels. Different MMPs have varying affinities for GelMA and degrade it at different rates; however, the degradation rate is a function of MMP9 enzyme concentration. Moreover, the concentration of specific MMPs in the surrounding environment influences the degradation kinetics.

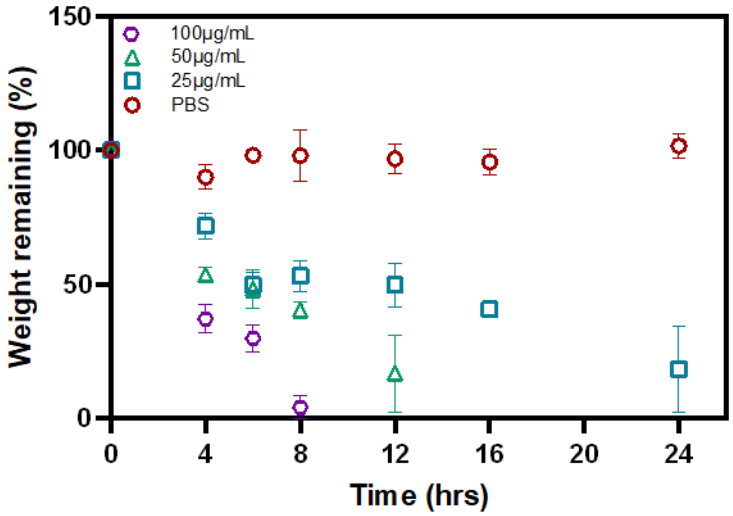


***Figure* 6.** Biodegradation profiles of 3D-printed conjunctival inserts in the presence of varying concentrations of MMP9 enzyme (Error bars indicate standard deviations).

No degradation was observed in the control groups incubated in PBS, at the end of the study duration of 24 h (Figure 7(A1,A2)) as there no enzyme was present. As previously stated, GelMA degrades in the presence of collagenases or MMPs, and these enzymes are found on the ocular surface. [7] MMP levels are elevated in certain ocular conditions such as corneal wound healing, ulceration, and uveitis, and they show collagenolytic activity [52]. Research shows that MMP-9 is elevated in the tears of dry eye patients [7, 30]. The gelatinase MMP9 enzyme cleaves collagen chains α1(V) and α(XI) between Gly-439 and Val-440 and the α2(V) chain between Gly-445 and Leu-446 [31, 32]. As degradation of gelatin chains occurs in the presence of MMPs [53], the mechanical properties of GelMA-based conjunctival inserts are also impacted by the MMP-mediated degradation process. The degradation profile of GelMA is affected by similar parameters that also influence the stiffness of the hydrogel, such as the degree of substitution [54], the concentration of photoinitiator used, and the intensity and time of UV exposure during the photocrosslinking process [55]. As the enzymes move through the polymer matrix, they break down crosslinks, effectively reducing the crosslink density (Figure 7(B1,B2)). This reduction leads to an expansion of the polymer mesh. Eventually, the degradation process reaches a critical point known as the reverse gelation point. At the reverse gelation point, the polymer undergoes a drastic shift in its structural integrity. The connectivity of the network declines sharply, causing a transition from a gel-like state to a more fluid-like state [56].

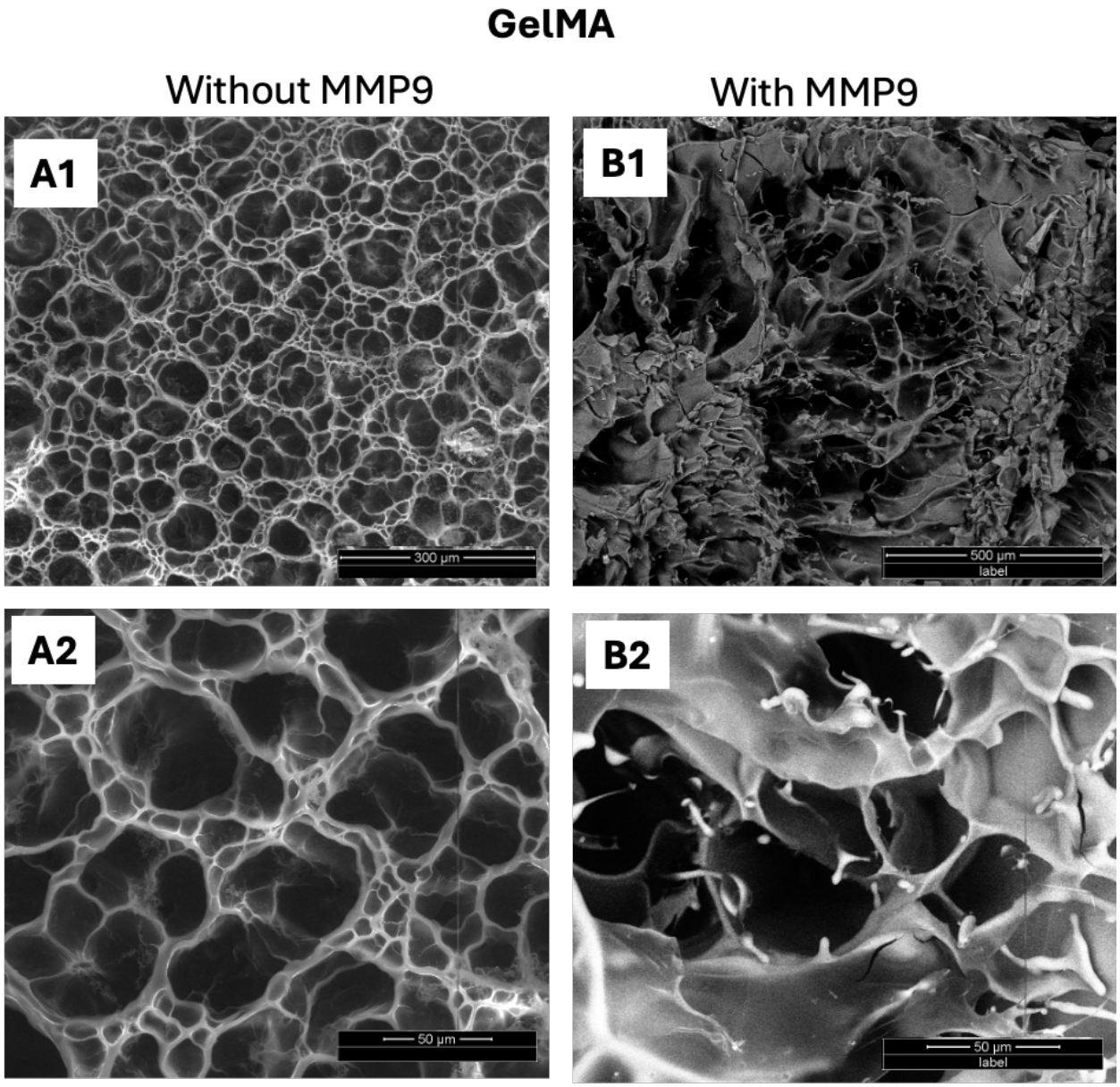


***Figure* 7.** Morphological changes in GelMA inserts (**A1**,**A2**) before and (**B1**,**B2**) after exposure to 50 µg/mL MMP9 enzyme for 24 h.

Interestingly, upon the addition of PVA to GelMA, hydrogen bonds are formed between PVA and GelMA.[36] Moreover, owing to the inherent crystalline nature of PVA, small ordered regions called crystalline domains are scattered inside the GelMA matrix, which leads to the formation of a relatively stiffer network (Figure 8(A1,A2)) [46]. This is further supported by previous reports, which

suggest that the reduced pore size in highly crosslinked GelMA-based soft hydrogels may create a membrane-like structure that is difficult for the MMP enzymes to penetrate through. Owing to the mechanically robust nature of P-Gel-5%, increased crosslinking density, and narrower pore size, the time needed for enzymatic cleavage is longer [26]. This could be the plausible explanation for the slower biodegradation rate of P-Gel-5% in the presence of MMP9 (Figure 8(B1,B2)) compared to GelMA alone, as shown in our previous works [57].

The concentration of MMP-9 used in the degradation assays (in the μg/mL range) was intentionally elevated to accelerate hydrogel breakdown and simulate an enzyme-rich inflammatory environment. In reality, physiological MMP-9 concentrations on the ocular surface are in the ng/mL range, even in patients with moderate-to-severe inflammation. Therefore, in vivo degradation is expected to be substantially slower, which would likely lead to prolonged drug release compared to in vitro observations. This discrepancy suggests that the current model may overestimate degradation rates, highlighting the need for more physiologically relevant enzyme concentrations in future studies. Additionally, it is possible that a threshold concentration of MMP-9 may be required to trigger degradation, suggesting that these materials might remain relatively stable under healthy ocular conditions but degrade more actively in inflamed environments—offering a form of pathology-responsive release.

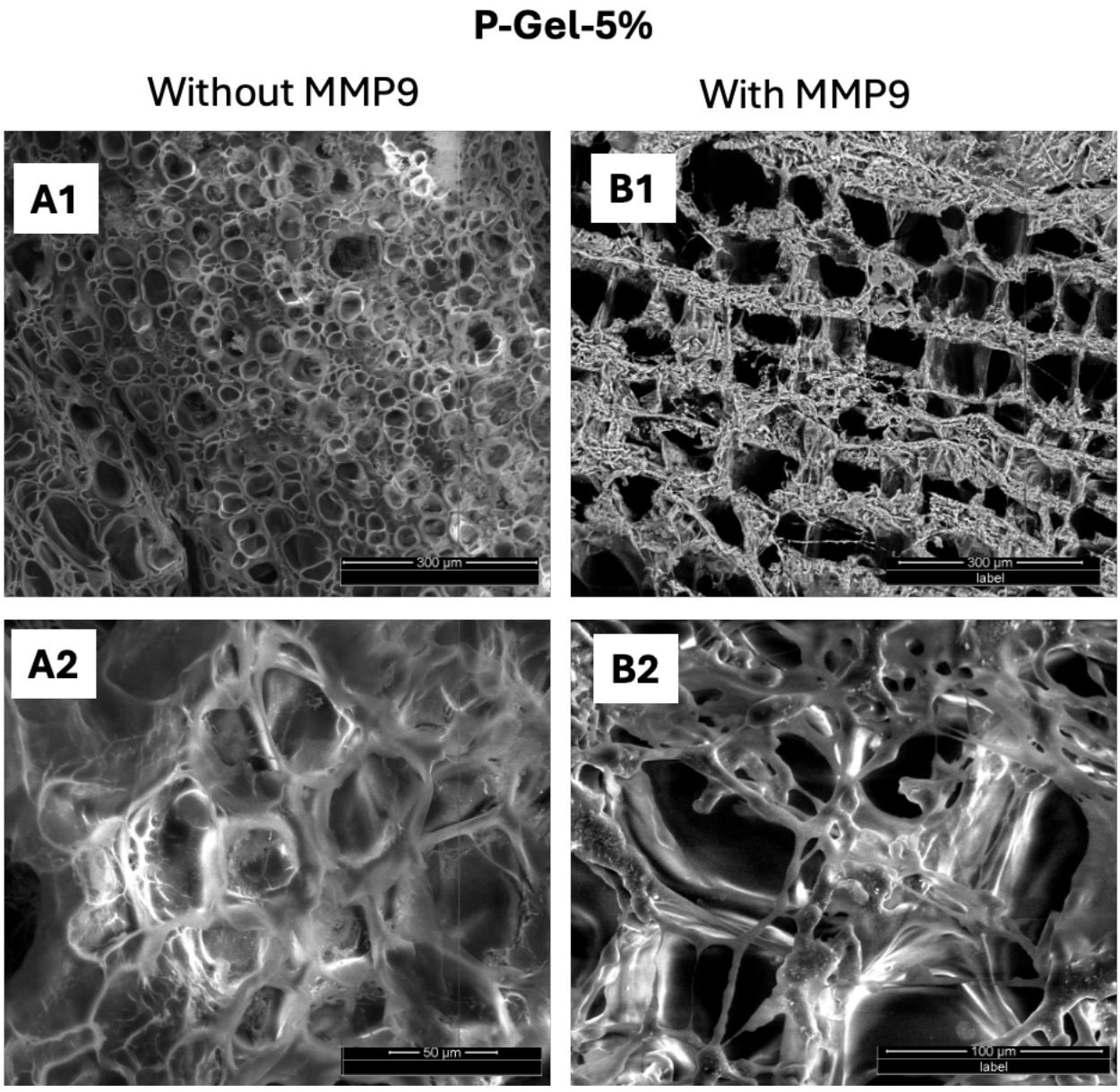


***Figure* 8.** Morphological changes in P-Gel-5% inserts (A1,A2) before and (B1,B2) after exposure to 100 µg/mL MMP9 enzyme for 24 h.

The incorporation of PVA into the GelMA network facilitates the formation of hydrogen bonds, leading to the development of crystalline domains that are dispersed within the GelMA matrix [36]. This suggests that the release of PVA is dependent on the rate of degradation of the GelMA network because the environmental conditions, such as incubation temperature and pH, are kept constant. Therefore,

disruption of this H-bonding, and, hence, PVA release, is mediated by MMP9 enzymes acting on the GelMA network structure. As discussed earlier, the rate of GelMA degradation is a function of MMP9 enzyme concentration; therefore, higher enzyme concentrations display faster degradation and, hence, the faster release of PVA (Figure 9d). As the enzyme concentration decreases to 50 µg/mL (Figure 9c) and 25 µg/mL (Figure 9b), the rate of degradation becomes slower, and, consequently, the rate at which the PVA-GelMA supramolecular interactions (H-bonding) are disrupted is slower. This is evident from the slope of the PVA release curves in Figure 9. However, in control samples where no enzyme was present, no degradation of the P-Gel-5% insert was observed (Figure 9a), and the PVA release from these samples was relatively low and at a slower rate, as observed from the slope of these curves in the first few hours of release.

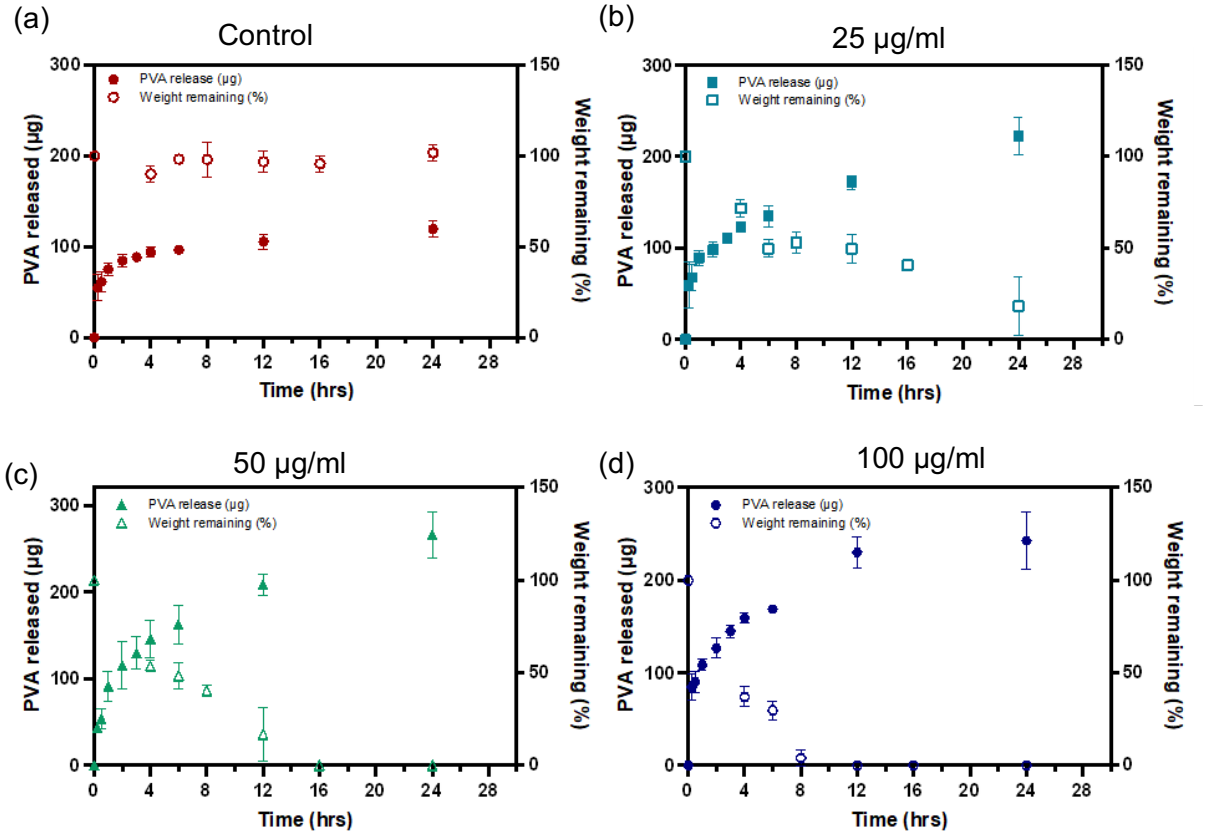


***Figure* 9.** Correlation between the biodegradation profiles and PVA release curves of 3D-printed conjunctival inserts in the presence of varying concentrations of MMP9 enzyme (**a**) control, (**b**) 25 µg/mL, (**c**) 50 µg/mL, and (**d**) 100 µg/mL.

6.4.5. Release Kinetics in the Presence of MMP9 Enzymes

Predicting the degradation pattern of these inserts is essential to optimize drug release timing and minimize discomfort associated with material breakdown or residue. This can be approached through a combination of mathematical modeling (e.g., enzyme-substrate kinetics or diffusion-degradation models) and empirical data on degradation profiles under various MMP9 concentrations. By correlating enzyme levels, crosslink density, and insert composition with observed mass loss or structural changes, it could be possible to forecast how long the insert remains intact and when it becomes fully resorbed. Such predictive tools would allow tailoring insert properties to individual patient needs—ensuring that degradation aligns with both therapeutic goals and comfort thresholds, such as avoiding fragmentation during wear or ensuring complete clearance from the ocular surface.

To study the drug release kinetics and how different factors affect the dissolution velocity and behaviors, various mathematical equations describing the release dependence on time were used. The drug release was evaluated through four main release kinetic models: zero-order, first-order, Higuchi model, and Korsmeyer–Peppas model by linear regression (Figure 10) and non-linear regression (Figure 11). To evaluate the best-fit model for the release profiles in our study, the goodness of fit for each model or the coefficient of determination (R^2) was calculated using GraphPad Prism 10 (Table 3). The release profiles of the P-Gel-5% containing hydrogels in the presence of different concentrations of MMP9 showed the highest linearity with the Korsmeyer–Peppas model, as shown in Table 3. The release exponent (n) for the Korsmeyer–Peppas model was calculated from the slope of the graph between $\log(M_t/M_\infty)$ versus $\log t$. The n-values indicate that these systems follow Fickian diffusion. The release exponent (n) values below 0.5 confirm the diffusion-controlled behavior rather than swelling or erosion-driven release. This finding has important practical implications: it suggests that the rate and duration of drug release can be effectively tuned by modifying polymer composition, crosslink density, or device geometry, without the need for complex reservoir systems. Moreover, understanding that diffusion is the dominant mechanism enables predictive modeling of release kinetics for different drugs or dosing needs, providing a robust framework for rational design of next-generation inserts with controlled and sustained drug delivery profiles.[58]

Table 3. The coefficient of determination (R^2) values of PVA release from P-Gel-5% in PBS and MMP9 (25 µg/mL, 50 µg/mL, and 100 µg/mL) calculated by using different kinetic models.

Kinetic Model	PBS	25 µg/mL	50 µg/mL	100 µg/mL
Zero-order	0.7143	0.9160	0.8490	0.8135
First order	0.9420	0.9420	0.8983	0.8399
Higuchi	0.8910	0.9947	0.9734	0.9528
Korsmeyer–Peppas	0.9785	0.9896	0.9812	0.9809
Diffusion exponent (*n*-value) *	0.1685	0.2852	0.3995	0.2518

* Calculated by the linear regression of Korsmeyer–Peppas equation of $\log(M_t/M_\infty)$ versus $\log t$.

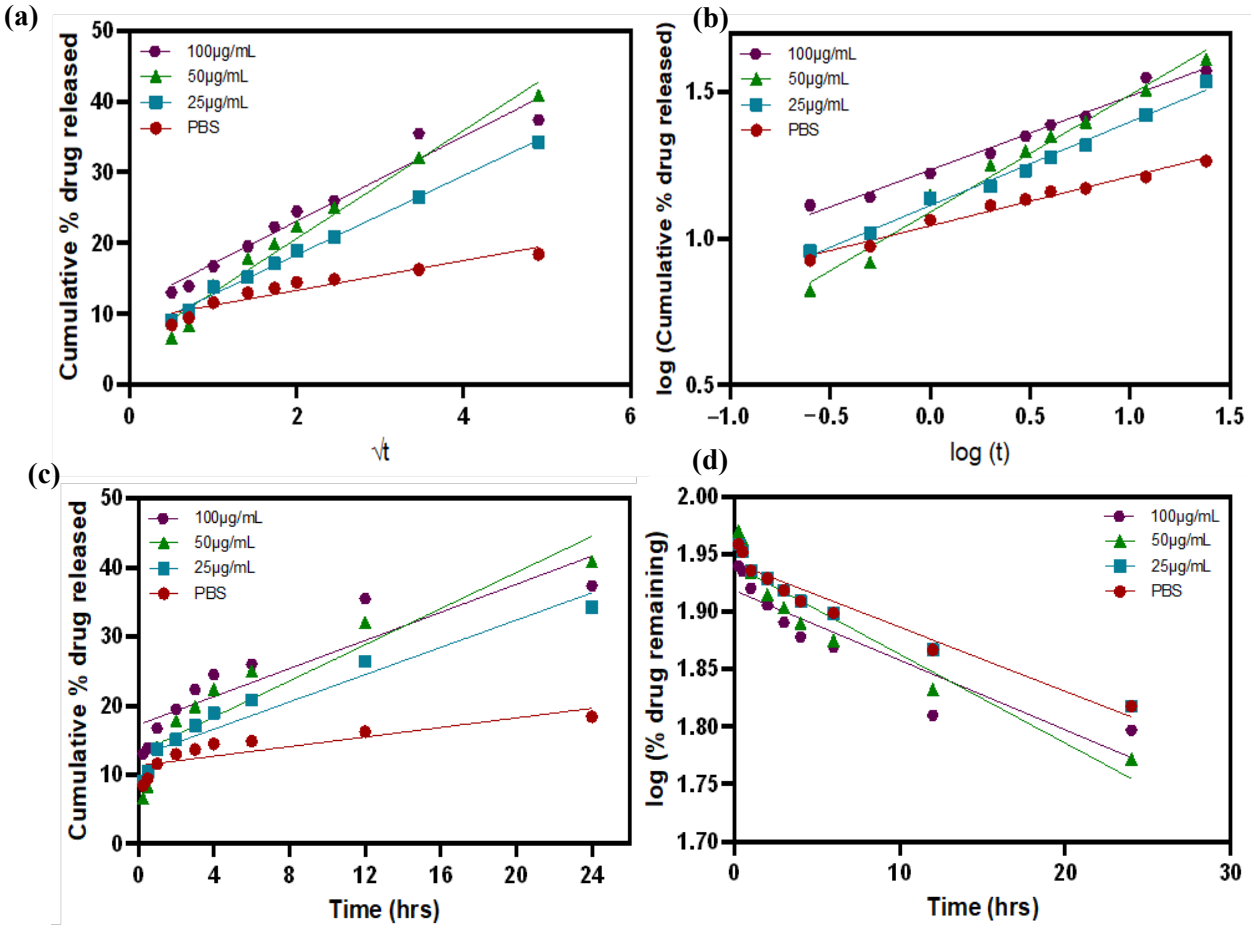


***Figure* 10.** Modeling of the PVA release data on well-known mathematical models: (**a**) zero order, (**b**) first order, (**c**) Higuchi's model, and (**d**) Korsmeyer–Peppas model.

In this study, release kinetics were analysed using linear regression of transformed data to assess fit against established models such as zero-order, first-order, Higuchi, and Korsmeyer–Peppas models. While this method offers straightforward implementation and interpretability, it relies on data transformation, which may introduce bias or distort variance structure. An alternative approach is nonlinear regression (*Figure* 11), which fits the original (untransformed) data directly to model equations, often yielding more accurate parameter estimation and better handling of residuals. Preliminary nonlinear fitting conducted for comparison in this study produced similar trends and model fits, supporting the robustness of the findings. Future studies may benefit from a fully nonlinear regression framework, especially when optimizing formulations or comparing across systems with more complex release behaviour.

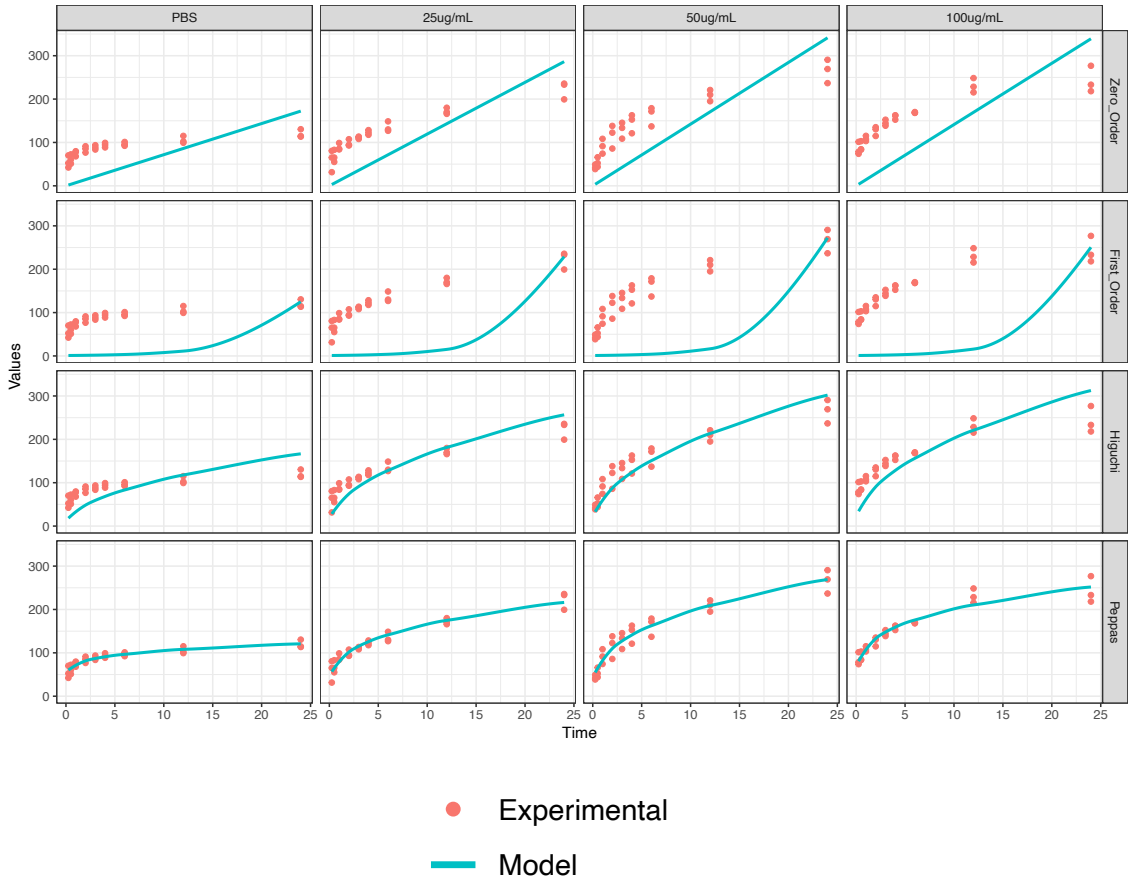


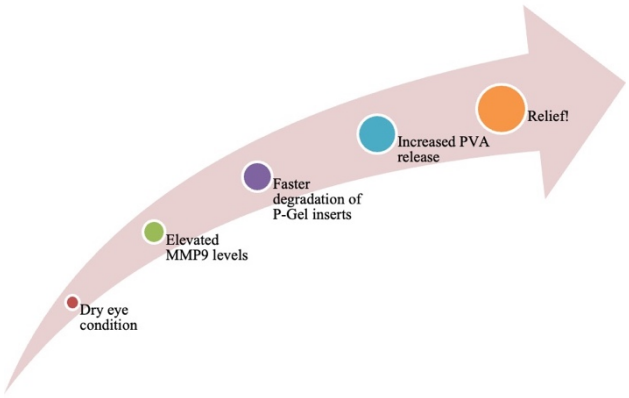
***Figure* 11.** Modelling of the PVA release data on well-known mathematical models: (a) zero order, (b) first order, (c) Higuchi's model, and (d) Korsmeyer-Peppas model using non-linear regression.

In vivo factors such as tear flow, blinking, and dilution effects can influence drug clearance and material degradation in ways that are not fully captured in static in vitro models. As a result, release kinetics in the eye may deviate from model predictions, and actual drug exposure could be either higher (due to prolonged retention) or lower (due to mechanical washout). Ideally, these inserts should demonstrate predictable, sustained degradation over 3–7 days, matching the typical duration between clinical visits or lens replacement cycles. The goal is to create a system that is biodegradable, self-eliminating, and capable of maintaining therapeutic drug levels within the tear film or ocular surface tissues throughout this period. Achieving this balance requires fine-tuning the crosslinking density, drug-polymer interactions, and responsiveness to ocular-specific stimuli, all of which are important directions for future development.

While this research focuses on achieving therapeutic efficacy through sustained ocular drug delivery, the question of maximum drug exposure and potential toxicity is equally important. Although in vitro cytotoxicity assays confirmed that the materials and released PVA concentrations were non-toxic to ocular cells, the cumulative exposure over time, especially under reduced tear turnover or compromised ocular clearance, could lead to localized accumulation. Future work should include in vivo studies to assess maximum tolerable exposure levels, drug retention dynamics, and any potential dose-dependent inflammatory responses, ensuring both safety and efficacy in real-world conditions.

4. Conclusions

In summary, this work highlights the versatile 3D-printing abilities of GelMA to design conjunctival inserts. The results from this study demonstrate the mechanism of degradation of GelMA/PVA-based conjunctival inserts by MMP9 enzymes and its correlation with the release of PVA, a well-known wetting agent for the treatment of dry eyes. Interestingly, these MMP9 enzymes are also found on the ocular surface and are elevated in ocular conditions such as dry eye disease. These elevated levels can be utilized as a feedback mechanism for regulating the degradation rate of PVA from the inserts. The degradation rate of GelMA/PVA is directly correlated with the concentration of the MMP9 enzyme. As the enzyme moves through the polymer matrix, it breaks down crosslinks, reducing the overall crosslink density. Consequently, higher enzyme concentrations accelerate the disruption of PVA-GelMA supramolecular interactions (H-bonding), leading to a faster release of PVA. The release profiles of the P-Gel-5% containing hydrogels in the presence of different concentrations of MMP9 showed the highest linearity with the Korsmeyer–Peppas model. These inserts hold promise as successful drug-delivery devices for the treatment of dry eyes. However, before these inserts can be considered as a commercial product, a complete set of in vitro and in vivo studies needs to be evaluated. These ocular inserts are most suitable for patients with moderate to severe dry eye, where elevated MMP9 levels can effectively trigger polymer degradation and subsequent drug release. The system offers a targeted, pathology-responsive approach that aligns well with the needs of patients who experience more persistent inflammation and may not respond adequately to conventional eye drops. In the future, these inserts could also be explored to deliver a variety of therapeutic molecules of interest to treat various ocular conditions, making them more clinically useful and commercially viable.



Chapter 7

General Discussion

The aim of this thesis was to develop a biodegradable contact lens as an ocular drug delivery system, with the ability of controlled release of PVA using a physical crosslinking method. To avoid the problems associated with contact lens storage such as material degradation and drug release, an on-demand 3D printing method to fabricate a proof-of-concept contact lens and conjunctival insert was developed in this thesis using a low-cost commercial 3D printer.

As mentioned in *Chapter 3*, the first aim was to evaluate the feasibility of fabricating contact lenses using 3D printing. Therefore, owing to its biocompatible nature, GelMA biomaterial-based ink was selected as a base material. Given the budget constraints which leads to lower accessibility of 3D printers, the printing conditions for GelMA-based soft hydrogel materials were optimized for a low-cost vat-based commercial 3D printer. The printer was retrofitted with a humidity and temperature control kit to enable printing at ~60-70% relative humidity and 37 °C temperature. As there are many parameters that can affect the photocuring process, and hence the final print quality, the effects of ink parameters (dye concentration) and print parameters (UV exposure time) on the 3D printing of GelMA hydrogels were discussed. The effectiveness of these optimized parameters was confirmed by successful printing of a prototype soft contact lens, which showed excellent shape fidelity. As an added benefit, 3D printing offers several advantages over traditional contact lens manufacturing processes in terms of fabrication of lenses with complex designs and geometries, customized lenses tailored to the unique topography of each patient's eye, and rapid prototyping, allowing manufacturers to experiment with new designs and materials more efficiently.

With growing advancements in technologies in next few years, latest 3D printers in the market could be explored which might prove to be more durable and maintain constant UV exposure throughout the printer’s lifecycle. Another key point that needs to be considered while retrofitting the 3D printer with the humidifier kit is to protect the electronic components of the 3D printer to increase the life expectancy of the machine. The process described in this thesis considers two key parameters (dye concentration and UV exposure time) to optimize the printing conditions for GelMA ink. As *Chapter 3* mentions several other parameters that influence the final properties of the 3D printed

materials, their effect could be analysed as well in the future. During the experiments, it was observed that if the relative humidity of the printing chamber falls below 50-70%, the GelMA ink starts drying up, thus increasing the ink viscosity in the vat. This, in turn, interrupted the printing process, leading to failed 3D prints. Therefore, 70% was considered as the threshold set value for relative humidity. Overall, these results highlighted that by tuning the print conditions and ink parameters, soft biomaterials from GelMA ink with better shape fidelity and accuracy can be efficiently printed even on a low-cost 3D printer.

Once the process of 3D printing was standardized for GelMA-based contact lenses, the next aim was to load a therapeutic molecule inside these lenses. To this end, *Chapter 4* of this thesis aimed to 3D print a prototype contact lens with PVA as a wetting agent for potential treatment of dry eye disease. As in the previous chapter, the conditions for 3D printing of a GelMA-based contact lens were optimized; it is also important to study the effects of addition of PVA on the ink parameters and overall 3D printing process. Therefore, to understand how PVA could impact the ink-based printing parameters, it is crucial to understand about the crosslinking mechanisms of PVA. Reports suggest that PVA could be either crosslinked physically via freeze thaw cycles or chemically by using aldehydes. However, the UV light used in the photocrosslinking reaction that takes place during the 3D printing process does not crosslink PVA component in the ink, resulting in formation of a semi-interpenetrating network of GelMA and PVA, where the PVA chains are entrapped inside the chemically crosslinked GelMA matrix.

An important consideration while fabricating the ink for PVA containing therapeutic contact lenses is to ensure proper mixing and phase compatibility between GelMA and PVA. This was achieved by mixing the ink using a magnetic stirrer for sufficient time or by addition of phase compatibilizer molecules. If the ink used for fabrication of these ophthalmic devices is not homogenous, it would be hard to predict the physico-chemical behaviour of these materials. For instance, at the interphase, if there is no/weak interaction between GelMA and PVA, structural integrity and mechanical properties of the blend hydrogel devices would be compromised. With development of various formulations for 3D printing with biomaterial inks and hydrogels, changing the chemical compositions and properties can have an impact on the final print quality. As a result, there is a need for an objective screening method to assess whether a new formulation meets or surpasses the required print quality compared to prior iterations. Therefore, in *Chapter 4,* the shape fidelity of the 3D printed CLs was evaluated using

circularity. Interestingly, it was observed that with addition of PVA, the mechanical strength of the hydrogels became more robust. This could be a potential reason behind increased circularity values and better shape fidelity for the PVA-loaded lenses owing to the interactions of -OH groups of PVA with -NH_2 of GelMA. However, increasing the PVA concentration to higher amounts (>7%) in the ink solution did not result in high quality prints. Next, the PVA release from the designed lenses was assessed along with its role to act as a viscosity enhancer. To build upon this, non-invasive keratograph break-up time measurements were assessed on a 3D printed eyeball model and as expected, PVA significantly improved the tear breakup time, supporting its role as a tear film stabilizer.

To further validate the effectiveness of PVA at a cellular level, a dry eye disease cell model was used. Generally, artificial tear formulations are engineered to mitigate tear evaporation by restoring the tear film. These formulations are crucial in preventing cellular desiccation, thereby safeguarding the ocular surface and maintaining cellular metabolic activity. This concept was utilized in this chapter to simulate dry eye conditions in vitro and design the dry eye disease cell model. The decline in metabolic function during dehydration was assessed with the help of the MTT assay. This concept has been previously used by researchers and the dry eye industry to test efficiency of their lubricating drops. In the cell model experiments, it was observed that cells treated with 2% (w/v) PVA showed a viability comparable to that of the control, further supporting the concept of using PVA-based therapeutic lenses to treat dry eyes. The PVA released from the lenses was not used to measure the tear breakup time, however, solutions with a known amount of PVA were made to carry out these experiments. This information is useful to tune the drug loading and release from these ophthalmic devices.

An important factor to consider is how tear film dynamics—particularly low tear volume in dry eye patients—may influence the behavior of the lenses. In conditions of reduced tear volume, traditional sink conditions may not be maintained, potentially affecting the diffusion gradient that drives PVA release. However, even in such scenarios, PVA is expected to be released until local equilibrium is reached between the device and the surrounding tear film. This released PVA may not only act as a carrier for any therapeutic agents but could itself provide viscosity-enhancing and lubricating effects, offering symptomatic relief. This was the rationale behind evaluating the viscosity enhancement properties of PVA in *Chapter* 4, which demonstrated that even modest PVA concentrations can improve tear film stability. Thus, while tear film limitations may alter release

kinetics, the system is still capable of delivering functional benefit in low-volume conditions characteristic of dry eye disease.

A key aspect in ocular drug delivery is to control the release rate of therapeutic agents from ophthalmic devices. There are different strategies that have been used for sustained drug release to deliver drugs from CLs, such as the inclusion of nanoparticles, liposomes, and vitamin E coatings.[1] Even though these techniques show sustained drug release, most of their release kinetics still exhibit a pattern of burst release. This is an issue because it causes drugs to be released at an uncontrollable rate over the initial period, which decreases the therapeutic effect of the drug at the later stages and raises some safety concerns due to potential excessive release.[2] Therefore, in *Chapter 5* the formation of a chemical-physical (double) interpenetrating network to control the release of PVA from GelMA network was discussed. PVA was specifically used as part of these degradable hydrogels because of its dual nature, to act as a wetting agent as well as its ability to be physically crosslinked using freeze thaw cycles, forming a drug-loaded interpenetrating network where the unbound PVA acts as the 'drug'. The interpenetrating polymer network was fabricated in a sequential manner where GelMA was chemically crosslinked by photocrosslinking, followed by physical crosslinking of PVA using a relatively short freeze thaw cycle. In the first step, ice crystal formation occurs during the freezing cycle. The subsequent thawing leads to the formation of hydrogen bonds between the PVA chains, creating 'physical crosslinks' without the need for any additional chemical crosslinkers.

With the help of a suite of characterizations, the mechanism behind formation of these freeze thaw induced crystalline domains and their role in taking control over the release of PVA was described. The results from this study highlight that upon applying relatively short freeze thaw cycles (of 1 or 2 hr), crystalline domain formation of PVA can be induced in the interpenetrating network. This can lead to the physical crosslinking of PVA within the network and can be used as a strategy to control the release rate of PVA.

As freeze-thaw (FT) time and cycle number increase, the density of physical crosslinks within the PVA matrix also increases, primarily due to the formation of crystalline domains through hydrogen bonding. This process causes a portion of the added PVA to become embedded within the network, while the remainder remains releasable—the fraction of most interest in the context of ocular drug delivery. The releasable PVA contributes directly to therapeutic effect by dissolving into the tear film,

whereas the crosslinked fraction provides structural stability but does not contribute to drug elution. While FT processing is most often associated with PVA, it has also shown applicability to other –OH containing polymers, such as alginate, albeit to a different extent and through different physical mechanisms. The balance between releasable and retained PVA is not governed solely by cycle number—it also depends on polymer characteristics such as molecular weight, polydispersity index, and initial concentration. Furthermore, the formation of hydrophobic crystalline regions alters the polymer's internal microenvironment, affecting the interplay between hydrophilic and hydrophobic interactions, which also modulate release behavior. Therefore, while FT processing offers a tunable approach to modifying both structure and release, effective control requires a deep understanding of system-level parameters that influence PVA partitioning and drug elution. Rather than viewing FT as a simple on/off switch for release, it should be regarded as part of a broader formulation toolkit—one that can be optimized through mechanistic insight into how each variable contributes to final device performance.

An important consideration while preparing medical devices is the method of sterilization to be used. While fabricating controlled release ophthalmic devices using PVA/GelMA, steam sterilization methods are generally not an option, because the high temperature used in the steam sterilization method can melt the crystalline domains. Therefore, other methods based on ethylene oxide or gamma irradiation could be considered. Although these methods are widely used for sterilization of medical devices, the effects of these sterilization methods need to be evaluated on these devices. [3, 4] Another important aspect is maintaining a balance between transparency and the formation of crystalline domains to control the release rate of PVA. There are reports in the literature that demonstrate how carrying out the freeze thaw process at higher temperatures (around 0°C) could facilitate the fabrication of transparent PVA hydrogels.

While contact lenses offer a promising platform for ocular drug delivery, they come with inherent limitations—they must maintain optical transparency, mechanical strength, oxygen permeability, and overall comfort to ensure patient safety and wearability. These stringent design requirements can constrain material choices and drug loading strategies. In contrast, ocular inserts are not subject to the same optical or mechanical demands, allowing for greater flexibility in material selection and drug release design. This makes them especially suitable for incorporating biodegradable polymers, which can provide sustained drug delivery without the need for removal. The concept of biodegradability,

therefore, extends naturally to ocular inserts, where self-degrading materials can enhance patient compliance, reduce intervention, and improve therapeutic outcomes—supporting the broader objective of developing advanced, low-maintenance ocular drug delivery systems.

The next step of the thesis focused more on conjunctival inserts, which can be placed in the lower eyelid and therefore, do not need to be transparent. These inserts are fabricated from GelMA, which degrades in the presence of collagenases or MMPs, which are enzymes found on the ocular surface. Additionally, in various ocular conditions, such as dry eyes, the levels of MMP9 enzymes are elevated [5, 6] and can be utilized as a feedback mechanism for regulating the degradation rate of PVA from these conjunctival inserts. *Chapter 6* of this thesis focused on the mechanism of degradation of GelMA-based hydrogels in presence of MMP9 and its correlation with the release of PVA. In all the chapters, the release kinetic mechanisms were examined, demonstrating that the release from these ophthalmic devices is influenced by multiple mechanisms, including diffusion, swelling, and/or degradation.

We anticipate that the system may function within a feedback-responsive loop. In dry eye disease, elevated MMP9 levels contribute to extracellular matrix degradation and disease progression. Our insert leverages this pathological elevation—using MMP9 to trigger controlled degradation and PVA release, which provides viscosity enhancement and symptomatic relief. As the therapeutic effect is achieved, MMP9 levels are expected to return to baseline, thereby naturally slowing or stopping further insert degradation. This self-limiting mechanism aligns drug release with disease severity. Nevertheless, this interaction warrants further exploration in in vivo models, where the balance between enzyme consumption and physiological function can be more accurately assessed. Such studies will help determine whether the insert serves only as a passive substrate or if it actively modulates the local protease environment.

An important consideration for future development is whether anti-inflammatory drugs, which are known to suppress MMP9 expression, are appropriate candidates for loading into these enzyme-responsive inserts. While these drugs could help resolve ocular surface inflammation, they may also downregulate the very enzyme (MMP9) responsible for triggering material degradation and drug release, potentially creating a negative feedback loop that limits their own elution. To fully understand this interaction, in vivo studies are needed to observe how MMP9 levels dynamically change in response to both disease progression and drug exposure. A controlled model system that allows

modulation of MMP9 expression over time would be particularly useful in evaluating whether therapeutic efficacy and release kinetics can be balanced effectively in such a system. Until these interactions are better understood, anti-inflammatory drugs should be considered with caution for enzyme-responsive platforms.

Another important consideration in the use of 3D printing—particularly for biomedical devices—is the issue of batch-to-batch variability, which can impact dimensional accuracy, surface quality, and drug loading uniformity. In this study, inserts were fabricated using stereolithography (SLA) under tightly controlled conditions, including consistent resin preparation, laser exposure settings, and print environment. While no formal statistical analysis of batch-to-batch variability was performed, qualitative assessments (e.g., visual inspection, dimensional consistency using calipers, and print fidelity) suggested minimal variation across multiple prints. Nonetheless, to ensure clinical and regulatory readiness, future work should include quantitative assessments of reproducibility, such as measuring intra- and inter-batch variance in print dimensions, weight, and drug loading. Incorporating quality control metrics and tolerance thresholds will be essential for validating 3D-printed ocular inserts as reliable, scalable medical products. In future, these inserts could be tested under physiological conditions such as in vitro and in vivo models to assess their therapeutic response.

Limitations and Future Work:

While this work presents promising developments in drug-eluting contact lenses and biodegradable ocular inserts, several limitations should be acknowledged. Firstly, in vitro models used for drug release and degradation studies, while useful for controlled observations, do not fully replicate the dynamic physiological environment of the ocular surface. Factors such as tear turnover, blinking, enzymatic variability, and ocular pH fluctuations were not fully simulated, which may influence both drug kinetics and material degradation in vivo. Secondly, the concentration of enzymes like MMP-9 used in degradation assays (μg/mL) exceeds the typical physiological range (ng/mL), potentially exaggerating degradation profiles. This discrepancy suggests that actual degradation rates in the eye could be slower, and future work should aim to refine models that better reflect pathophysiological conditions.

Material selection also posed some challenges. While GelMA was chosen for its biodegradability and printability, its mechanical properties, transparency, and oxygen permeability may not yet fully

meet the demands of long-term ocular use, particularly in contact lens formats. Additionally, the 3D printing techniques employed—although offering excellent design control—require further optimization for reproducibility and scalability, especially when integrating therapeutic agents.

Finally, while drug release studies focused on model compounds, the translation of these findings to clinically relevant therapeutics (e.g., cyclosporine, lifitegrast) will require detailed pharmacokinetic and safety assessments, including in vivo validation in appropriate animal models or human trials.

Building on the insights gained through this research, several avenues for future investigation are proposed. First, refining in vitro models to better mimic ocular conditions—such as tear fluid dynamics, temperature, blinking, and ocular enzymes—would improve the predictive value of degradation and drug release studies. Developing ex vivo or in vivo models, particularly in dry eye or inflammation-induced animal models, would also allow for evaluation of material-tissue interactions, retention time, and therapeutic efficacy.

In terms of materials, further exploration of hybrid polymers or nanocomposite hydrogels could enhance mechanical strength, transparency, and oxygen permeability without compromising biodegradability. There is also potential in integrating stimuli-responsive elements (e.g., pH-, enzyme-, or inflammation-sensitive linkers) for more intelligent, condition-responsive drug release.

From a fabrication perspective, optimizing 3D printing reproducibility and transitioning to scalable manufacturing techniques (e.g., microfabrication, stereolithography) will be essential for clinical translation. Future work may also include multi-drug systems or layered printing approaches for more complex therapeutic regimens, such as combining anti-inflammatory and lubricating agents.

Lastly, clinical development pathways must be considered. Collaborations with clinicians and industry partners could guide regulatory considerations, patient-specific customization, and clinical trial design, accelerating the path from lab to clinic.

Conclusions:

In summary, this thesis developed a proof-of-concept 3D printed CLs and conjunctival inserts for controlled ocular drug delivery. Therefore, the initial hypothesis that a biodegradable contact lens fabricated via on-demand 3D printing technique, utilizing a physically crosslinked polyvinyl alcohol (PVA) matrix, will enable controlled PVA release is successfully validated. Several important findings have been reported, and the shortcomings discussed in this chapter. With the advancements in 3D printing, personalized ophthalmic devices fabricated from 3D printing could be a commercially viable option, but the cost also needs to be considered. This work demonstrates the potential of 3D-printed biodegradable contact lenses to provide precise, patient-specific customization, offering a promising step towards personalized vision correction solutions.

Copyright Permissions

Chapter 1

Figure 2. Concept of drug eluting contact lenses

ELSEVIER LICENSE
TERMS AND CONDITIONS

Oct 16, 2024

This Agreement between Piyush Garg ("You") and Elsevier ("Elsevier") consists of your license details and the terms and conditions provided by Elsevier and Copyright Clearance Center.

License Number	5890901306487
License date	Oct 16, 2024
Licensed Content Publisher	Elsevier
Licensed Content Publication	Acta Biomaterialia
Licensed Content Title	Evaluation of commercial soft contact lenses for ocular drug delivery: A review
Licensed Content Author	Xin Fan,Cesar Torres-Luna,Marjan Azadi,Roman Domszy,Naiping Hu,Arthur Yang,Allan E. David
Licensed Content Date	Oct 1, 2020
Licensed Content Volume	115
Licensed Content Issue	n/a
Licensed Content Pages	15

Start Page	60
End Page	74
Type of Use	reuse in a thesis/dissertation
Portion	figures/tables/illustrations
Number of figures/tables/illustrations	1
Format	electronic
Are you the author of this Elsevier article?	No
Will you be translating?	No
Title of new work	Development of a biodegradable contact lens system for ocular drug delivery
Institution name	University of Waterloo
Expected presentation date	Apr 2025
Order reference number	CORE_GARG_THESIS
Portions	Graphical Abstract
The Requesting Person / Organization to Appear on the License	Piyush Garg

	Mr. Piyush Garg 200 University Ave W
Requestor Location	WATERLOO, ON N2L3G1 Canada Attn: Mr. Piyush Garg
Publisher Tax ID	GB 494 6272 12
Total	0.00 CAD

Terms and Conditions

INTRODUCTION

1. The publisher for this copyrighted material is Elsevier. By clicking "accept" in connection with completing this licensing transaction, you agree that the following terms and conditions apply to this transaction (along with the Billing and Payment terms and conditions established by Copyright Clearance Center, Inc. ("CCC"), at the time that you opened your RightsLink account and that are available at any time at https://myaccount.copyright.com).

GENERAL TERMS

2. Elsevier hereby grants you permission to reproduce the aforementioned material subject to the terms and conditions indicated.

3. Acknowledgement: If any part of the material to be used (for example, figures) has appeared in our publication with credit or acknowledgement to another source, permission must also be sought from that source. If such permission is not obtained then that material may not be included in your publication/copies. Suitable acknowledgement to the source must be made, either as a footnote or in a reference list at the end of your publication, as follows:

"Reprinted from Publication title, Vol /edition number, Author(s), Title of article / title of chapter, Pages No., Copyright (Year), with permission from Elsevier [OR APPLICABLE SOCIETY COPYRIGHT OWNER]." Also Lancet special credit - "Reprinted from The Lancet, Vol. number, Author(s), Title of article, Pages No., Copyright (Year), with permission from Elsevier."

4. Reproduction of this material is confined to the purpose and/or media for which permission is hereby given. The material may not be reproduced or used in any other way, including use in combination with an artificial intelligence tool (including to train an

Figure 9. Schematic illustration of enzyme diffusion and degradation reaction in the biodegradable polymer.

American Physical Society
Reuse and Permissions License

16-Oct-2024

This license agreement between the American Physical Society ("APS") and Piyush Garg ("You") consists of your license details and the terms and conditions provided by the American Physical Society and SciPris.

Licensed Content Information

License Number:	**RNP/24/OCT/084462**
License date:	16-Oct-2024
DOI:	10.1103/PhysRevApplied.9.031001
Title:	Localized Enzymatic Degradation of Polymers: Physics and Scaling Laws
Author:	Shankar Lalitha Sridhar and Franck Vernerey
Publication:	Physical Review Applied
Publisher:	American Physical Society
Cost:	USD $ 0.00

Request Details

Does your reuse require significant modifications: No

Specify intended distribution locations:	Worldwide
Reuse Category:	Reuse in a thesis/dissertation
Requestor Type:	Student
Items for Reuse:	Figures/Tables
Number of Figure/Tables:	1
Figure/Tables Details:	Figure 1: Schematic illustrating the propagation of a fuzzy interface due to enzyme diffusion and degradation reaction in the biodegradable polymer.
Format for Reuse:	Electronic

Information about New Publication:

University/Publisher:	University of Waterloo
Title of dissertation/thesis:	Development of a biodegradable contact lens system for ocular drug delivery
Author(s):	Piyush Garg
Expected completion date:	Apr. 2025

License Requestor Information

Name:	Piyush Garg
Affiliation:	Individual
Email Id:	piyushgarg555@gmail.com
Country:	Canada



American Physical Society
Reuse and Permissions License

TERMS AND CONDITIONS

The American Physical Society (APS) is pleased to grant the Requestor of this license a non-exclusive, non-transferable permission, limited to Electronic format, provided all criteria outlined below are followed.

1. You must also obtain permission from at least one of the lead authors for each separate work, if you haven't done so already. The author's name and affiliation can be found on the first page of the published Article.
2. For electronic format permissions, Requestor agrees to provide a hyperlink from the reprinted APS material using the source material's DOI on the web page where the work appears. The hyperlink should use the standard DOI resolution URL, http://dx.doi.org/{DOI}. The hyperlink may be embedded in the copyright credit line.
3. For print format permissions, Requestor agrees to print the required copyright credit line on the first page where the material appears: "Reprinted (abstract/excerpt/figure) with permission from [(FULL REFERENCE CITATION) as follows: Author's Names, APS Journal Title, Volume Number, Page Number and Year of Publication.] Copyright (YEAR) by the American Physical Society."
4. Permission granted in this license is for a one-time use and does not include permission for any future editions, updates, databases, formats or other matters. Permission must be sought for any additional use.
5. Use of the material does not and must not imply any endorsement by APS.
6. APS does not imply, purport or intend to grant permission to reuse materials to which it does not hold copyright. It is the requestor's sole responsibility to ensure the licensed material is original to APS and does not contain the copyright of another entity, and that the copyright notice of the figure, photograph, cover or table does not indicate it was reprinted by APS with permission from another source.
7. The permission granted herein is personal to the Requestor for the use specified and is not transferable or assignable without express written permission of APS. This license may not be amended except in writing by APS.
8. You may not alter, edit or modify the material in any manner.
9. You may translate the materials only when translation rights have been granted.
10. APS is not responsible for any errors or omissions due to translation.
11. You may not use the material for promotional, sales, advertising or marketing purposes.
12. The foregoing license shall not take effect unless and until APS or its agent, Aptara, receives payment in full in accordance with Aptara Billing and Payment Terms and Conditions, which are incorporated herein by reference.
13. Should the terms of this license be violated at any time, APS or Aptara may revoke the license with no refund to you and seek relief to the fullest extent of the laws of the USA. Official written notice will be made using the contact information provided with the permission request. Failure to receive such notice will not nullify revocation of the permission.
14. APS reserves all rights not specifically granted herein.
15. This document, including the Aptara Billing and Payment Terms and Conditions, shall be the entire agreement between the parties relating to the subject matter hereof.

References

Chapter 1

1. Lanier OL, Banerjee A, Su SH, Mitra AK. Review of approaches for increasing ophthalmic bioavailability for eye drop formulations. *AAPS PharmSciTech* 2021; 22: 107.
2. Rykowska I, Nowak I, Nowak R. Soft contact lenses as drug delivery systems: A review. *Molecules* 2021; 26(7): 2139.
3. Bengani LC, Hsu KH, Gause S, Chauhan A. Contact lenses as a platform for ocular drug delivery. *Expert Opin Drug Deliv* 2013; 10(10): 1483–1496.
4. Moreddu R, Vigolo D, Yetisen AK. Contact lens technology: From fundamentals to applications. *Adv Healthc Mater*2019; 8(13): e1900368.
5. Statista. Value of the global contact lens market from 2017 to 2024. *Statista Res Dep*. [n.d.].
6. Li CC, Chauhan A. Modeling ophthalmic drug delivery by soaked contact lenses. *Ind Eng Chem Res* 2006; 45(10): 3718–3734.
7. Gote V, Sikder S, Sicotte J, Pal D. Ocular drug delivery: Present innovations and future challenges. *J Pharmacol Exp Ther*2019; 370(3): 602–624.
8. Carvalho IM, Marques CS, Oliveira RS, Coelho PB, Gil MH, Alvarez-Lorenzo C. Sustained drug release by contact lenses for glaucoma treatment—A review. *J Control Release* 2015; 202: 76–82.
9. Peng CC, Kim J, Chauhan A. Extended delivery of hydrophilic drugs from silicone-hydrogel contact lenses containing vitamin E diffusion barriers. *Biomaterials* 2010; 31(14): 4032–4047.
10. Ranch K, Patel P, Mistry M, Vyas B. Development of in situ ophthalmic gel of dexamethasone sodium phosphate and chloramphenicol: A viable alternative to conventional eye drops. *J Appl Pharm Sci* 2017; 7(9): 101–108.
11. Thakkar FMV, Soni T, Gohel M, Gandhi T. Supercritical fluid technology: A promising approach to enhance the drug solubility. *J Pharm Sci Res* 2009; 1(1): 1–10.
12. Alam F, Islam MA, Ahmad S, Janjua TI, Arjmand M. 3D printed contact lenses. *ACS Biomater Sci Eng* 2021; 7(2): 794–803.

Chapter 2

1. Di Zazzo A, Barabino S, Fasciani R, Aragona P, Giannaccare G, Villani E, Rolando M. One soul and several faces of evaporative dry eye disease. J Clin Med 2024; 13: 1220.
2. Willcox MD, Argüeso P, Georgiev GA, Holopainen JM, Laurie GW, Millar TJ. TFOS DEWS II tear film report. Ocul Surf 2017; 15: 366–403.
3. Mantelli F, Mauris J, Argüeso P. The ocular surface epithelial barrier and other mechanisms of mucosal protection: From allergy to infectious diseases. Curr Opin Allergy Clin Immunol 2013; 13: 563–568.
4. Kautto L, Nguyen-Khuong T, Everest-Dass A, Packer NH, Quah BJ, Grinyer J, Thaysen-Andersen M. Glycan involvement in the adhesion of Pseudomonas aeruginosa to tears. Exp Eye Res 2016; 145: 278–288.
5. Gipson IK, Argüeso P. Role of mucins in the function of the corneal and conjunctival epithelia. Int Rev Cytol 2003; 231: 1–49.
6. Adrianto MF, Annuryanti F, Wilson CG, Sheshala R, Thakur RRS. In vitro dissolution testing models of ocular implants for posterior segment drug delivery. Drug Deliv Transl Res 2022; 12: 1355–1375.
7. Chang AY, Purt B. Biochemistry, tear film. StatPearls 2021.
8. Lanier OL, Manfre MG, Bailey C, Liu Z, Sparks Z, Kulkarni S, Chauhan A. Review of approaches for increasing ophthalmic bioavailability for eye drop formulations. AAPS PharmSciTech 2021; 22: 107.
9. Rykowska I, Nowak I, Nowak R. Soft contact lenses as drug delivery systems: A review. Molecules 2021; 26: 5577.
10. Ross AE, Bengani LC, Tulsan R, Maidana DE, Salvador-Culla B, Kobashi H, Kolovou PE, Zhai H, Taghizadeh K, Kuang L, Mehta M, Vavvas DG, Freeman MW, Chauhan A. Topical sustained drug delivery to the retina with a drug-eluting contact lens. Biomaterials 2019; 217: 119285.
11. Liu Z, Overton M, Chauhan A. Transport of vitamin E from ethanol/water solution into contact lenses and impact on drug transport. J Ocul Pharmacol Ther 2022; 38: 684–694.
12. Bengani LC, Hsu KH, Gause S, Chauhan A. Contact lenses as a platform for ocular drug delivery. Expert Opin Drug Deliv 2013; 10: 1483–1496.
13. Fan X, Wang J, Zhang Y, Xu X, Yu Q, Wu Y, Li L. Evaluation of commercial soft contact lenses for ocular drug delivery: A review. Acta Biomater 2020; 115: 60–74.
14. Moreddu R, Vigolo D, Yetisen AK. Contact lens technology: From fundamentals to applications. Adv Healthc Mater 2019; 8: e1900368.
15. Statista. Value of the global contact lens market from 2017 to 2024. Available at: https://www.statista.com/statistics/485820/global-value-of-the-contact-lens-market/. Accessed 3 June 2024.
16. Li C-C, Chauhan A. Modeling ophthalmic drug delivery by soaked contact lenses. Ind Eng Chem Res 2006; 45: 3718–3734.
17. Stapleton F, Hickson-Curran SB, Chalmers RL, Morgan PB, Razmaria N, Keay L, Jones LW. BCLA CLEAR—Contact lens complications. Cont Lens Anterior Eye 2021; 44: 330–367.
18. Richdale K, Sinnott LT, Skadahl E, Nichols JJ. Frequency of and factors associated with contact lens dissatisfaction and discontinuation. Cornea 2007; 26: 168–174.

19. Pritchard N, Fonn D, Brazeau D. Discontinuation of contact lens wear: A survey. Int Contact Lens Clin 1999; 26: 157–162.
20. Guillon M, Maissa C. Contact lens wear affects tear film evaporation. Eye Contact Lens 2008; 34: 326–330.
21. Willcox M, Keir N, Mase T, Morgan PB, Maldonado-Codina C, Subbaraman LN. BCLA CLEAR—Contact lens wettability, cleaning, disinfection and interactions with tears. Cont Lens Anterior Eye 2021; 44: 157–191.
22. Koh S. Contact lens wear and dry eye: Beyond the known. Asia Pac J Ophthalmol 2020; 9: 498–504.
23. Yokoi N, Georgiev GA. Tear-film-oriented diagnosis for dry eye. Jpn J Ophthalmol 2019; 63: 127–136.
24. Labetoulle M, Benitez-del-Castillo JM, Barabino S, Herrero Vanrell R, Daull P, Garrigue J-S. Artificial tears: Biological role of their ingredients in the management of dry eye disease. Int J Mol Sci 2022; 23: 2434.
25. Barabino S, Benitez-Del-Castillo JM, Fariselli C, Jukic A, Marcet MM, Martinez-Soroa I, Rolando M, Tinley C. Dry eye disease treatment: The role of tear substitutes, their future, and an updated classification. Eur Rev Med Pharmacol Sci 2020; 24: 8642–8652.
26. Yokoi N, Georgiev GA. Tear film–oriented diagnosis and tear film–oriented therapy for dry eye based on tear film dynamics. Investig Ophthalmol Vis Sci 2018; 59: DES13–DES22.
27. Jones L, Hui A, Phan CM, Read ML, Azar D, Buch J. CLEAR—Contact lens technologies of the future. Cont Lens Anterior Eye 2021; 44: 398–430.
28. Papas EB, Ciolino JB, Jacobs D, Miller KM, Paugh JR, Pult H, Srinivasan S, Tauber J, Wolffsohn JS. The TFOS International Workshop on Contact Lens Discomfort: Report of the management and therapy subcommittee. Investig Ophthalmol Vis Sci 2013; 54: 183–203.
29. Weeks A, Luensmann D, Boone A, Jones L, Sheardown H. Hyaluronic acid as an internal wetting agent in model DMAA/TRIS contact lenses. J Biomater Appl 2012; 27: 423–432.
30. Phan CM, Walther H, Riederer D, Lau C, Lorenz KO, Subbaraman LN. Analysis of polyvinyl alcohol release from commercially available daily disposable contact lenses using an in vitro eye model. J Biomed Mater Res B Appl Biomater 2019; 107: 1662–1668.
31. Winterton LC, Lally JM, Sentell KB, Chapoy LL. The elution of poly(vinyl alcohol) from a contact lens: The realization of a time release moisturizing agent/artificial tear. J Biomed Mater Res B Appl Biomater 2007; 80: 424–432.
32. CFR—Code of Federal Regulations Title 21. Available at: https://www.accessdata.fda.gov/scripts/cdrh/cfdocs/cfcfr/CFRSearch.cfm?CFRPart=349&showFR=1. Accessed 3 June 2024.
33. Lynch C, Perera S, Konduri S, Bennani S, Shinde R, Pearce-Kelly A. Advances in biodegradable nano-sized polymer-based ocular drug delivery. Polymers 2019; 11: 1371.
34. Wu F, Gao J, Xiang Y, Yang J. Enhanced mechanical properties of PVA hydrogel by low-temperature segment self-assembly vs. freeze–thaw cycles. Polymers 2023; 15: 3782.
35. Teixeira MA, Amorim MTP, Felgueiras HP. Poly(vinyl alcohol)-based nanofibrous electrospun scaffolds for tissue engineering applications. Polymers 2020; 12: 7.
36. Alves MH, Jensen BE, Smith AA, Zelikin AN. Poly(vinyl alcohol) physical hydrogels: New vista on a long serving biomaterial. Macromol Biosci 2011; 11: 1293–1313.
37. Xu J, Li X, Sun F, Cao P. PVA hydrogels containing β-cyclodextrin for enhanced loading and sustained release of ocular therapeutics. J Biomater Sci Polym Ed 2010; 21: 1023–1038.
38. Adelnia H, Ensandoost R, Moonshi SS, Gavgani JN, Vasafi EI, Ta HT. Freeze/thawed polyvinyl alcohol hydrogels: Present, past and future. Eur Polym J 2022; 164: 110974.

39. Kasselkus A, Weiskircher-Hildebrandt E, Schornick E, Bauer F, Zheng M. Polyvinyl alcohol: Revival of a long-lost polymer. TIC Mag 2018; 10: 15.
40. Rajput S, Gosavi H. Overcoming challenges in ophthalmic formulations through polymer selection—A closer look at polyvinyl alcohol. Merck KGaA, Darmstadt, Germany 2022.
41. Calles JA, Bermúdez J, Vallés E, Allemandi D, Palma S. Polymers in ophthalmology. Adv Polym Med 2015; 147–176.
42. Phan C-M, Subbaraman LN, Jones LW. Uptake and release of polyvinyl alcohol from hydrogel daily disposable contact lenses. Optom Vis Sci 2019; 96: 180–186.
43. Kaniuk Ł, Stachewicz U. Development and advantages of biodegradable PHA polymers based on electrospun PHBV fibers for tissue engineering and other biomedical applications. ACS Biomater Sci Eng 2021; 7: 5339–5362.
44. Wu DT, Eberle APR, Mikos AG, Eberle APR. Polymeric scaffolds for dental, oral, and craniofacial regenerative medicine. Molecules 2021; 26: 7453.
45. Kirillova A, Yeazel TR, Asheghali D, Petersen SR, Dort S, Gall K, Becker ML. Fabrication of biomedical scaffolds using biodegradable polymers. Chem Rev 2021; 121: 11238–11304.
46. Bedell ML, Navara AM, Du Y, Zhang S, Mikos AG. Polymeric systems for bioprinting. Chem Rev 2020; 120: 10744–10792.
47. Kamaly N, Yameen B, Wu J, Farokhzad OC. Degradable controlled-release polymers and polymeric nanoparticles: Mechanisms of controlling drug release. Chem Rev 2016; 116: 2602–2663.
48. Makadia HK, Siegel SJ. Poly lactic-co-glycolic acid (PLGA) as biodegradable controlled drug delivery carrier. Polymers 2011; 3: 1377–1397.
49. Woodruff MA, Hutmacher DW. The return of a forgotten polymer—Polycaprolactone in the 21st century. Prog Polym Sci 2010; 35: 1217–1256.
50. Garg U, Chauhan A, Upadhyay P, Rakshit T, Jain D, Goyal G, Gupta U, Jain A, Goyal AK. The emerging role of 3D-printing in ocular drug delivery: Challenges, current status, and future prospects. J Drug Deliv Sci Technol 2022; 76: 103798.
51. Uhrich KE, Cannizzaro SM, Langer RS, Shakesheff KM. Polymeric systems for controlled drug release. Chem Rev 1999; 99: 3181–3198.
52. Hu B, Gao J, Lu Y, Wang Y. Applications of degradable hydrogels in novel approaches to disease treatment and new modes of drug delivery. Pharmaceutics 2023; 15: 2181.
53. Lyu S, Untereker D. Degradability of polymers for implantable biomedical devices. Int J Mol Sci 2009; 10: 4033–4065.
54. Kimura H, Ogura Y. Biodegradable polymers for ocular drug delivery. Ophthalmologica 2001; 215: 143–155.
55. Zhao L, Qi X, Cai T, Fan Z, Wang H, Du X. Gelatin hydrogel/contact lens composites as rutin delivery systems for promoting corneal wound healing. Drug Deliv 2021; 28: 1951–1961.
56. Yue K, Trujillo-de Santiago G, Alvarez MM, Tamayol A, Annabi N, Khademhosseini A. Synthesis, properties, and biomedical applications of gelatin methacryloyl (GelMA) hydrogels. Biomaterials 2015; 73: 254–271.
57. Rastin H, Ormsby RT, Atkins GJ, Losic D. 3D bioprinting of methylcellulose/gelatin-methacryloyl (MC/GelMA) bioink with high shape integrity. ACS Appl Bio Mater 2020; 3: 1815–1826.
58. Nguyen AK, Goering PL, Reipa V, Narayan RJ. Toxicity and photosensitizing assessment of gelatin methacryloyl-based hydrogels photoinitiated with lithium phenyl-2,4,6-trimethylbenzoylphosphinate in human primary renal proximal tubule epithelial cells. Biointerphases 2019; 14: 021007.

59. Sun Y, Deng R, Ren X, Zhang K, Li J. 2D gelatin methacrylate hydrogels with tunable stiffness for investigating cell behaviors. ACS Appl Bio Mater 2019; 2: 570–576.
60. Ding H, Illsley NP, Chang RC. 3D bioprinted GelMA based models for the study of trophoblast cell invasion. Sci Rep 2019; 9: 18854.
61. Lv B, Liu F, Wang X, Cao C, Liu J, Wu Z, Lu G, Wang S. Recent advances in GelMA hydrogel transplantation for musculoskeletal disorders and related disease treatment. Theranostics 2023; 13: 2015–2039.
62. Tse JW, Rizwan M, Rasmussen J, Jones L, Yim EKF. Gelatin methacrylate as an enzyme-controlled release vehicle of hyaluronic acid for the treatment of recurrent corneal erosion. ACS Appl Bio Mater 2020; 3: 6214–6223.
63. Woessner JF Jr. Matrix metalloproteinases and their inhibitors in connective tissue remodeling. FASEB J 1991; 5: 2145–2154.
64. Wu S, Zhou X, Jin Z, Cheng H. Collagenases and their inhibitors: A review. Collagen Leather 2023; 5: 19.
65. Jamerson EC, Elhusseiny AM, ElSheikh RH, Eleiwa TK, El Sayed YM. Role of matrix metalloproteinase 9 in ocular surface disorders. Eye Contact Lens 2020; 46: S57–S63.
66. Lalitha Sridhar S, Vernerey F. Localized enzymatic degradation of polymers: Physics and scaling laws. Phys Rev Appl 2018; 9: 031001.
67. Sivak JM, Fini ME. MMPs in the eye: Emerging roles for matrix metalloproteinases in ocular physiology. Prog Retin Eye Res 2002; 21: 1–14.
68. Sambursky R, Davitt WF III, Friedberg M, Tauber S. Prospective, multicenter, clinical evaluation of point-of-care matrix metalloproteinase-9 test for confirming dry eye disease. Cornea 2014; 33: 812–818.
69. Pflugfelder SC, Farley W, Luo L, Chen LZ, de Paiva CS, Olmos LC, Li DQ, Fini ME. Matrix metalloproteinase-9 knockout confers resistance to corneal epithelial barrier disruption in experimental dry eye. Am J Pathol 2005; 166: 61–71.
70. Bhaskaran R, Palmier MO, Lauer-Fields JL, Fields GB, Van Doren SR. MMP-12 catalytic domain recognizes triple helical peptide models of collagen V with exosites and high activity. J Biol Chem 2008; 283: 21779–21788.
71. Lauer-Fields JL, Sritharan T, Stack MS, Nagase H, Fields GB. Selective hydrolysis of triple-helical substrates by matrix metalloproteinase-2 and -9. J Biol Chem 2003; 278: 18140–18145.
72. Alvarado E, Castro R, Castro-Rodríguez JA, Navarro A, Farrés A. Poly(lactic acid) degradation by recombinant cutinases from Aspergillus nidulans. Polymers 2024; 16: 1994.
73. Rizzarelli P, Rapisarda M, Valenti G. Mass spectrometry in bioresorbable polymer development, degradation and drug-release tracking. Rapid Commun Mass Spectrom 2020; 34: e8697.
74. Santamaria M, Montes L, Garzon R, Moreira R, Rosell CM. Performance of starch gels on in vitro enzymatic hydrolysis assessed by rheological methodologies. Starch-Stärke 2023; 75: 2200189.
75. Rydz J, Šišková A, Andicsová Eckstein A. Scanning electron microscopy and atomic force microscopy: Topographic and dynamical surface studies of blends, composites, and hybrid functional materials for sustainable future. Adv Mater Sci Eng 2019; 2019: 6871785.
76. Phan CM, Subbaraman L, Jones L. Contact lenses for antifungal ocular drug delivery: A review. Expert Opin Drug Deliv 2014; 11: 537–546.
77. White C, Tieppo A, Byrne M. Controlled drug release from contact lenses: A comprehensive review from 1965-present. J Drug Deliv Sci Technol 2011; 21: 369–384.

78. Yoo J, Won Y-Y. Phenomenology of the initial burst release of drugs from PLGA microparticles. ACS Biomater Sci Eng 2020; 6: 6053–6062.
79. Vert M, Doi Y, Hellwich K-H, Hess M, Hodge P, Kubisa P, Rinaudo M, Schué F. Terminology for biorelated polymers and applications (IUPAC Recommendations 2012). Pure Appl Chem 2012; 84: 377–410.
80. Yasukawa T, Ogura Y, Kimura H, Sakurai E, Tabata Y. Drug delivery from ocular implants. Expert Opin Drug Deliv 2006; 3: 261–273.
81. Alam F, Elsherif M, AlQattan B, Salih A, Lee SM, Yetisen AK. 3D printed contact lenses. ACS Biomater Sci Eng 2021; 7: 794–803.
82. Hull CW. Apparatus for production of three-dimensional objects by stereolithography. US patent 1986.
83. Yu C, Schimelman J, Wang P, Miller KL, Ma X, You S, Guan J, Sun B, Zhu W, Chen S. Photopolymerizable biomaterials and light-based 3D printing strategies for biomedical applications. Chem Rev 2020; 120: 10695–10743.
84. Bagheri A, Jin J. Photopolymerization in 3D printing. ACS Appl Polym Mater 2019; 1: 593–611.
85. Lai JH, Wang C, Wang M. 3D printing in biomedical engineering: Processes, materials, and applications. Appl Phys Rev 2021; 8: 021322.
86. Badanova N, Perveen A, Talamona D. Study of SLA printing parameters affecting the dimensional accuracy of the pattern and casting in rapid investment casting. J Manuf Mater Process 2022; 6: 136.
87. Chakraborty A, Roy A, Ravi SP, Paul A. Exploiting the role of nanoparticles for use in hydrogel-based bioprinting applications: Concept, design, and recent advances. Biomater Sci 2021; 9: 6337–6354.
88. Chimene D, Kaunas R, Gaharwar AK. Hydrogel bioink reinforcement for additive manufacturing: A focused review of emerging strategies. Adv Mater 2020; 32: 1902026.
89. Zennifer A, Senthilvelan P, Sethuraman S, Sundaramurthi D. Key advances of carboxymethyl cellulose in tissue engineering & 3D bioprinting applications. Carbohydr Polym 2021; 256: 117561.
90. Shahbazi M, Jäger H. Current status in the utilization of biobased polymers for 3D printing process: A systematic review of the materials, processes, and challenges. ACS Appl Bio Mater 2021; 4: 325–369.
91. Ho BD, Phan CM, Garg P, Shokrollahi P, Jones L. A rapid screening platform for simultaneous evaluation of biodegradation and therapeutic release of an ocular hydrogel. Pharmaceutics 2023; 15: 2625.
92. Quan H. Photo-curing 3D printing technique and its challenges. Bioact Mater 2021; 6: 1789.
93. Das S, Jegadeesan JT, Basu B. Gelatin methacryloyl (GelMA)-based biomaterial inks: Process science for 3D/4D printing and current status. Biomacromolecules 2024; 25: 2156–2221.
94. He J, Zhu Y, Wu Q, Ma C, Sun W, Zhang J, Mao X, Cui Z. Gelatin methacryloyl hydrogel, from standardization, performance, to biomedical application. Adv Healthc Mater 2023; 12: 2300398.
95. Schwab A, Levato R, D'Este M, Piluso S, Eglin D, Malda J. Printability and shape fidelity of bioinks in 3D bioprinting. Chem Rev 2020; 120: 11028–11055.

Chapter 3

1. Taneja H, Salodkar SM, Parmar AS, Chaudhary S. Hydrogel based 3D printing: Bio ink for tissue engineering. *J Mol Liq*2022; 367.
2. Chakraborty A, Roy A, Ravi SP, Paul A. Exploiting the role of nanoparticles for use in hydrogel-based bioprinting applications: concept, design, and recent advances. *Biomater Sci* 2021; 9(19): 6337–6354.
3. Zennifer A, Senthilvelan P, Sethuraman S, Sundaramurthi D. Key advances of carboxymethyl cellulose in tissue engineering & 3D bioprinting applications. *Carbohydr Polym* 2021; 256.
4. Chimene D, Kaunas R, Gaharwar AK. Hydrogel bioink reinforcement for additive manufacturing: A focused review of emerging strategies. *Adv Mater* 2020; 32(1).
5. Zhou LY, Fu JZ, He Y. A review of 3D printing technologies for soft polymer materials. *Adv Funct Mater* 2020; 30(28).
6. Bao YY, Paunovic N, Leroux JC. Challenges and opportunities in 3D printing of biodegradable medical devices by emerging photopolymerization techniques. *Adv Funct Mater* 2022; 32(15).
7. Poomathi N, Singh S, Prakash C, Subramanian A, Sahay R, Cinappan A et al. 3D printing in tissue engineering: a state-of-the-art review of technologies and biomaterials. *Rapid Prototyp J* 2020; 26(7): 1313–1334.
8. Bose S, Phan CM, Rizwan M, Tse JW, Yim E, Jones L et al. Fabrication and characterization of an enzyme-triggered, therapeutic-releasing hydrogel bandage contact lens material. *Pharmaceutics* 2024; 16(1).
9. Zhu MX, Wang YY, Ferracci G, Zheng J, Cho NJ, Lee BH. Gelatin methacryloyl and its hydrogels with an exceptional degree of controllability and batch-to-batch consistency. *Sci Rep* 2019; 9.
10. 10. Mamidi N, Ijadi F, Norahan MH. Leveraging the recent advancements in GelMA scaffolds for bone tissue engineering: An assessment of challenges and opportunities. Biomacromolecules 2023; 25(4): 2075–2113.
11. Yang XL, Li XJ, Wu ZP, Cao LL. Photocrosslinked methacrylated natural macromolecular hydrogels for tissue engineering: A review. *Int J Biol Macromol* 2023; 246.
12. Das S, Jegadeesan JT, Basu B. Advancing peripheral nerve regeneration: 3D bioprinting of GelMA-based cell-laden electroactive bioinks for nerve conduits. *ACS Biomater Sci Eng* 2024; 10(3): 1620–1645.
13. Das S, Jegadeesan JT, Basu B. Gelatin methacryloyl (GelMA)-based biomaterial inks: Process science for 3D/4D printing and current status. *Biomacromolecules* 2024; 25(4): 2156–2221.
14. Lai JH, Wang C, Wang M. 3D printing in biomedical engineering: Processes, materials, and applications. *Appl Phys Rev*2021; 8(2).
15. He J, Sun Y, Gao Q, He CF, Yao K, Wang TY et al. Gelatin methacryloyl hydrogel, from standardization, performance, to biomedical application. *Adv Healthc Mater* 2023; 12(23).
16. Badanova N, Perveen A, Talamona D. Study of SLA printing parameters affecting the dimensional accuracy of the pattern and casting in rapid investment casting. *J Manuf Mater Process* 2022; 6(5).
17. Arif ZU, Khalid MY, Tariq A, Hossain M, Umer R. 3D printing of stimuli-responsive hydrogel materials: Literature review and emerging applications. *Giant* 2023: 100209.
18. Quan H. Photo-curing 3D printing technique and its challenges. *Bioact Mater* 2021; 6(6): 1789–1789.

19. Shin SH, Kwon JS, Shim JS, Kim JE. Evaluating the three-dimensional printing accuracy of partial-arch models according to outer wall thickness: An in vitro study. *Materials (Basel)* 2021; 14(22).
20. Kim I, Kim S, Andreu A, Kim JH, Yoon YJ. Influence of dispersant concentration toward enhancing printing precision and surface quality of vat photopolymerization 3D printed ceramics. *Addit Manuf* 2022; 52.
21. Li WL, Mille LS, Robledo JA, Uribe T, Huerta V, Zhang YS. Recent advances in formulating and processing biomaterial inks for vat polymerization-based 3D printing. *Adv Healthc Mater* 2020; 9(15).
22. McGregor DJ, Rylowicz S, Brenzel A, Baker D, Wood C, Pick D et al. Analyzing part accuracy and sources of variability for additively manufactured lattice parts made on multiple printers. *Addit Manuf* 2021; 40.
23. Ouyang LL, Yao R, Zhao Y, Sun W. Effect of bioink properties on printability and cell viability for 3D bioplotting of embryonic stem cells. *Biofabrication* 2016; 8(3).
24. Shahbazi M, Jäger H. Current status in the utilization of biobased polymers for 3D printing process: A systematic review of the materials, processes, and challenges. *ACS Appl Bio Mater* 2021; 4(1): 325–369.
25. Ho BD, Phan CM, Garg P, Shokrollahi P, Jones L. A rapid screening platform for simultaneous evaluation of biodegradation and therapeutic release of an ocular hydrogel. *Pharmaceutics* 2023; 15(11).
26. Karamzadeh V, Shen ML, Ravanbakhsh H, Sohrabi-Kashani A, Okhovatian S, Savoji H et al. High-resolution additive manufacturing of a biodegradable elastomer with a low-cost LCD 3D printer. *Adv Healthc Mater* 2024; 13(9).
27. Shirahama H, Lee BH, Tan LP, Cho NJ. Precise tuning of facile one-pot gelatin methacryloyl (GelMA) synthesis. *Sci Rep*2016; 6.
28. Zhang J, Xiao P. 3D printing of photopolymers. *Polym Chem* 2018; 9(13): 1530–1540.
29. Zanon M, Cue-López R, Martínez-Campos E, Bosch P, Versace DL, Hayek H et al. Bioderived dyes-mediated vat photopolymerization 3D printing of chitosan hydrogels for tissue engineering. *Addit Manuf* 2023; 69.
30. Gastaldi M, Cardano F, Zanetti M, Viscardi G, Barolo C, Bordiga S et al. Functional dyes in polymeric 3D printing: applications and perspectives. *ACS Mater Lett* 2020; 3(1): 1–17.
31. Arif ZU, Khalid MY, Noroozi R, Sadeghianmaryan A, Jalalvand M, Hossain M. Recent advances in 3D-printed polylactide and polycaprolactone-based biomaterials for tissue engineering applications. *Int J Biol Macromol* 2022; 218: 930–968.
32. Anandakrishnan N, Ye H, Guo ZP, Chen ZW, Mentkowski KI, Lang JK et al. Fast stereolithography printing of large-scale biocompatible hydrogel models. *Adv Healthc Mater* 2021; 10(10).
33. Wang TZ, Liu XX, Wang SY, Liu Y, Pan XY, Wang JJ et al. Engineering advanced drug delivery systems for dry eye: A review. *Bioeng (Basel)* 2022; 10(1).
34. Hosseinabadi HG, Nieto D, Yousefinejad A, Fattel H, Ionov L, Miri AK. Ink material selection and optical design considerations in DLP 3D printing. *Appl Mater Today* 2023; 30.
35. Leone G, Consumi M, Pepi S, Pardini A, Bonechi C, Tamasi G et al. Modified low molecular weight poly-vinyl alcohol as viscosity enhancer. *Mater Today Commun* 2019; 21: 100634.
36. Garg P, Shokrollahi P, Phan C-M, Jones L. 3D printing of PVA loaded ocular inserts for ocular drug delivery. *Invest Ophthalmol Vis Sci* 2024; 65(7): 6548–6548.

Chapter 4

1. Willcox MD, Argüeso P, Georgiev GA, Holopainen JM, Laurie GW, Millar TJ. TFOS DEWS II tear film report. Ocul Surf 2017; 15(3): 366–403.
2. Jones L, Hui A, Phan CM, Read ML, Azar D, Buch J. CLEAR - Contact lens technologies of the future. Cont Lens Anterior Eye 2021; 44(2): 398–430.
3. Phan CM, Walther H, Riederer D, Lau C, Lorenz KO, Subbaraman LN. Analysis of polyvinyl alcohol release from commercially available daily disposable contact lenses using an in vitro eye model. J Biomed Mater Res B Appl Biomater 2019; 107(5): 1662–1668.
4. Winterton LC, Lally JM, Sentell KB, Chapoy LL. The elution of poly(vinyl alcohol) from a contact lens: The realization of a time release moisturizing agent/artificial tear. J Biomed Mater Res B Appl Biomater 2007; 80(2): 424–432.
5. Alam F, Elsherif M, AlQattan B, Salih A, Lee SM, Yetisen AK. 3D printed contact lenses. ACS Biomater Sci Eng 2021; 7(2): 794–803.
6. Aravind M, Chidangil S, George SD. Self-moisturizing contact lens employing capillary flow. Addit Manuf 2022; 55: 102842.
7. Schwab A, Levato R, D'Este M, Piluso S, Eglin D, Malda J. Printability and shape fidelity of bioinks in 3D bioprinting. Chem Rev 2020; 120(19): 11028–11055.
8. Ouyang LL, Yao R, Zhao Y, Sun W. Effect of bioink properties on printability and cell viability for 3D bioplotting of embryonic stem cells. Biofabrication 2016; 8(3): 035020.
9. Leone G, Consumi M, Pepi S, Pardini A, Bonechi C, Tamasi G. Modified low molecular weight poly-vinyl alcohol as viscosity enhancer. Mater Today Commun 2019; 21: 100634.
10. Phan C-M, Subbaraman LN, Jones LW. Uptake and release of polyvinyl alcohol from hydrogel daily disposable contact lenses. Optom Vis Sci 2019; 96(3): 180–186.
11. Schindelin J, Arganda-Carreras I, Frise E, Kaynig V, Longair M, Pietzsch T. Fiji: An open-source platform for biological-image analysis. Nat Methods 2012; 9(7): 676–682.
12. Procházková L, Rodríguez-Muñoz Y, Procházka J, Wanner J. Simple spectrophotometric method for determination of polyvinylalcohol in different types of wastewater. Int J Environ Anal Chem 2014; 94(4): 399–410.
13. Liu Y, Fan Q, Huo Y, Liu C, Li B, Li Y. Construction of a mesoporous polydopamine@GO/cellulose nanofibril composite hydrogel with an encapsulation structure for controllable drug release and toxicity shielding. ACS Appl Mater Interfaces 2020; 12(51): 57410–57420.
14. Elmas A, Akyüz G, Bergal A, Andaç M, Andaç Ö. Mathematical modelling of drug release. Res Eng Struct Mater 2020; 6(4): 327–339.
15. Madhavi BB, Kusum B, Chatanya CK, Madhu MN, Harsha VS, Banji D. Dissolution enhancement of efavirenz by solid dispersion and PEGylation techniques. Int J Pharm Investig 2011; 1(1): 29–34.
16. Rosencranz R, Bogen SA. Clinical laboratory measurement of serum, plasma, and blood viscosity. Pathol Patterns Rev 2006; 125(Suppl_1): S78–S86.
17. Phan C-M, Chan VW, Drolle E, Hui A, Ngo W, Bose S. Evaluating the in vitro wettability and coefficient of friction of a novel and contemporary reusable silicone hydrogel contact lens materials using an in vitro blink model. Cont Lens Anterior Eye 2024; 47(2): 102129.
18. Phan C-M, Ross M, Fahmy K, McEwen B, Hofmann I, Chan VW. Evaluating viscosity and tear breakup time of contemporary commercial ocular lubricants on an in vitro eye model. Transl Vis Sci Technol 2023; 12(6): 29.

19. Rangarajan R, Ketelson HA, Do R, McCanna DJ, Suko A, Enstone D. Effect of artificial tear formulations on the metabolic activity of human corneal epithelial cells after exposure to desiccation. J Vis Exp 2020; (159): e60812.
20. Yu K, Zhang XJ, Sun Y, Gao Q, Fu JZ, Cai XJ. Printability during projection-based 3D bioprinting. Bioact Mater 2022; 11: 254–267.
21. Bose S, Phan CM, Rizwan M, Tse JW, Yim E, Jones L. Fabrication and characterization of an enzyme-triggered, therapeutic-releasing hydrogel bandage contact lens material. Pharmaceutics 2024; 16(1): 26.
22. Zhu MX, Wang YY, Ferracci G, Zheng J, Cho NJ, Lee BH. Gelatin methacryloyl and its hydrogels with an exceptional degree of controllability and batch-to-batch consistency. Sci Rep 2019; 9: 6863.
23. Caprioli M, Roppolo I, Chiappone A, Larush L, Pirri CF, Magdassi S. 3D-printed self-healing hydrogels via digital light processing. Nat Commun 2021; 12(1): 2462.
24. Zhang J, Xiao P. 3D printing of photopolymers. Polym Chem 2018; 9(13): 1530–1540.
25. Guo A, Zhang S, Yang R, Sui C. Enhancing the mechanical strength of 3D printed GelMA for soft tissue engineering applications. Mater Today Bio 2023; 100939.
26. Xue Q, Hu H, Wang W, Li Q, Ma L, Ma J. Liquid-phase integrated 3D printed biological lenses for lamellar corneal substitute. Adv Healthc Mater 2023; 12(27): 2300600.
27. Bernal-Chávez SA, Romero-Montero A, Hernández-Parra H, Peña-Corona SI, Del Prado-Audelo ML, Alcalá-Alcalá S. Enhancing chemical and physical stability of pharmaceuticals using freeze-thaw method: Challenges and opportunities for process optimization through quality by design approach. J Biol Eng 2023; 17(1): 35.
28. Mandal P, Stokes K, Hernández G, Brandell D, Mindemark J. Influence of binder crystallinity on the performance of Si electrodes with poly(vinyl alcohol) binders. ACS Appl Energy Mater 2021; 4(4): 3008–3016.
29. Adelnia H, Ensandoost R, Moonshi SS, Gavgani JN, Vasafi-Seifi M, Ta HT. Freeze/thawed polyvinyl alcohol hydrogels: Present, past and future. Eur Polym J 2022; 164: 110974.
30. Hu Q, Lu R, Liu S, Liu Y, Gu Y, Zhang H. 3D printing GelMA/PVA interpenetrating polymer networks scaffolds mediated with CuO nanoparticles for angiogenesis. Macromol Biosci 2022; 22(10): 2200208.
31. Ino JM, Sju E, Ollivier V, Yim EK, Letourneur D, Le Visage C. Evaluation of hemocompatibility and endothelialization of hybrid poly(vinyl alcohol)(PVA)/gelatin polymer films. J Biomed Mater Res B Appl Biomater 2013; 101(8): 1549–1559.
32. Thangprasert A, Tansakul C, Thuaksubun N, Meesane J. Mimicked hybrid hydrogel based on gelatin/PVA for tissue engineering in subchondral bone interface for osteoarthritis surgery. Mater Des 2019; 183: 108113.
33. Marcos Luciano B. Mathematical models of drug release. In Strategies to modify the drug release from pharmaceutical systems; Woodhead Publishing: Sawston, UK, 2015; 63–86.
34. Onogi S, Masuda T, Miyanaga N, Kimura Y. Dependence of viscosity of concentrated polymer solutions upon molecular weight and concentration. J Polym Sci A-2 Polym Phys 1967; 5(5): 899–913.
35. Jones L, Downie LE, Korb D, Benitez-del-Castillo JM, Dana R, Deng SX. TFOS DEWS II management and therapy report. Ocul Surf 2017; 15(3): 575–628.
36. CFR - Code of Federal Regulations Title 21. Available at: https://www.accessdata.fda.gov/scripts/cdrh/cfdocs/cfcfr/CFRSearch.cfm?CFRPart=349&showFR=1. Accessed 3 June 2024.

37. Labetoulle M, Benitez-del-Castillo JM, Barabino S, Herrero Vanrell R, Daull P, Garrigue J-S. Artificial tears: Biological role of their ingredients in the management of dry eye disease. Int J Mol Sci 2022; 23(5): 2434.
38. Leone G, Consumi M, Greco G, Bonechi C, Lamponi S, Rossi C. A PVA/PVP hydrogel for human lens substitution: Synthesis, rheological characterization, and in vitro biocompatibility. J Biomed Mater Res B Appl Biomater 2011; 97(2): 278–288.

Chapter 5

1. Seo H, Chung WG, Kwon YW, Kim S, Hong Y-M, Park W, Kim E, Lee J, Lee S, Kim M. Smart contact lenses as wearable ophthalmic devices for disease monitoring and health management. Chem Rev 2023; 123(19): 11488–11558.
2. Lanier OL, Manfre MG, Bailey C, Liu Z, Sparks Z, Kulkarni S, Chauhan A. Review of approaches for increasing ophthalmic bioavailability for eye drop formulations. AAPS PharmSciTech 2021; 22(3): Article 107.
3. Rykowska I, Nowak I, Nowak R. Soft contact lenses as drug delivery systems: A review. Molecules 2021; 26(18): Article 5577.
4. Maulvi FA, Soni TG, Shah DO. Extended release of hyaluronic acid from hydrogel contact lenses for dry eye syndrome. J Biomater Sci Polym Ed 2015; 26(15): 1035–1050.
5. Li R, Guan X, Lin X, Guan P, Zhang X, Rao Z, Du L, Zhao J, Rong J, Zhao J. Poly(2-hydroxyethyl methacrylate)/β-cyclodextrin-hyaluronan contact lens with tear protein adsorption resistance and sustained drug delivery for ophthalmic diseases. Acta Biomater 2020; 110: 105–118.
6. Yu Y, Chow DWY, Lau CML, Zhou G, Back W, Xu J, Carim S, Chau Y. A bioinspired synthetic soft hydrogel for the treatment of dry eye. Bioeng Transl Med 2021; 6(3): Article e10227.
7. Dana R, Meunier J, Markowitz JT, Joseph C, Siffel C. Patient-reported burden of dry eye disease in the United States: Results of an online cross-sectional survey. Am J Ophthalmol 2020; 216: 7–17.
8. Stapleton F, Alves M, Bunya VY, Jalbert I, Lekhanont K, Malet F, Na KS, Schaumberg D, Uchino M, Vehof J, Viso E. TFOS DEWS II epidemiology report. Ocul Surf 2017; 15(3): 334–365.
9. Nicolson PC, Vogt J. Soft contact lens polymers: An evolution. Biomaterials 2001; 22(24): 3273–3283.
10. Ruskowitz ER, DeForest CA. Photoresponsive biomaterials for targeted drug delivery and 4D cell culture. Nat Rev Mater 2018; 3(2): 1–17.
11. Ooi HW, Hafeez S, van Blitterswijk C, Moroni L, Baker MB. Hydrogels that listen to cells: A review of cell-responsive strategies in biomaterial design for tissue regeneration. Mater Horiz 2017; 4(6): 1020–1040.
12. White CJ, DiPasquale SA, Byrne ME. Controlled release of multiple therapeutics from silicone hydrogel contact lenses. Optom Vis Sci 2016; 93(4): 377–386.
13. DiPasquale SA, Uricoli B, DiCerbo MC, Brown TL, Byrne ME. Controlled release of multiple therapeutics from silicone hydrogel contact lenses for post-cataract/post-refractive surgery and uveitis treatment. Transl Vis Sci Technol 2021; 10(14): 5.

14. Fang G, Yang X, Wang Q, Zhang A, Tang B. Hydrogels-based ophthalmic drug delivery systems for treatment of ocular diseases. Mater Sci Eng C 2021; 127: 112212.
15. Yue K, Trujillo-de Santiago G, Alvarez MM, Tamayol A, Annabi N, Khademhosseini A. Synthesis, properties, and biomedical applications of gelatin methacryloyl (GelMA) hydrogels. Biomaterials 2015; 73: 254–271.
16. Zhao L, Qi X, Cai T, Fan Z, Wang H, Du X. Gelatin hydrogel/contact lens composites as rutin delivery systems for promoting corneal wound healing. Drug Deliv 2021; 28(1): 1951–1961.
17. Nguyen AK, Goering PL, Reipa V, Narayan RJ. Toxicity and photosensitizing assessment of gelatin methacryloyl-based hydrogels photoinitiated with lithium phenyl-2,4,6-trimethylbenzoylphosphinate in human primary renal proximal tubule epithelial cells. Biointerphases 2019; 14(2): Article 021007.
18. Park BC, Kim HT, Koh JW. New biodegradable drug delivery system for patients with dry eye. Korean J Ophthalmol 2021; 35(6): 455.
19. Li S, Zhao X, Wang Q, Yu F, Li W, Bai Y, Shen X, Du X, He D, Yuan J. Mechanoresponsive drug loading system with tunable host–guest interactions for ocular disease treatment. ACS Biomater Sci Eng 2022; 8(11): 4850–4862.
20. Shen C, Zhao X, Ren Z, Yang B, Wang X, Hu A, Hu J. In situ formation of injectable gelatin methacryloyl (GelMA) hydrogels for effective intraocular delivery of triamcinolone acetonide. Int J Mol Sci 2023; 24(5): 4957.
21. Tse JW, Rizwan M, Rasmussen J, Jones L, Yim EKF. Gelatin methacrylate as an enzyme-controlled release vehicle of hyaluronic acid for the treatment of recurrent corneal erosion. ACS Appl Bio Mater 2020; 3(9): 6214–6223.
22. Kilic Bektas C, Hasirci V. Cell loaded GelMA: HEMA IPN hydrogels for corneal stroma engineering. J Mater Sci Mater Med 2020; 31: 1–15.
23. Ayran M, Goyuk Y, Tiryaki A, Ulag S, Koyuncu ACC, Turhan S, Gunduz O. Light-processed 3D bioprinting of symblepharon rings fortified with L-ascorbic acid for ocular tissue engineering. Macromol Mater Eng 2024; 2400057.
24. Sharifi S, Islam MM, Sharifi H, Islam R, Koza D, Reyes-Ortega F, Alba-Molina D, Nilsson PH, Dohlman CH, Mollnes TE. Tuning gelatin-based hydrogel towards bioadhesive ocular tissue engineering applications. Bioact Mater 2021; 6(11): 3947–3961.
25. Piao Y, You H, Xu T, Bei H-P, Piwko IZ, Kwan YY, Zhao X. Biomedical applications of gelatin methacryloyl hydrogels. Eng Regen 2021; 2: 47–56.
26. Yang H, Fustin CA. Design and applications of dynamic hydrogels based on reversible C═N bonds. Macromol Chem Phys 2023; 224(20): 2300211.
27. Sperling LH. Interpenetrating polymer networks: An overview. Adv Chem Ser 1994; 239: 3–38.
28. Zhao X, Chen X, Yuk H, Lin S, Liu X, Parada G. Soft materials by design: Unconventional polymer networks give extreme properties. Chem Rev 2021; 121(8): 4309–4372.
29. Leone G, Consumi M, Pepi S, Pardini A, Bonechi C, Tamasi G, Donati A, Rossi C, Magnani A. Modified low molecular weight poly-vinyl alcohol as viscosity enhancer. Mater Today Commun 2019; 21: 100634.
30. Chaudhari P, Birangal S, Mavlankar N, Pal A, Mallela LS, Roy S, Kodoth AK, Ghate V, Nampoothiri M, Lewis S. Oil-free eye drops containing cyclosporine A/cyclodextrin/PVA supramolecular complex as a treatment modality for dry eye disease. Carbohydr Polym 2022; 297: 120007.
31. Hassan CM, Peppas NA. Structure and morphology of freeze/thawed PVA hydrogels. Macromolecules 2000; 33(7): 2472–2479.

32. Suneetha M, Hemalatha D, Kim H, Rao KK, Han SS. Vanillin/fungal-derived carboxy methyl chitosan/polyvinyl alcohol hydrogels prepared by freeze-thawing for wound dressing applications. Int J Biol Macromol 2024; 130910.
33. Waresindo WX, Luthfianti HR, Edikresnha D, Suciati T, Noor FA, Khairurrijal K. A freeze–thaw PVA hydrogel loaded with guava leaf extract: Physical and antibacterial properties. RSC Adv 2021; 11(48): 30156–30171.
34. Edikresnha D, Suciati T, Khairurrijal K. Freeze-thawed hydrogel loaded by Piper crocatum extract with in-vitro antibacterial and release tests. J Mater Res Technol 2021; 15: 17–36.
35. Figueroa-Pizano M, Vélaz I, Peñas F, Zavala-Rivera P, Rosas-Durazo A, Maldonado-Arce A, Martínez-Barbosa M. Effect of freeze-thawing conditions for preparation of chitosan-poly (vinyl alcohol) hydrogels and drug release studies. Carbohydr Polym 2018; 195: 476–485.
36. Wu Y, Li Y, Han R, Long Z, Si P, Zhang D. Dual-cross-linked PEI/PVA hydrogel for pH-responsive drug delivery. Biomacromolecules 2023; 24(11): 5364–5370.
37. Ye J, Liu L, Lan W, Xiong J. Targeted release of soybean peptide from CMC/PVA hydrogels in simulated intestinal fluid and their pharmacokinetics. Carbohydr Polym 2023; 310: 120713.
38. Hu Q, Lu R, Liu S, Liu Y, Gu Y, Zhang H. 3D printing GelMA/PVA interpenetrating polymer networks scaffolds mediated with CuO nanoparticles for angiogenesis. Macromol Biosci 2022; 22(10): 2200208.
39. Bernal-Chávez SA, Romero-Montero A, Hernández-Parra H, Peña-Corona SI, Del Prado-Audelo ML, Alcalá-Alcalá S, Cortés H, Kiyekbayeva L, Sharifi-Rad J, Leyva-Gómez G. Enhancing chemical and physical stability of pharmaceuticals using freeze-thaw method: Challenges and opportunities for process optimization through quality by design approach. J Biol Eng 2023; 17(1): 35.
40. Boran F. The influence of freeze-thawing conditions on swelling and long-term stability properties of poly(vinyl alcohol) hydrogels for controlled drug release. Polym Bull 2021; 78(12): 7369–7387.
41. Phan C-M, Subbaraman LN, Jones LW. Uptake and release of polyvinyl alcohol from hydrogel daily disposable contact lenses. Optom Vis Sci 2019; 96(3): 180–186.
42. Phan CM, Walther H, Riederer D, Lau C, Lorenz KO, Subbaraman LN, Jones L. Analysis of polyvinyl alcohol release from commercially available daily disposable contact lenses using an in vitro eye model. J Biomed Mater Res B Appl Biomater 2019; 107(5): 1662–1668.
43. Rizwan M, Peh GS, Ang H-P, Lwin NC, Adnan K, Mehta JS, Tan WS, Yim EKF. Sequentially-crosslinked bioactive hydrogels as nano-patterned substrates with customizable stiffness and degradation for corneal tissue engineering applications. Biomaterials 2017; 120: 139–154.
44. Nakano T, Nakaoki T. Coagulation size of freezable water in poly(vinyl alcohol) hydrogels formed by different freeze/thaw cycle periods. Polym J 2011; 43(11): 875–880.
45. Procházková L, Rodríguez-Muñoz Y, Procházka J, Wanner J. Simple spectrophotometric method for determination of polyvinylalcohol in different types of wastewater. Int J Environ Anal Chem 2014; 94(4): 399–410.
46. Liu Y, Fan Q, Huo Y, Liu C, Li B, Li Y. Construction of a mesoporous polydopamine@GO/cellulose nanofibril composite hydrogel with an encapsulation structure for controllable drug release. ACS Appl Mater Interfaces 2020; 12(51): 57410–57420.
47. Elmas A, Akyüz G, Bergal A, Andaç M, Andaç Ö. Mathematical modelling of drug release. Res Eng Struct Mater 2020; 6(4): 327–339.
48. Madhavi BB, Kusum B, Chatanya CK, Madhu MN, Harsha VS, Banji D. Dissolution enhancement of efavirenz by solid dispersion and PEGylation techniques. Int J Pharm Investig 2011; 1(1): 29–34.

49. Shakeel A, Bhattacharya R, Jeevanandham S, Kochhar D, Singh A, Mehra L, Ghufran M, Garg P, Sangam S, Biswas S. Graphene quantum dots in the game of directing polymer self-assembly to exotic kagome lattice and janus nanostructures. ACS Nano 2019; 13(8): 9397–9407.
50. Li H, Wu C-W, Wang S, Zhang W. Mechanically strong poly(vinyl alcohol) hydrogel with macropores and high porosity. Mater Lett 2020; 266: 127504.
51. Zeng M, Fang Z, Xu C. Effect of compatibility on the structure of the microporous membrane prepared by selective dissolution of chitosan/synthetic polymer blend membrane. J Membr Sci 2004; 230(1-2): 175–181.
52. Adelnia H, Ensandoost R, Moonshi SS, Gavgani JN, Vasafi EI, Ta HT. Freeze/thawed polyvinyl alcohol hydrogels: Present, past and future. Eur Polym J 2022; 164: 110974.
53. Labus K, Radosinski L, Kotowski P. Functional properties of two-component hydrogel systems based on gelatin and polyvinyl alcohol—Experimental studies supported by computational analysis. Int J Mol Sci 2021; 22(18): 9909.
54. Jipa IM, Stoica A, Stroescu M, Dobre L-M, Dobre T, Jinga S, Tardei C. Potassium sorbate release from poly(vinyl alcohol)-bacterial cellulose films. Chem Pap 2012; 66(2): 138–143.
55. Aldana AA, Malatto L, Rehman MAU, Boccaccini AR, Abraham GA. Fabrication of gelatin methacrylate (GelMA) scaffolds with nano- and micro-topographical and morphological features. Nanomaterials 2019; 9(1): 120.
56. Fonseca DF, Costa PC, Almeida IF, Dias-Pereira P, Correia-Sá I, Bastos V, Oliveira H, Vilela C, Silvestre AJ, Freire CS. Swellable gelatin methacryloyl microneedles for extraction of interstitial skin fluid toward minimally invasive monitoring of urea. Macromol Biosci 2020; 20(10): 2000195.
57. Velasco-Rodriguez B, Diaz-Vidal T, Rosales-Rivera LC, García-González CA, Alvarez-Lorenzo C, Al-Modlej A, Domínguez-Arca V, Prieto G, Barbosa S, Soltero Martínez JF. Hybrid methacrylated gelatin and hyaluronic acid hydrogel scaffolds. Preparation and systematic characterization for prospective tissue engineering applications. Int J Mol Sci 2021; 22(13): 6758.
58. Pawde S, Deshmukh K. Characterization of polyvinyl alcohol/gelatin blend hydrogel films for biomedical applications. J Appl Polym Sci 2008; 109(5): 3431–3437.
59. Tozar T, Nistorescu S, Boni M, Gradisteanu Pircalabioru G, Negut I, Staicu A. Pulsed laser photo-crosslinking of gelatin methacryloyl hydrogels for the controlled delivery of chlorpromazine to combat antimicrobial resistance. Pharmaceutics 2022; 14(10): 2121.
60. El-Nemr KF, Mohamed HR, Ali MA, Fathy RM, Dhmees AS. Polyvinyl alcohol/gelatin irradiated blends filled by lignin as green filler for antimicrobial packaging materials. Int J Environ Anal Chem 2020; 100(14): 1578–1602.
61. Shirahama H, Lee BH, Tan LP, Cho NJ. Precise tuning of facile one-pot gelatin methacryloyl (GelMA) synthesis. Sci Rep 2016; 6: 31036.
62. Li XM, Chen SW, Li JC, Wang XL, Zhang J, Kawazoe N, Chen GP. 3D culture of chondrocytes in gelatin hydrogels with different stiffness. Polymers 2016; 8(8): 269.
63. Wang J, Wang X, Liang Z, Lan W, Wei Y, Hu Y, Wang L, Lei Q, Huang D. Injectable antibacterial Ag-HA/GelMA hydrogel for bone tissue engineering. Front Bioeng Biotechnol 2023; 11: 1219460.
64. Mehto A, Mehto VR, Chauhan J. Preparation and characterization of polyvinyl alcohol (PVA)/ZrO2 composite membranes. Phys Status Solidi B 2023; 260(10): 2300164.
65. Song X, He T, Qi Y, Liu Y, Wu H, Liu C, Zhang Y. Properties of cell-compatible poly(vinyl alcohol) hydrogels cross-linked with hydrophobic luteolin. ACS Appl Polym Mater 2021; 3(6): 3019–3027.

66. Wang Y, Wang J, Ma Z, Yan L. A highly conductive, self-recoverable, and strong eutectogel of a deep eutectic solvent with polymer crystalline domain regulation. ACS Appl Mater Interfaces 2021; 13(45): 54409–54416.
67. Chen L, Qiang T, Chen X, Ren W, Zhang HJ. Tough and biodegradable gelatin-based film via the synergistic effect of multi-cross-linking. ACS Appl Polym Mater 2021; 4(1): 357–368.
68. Darabi MA, Khosrozadeh A, Wang Y, Ashammakhi N, Alem H, Erdem A, Chang Q, Xu K, Liu Y, Luo G. An alkaline based method for generating crystalline, strong, and shape memory polyvinyl alcohol biomaterials. Adv Sci 2020; 7(21): 1902740.
69. Thomas D, Zhuravlev E, Wurm A, Schick C, Cebe P. Fundamental thermal properties of polyvinyl alcohol by fast scanning calorimetry. Polymer 2018; 137: 145–155.
70. Brazel CS, Peppas NA. Mechanisms of solute and drug transport in relaxing, swellable, hydrophilic glassy polymers. Polymer 1999; 40(12): 3383–3398.
71. Zhang Y, Sun M, Liu T, Hou M, Yang H. Effect of different additives on the mechanical properties of gelatin methacryloyl hydrogel: A meta-analysis. ACS Omega 2021; 6(13): 9112–9128.
72. Ahmed L, Atif R, Eldeen TS, Yahya I, Omara A, Eltayeb M. Study the using of nanoparticles as drug delivery system based on mathematical models for controlled release. IJLTEMAS 2019; 8: 52–56.
73. Bruschi ML. Strategies to modify the drug release from pharmaceutical systems. Woodhead Publishing 2015.
74. Justine RY, Janssen M, Liang BJ, Huang H-C, Fisher JP. A liposome/gelatin methacrylate nanocomposite hydrogel system for delivery of stromal cell-derived factor-1α and stimulation of cell migration. Acta Biomater 2020; 108: 67–76.

Chapter 6

1. Craig JP, Nichols KK, Akpek EK, Caffery B, Dua HS, Joo C-K, Liu Z, Nelson JD, Nichols JJ, Tsubota K, Stapleton F. TFOS DEWS II definition and classification report. Ocul Surf 2017; 15: 276–283.
2. Lemp MA, Bron AJ, Baudouin C, Del Castillo JMB, Geffen D, Tauber J, Foulks GN, Pepose JS, Sullivan BD. Tear osmolarity in the diagnosis and management of dry eye disease. Am J Ophthalmol 2011; 151: 792–798.
3. Stapleton F, Alves M, Bunya VY, Jalbert I, Lekhanont K, Malet F, Na KS, Schaumberg D, Uchino M, Vehof J. TFOS DEWS II epidemiology report. Ocul Surf 2017; 15: 334–365.
4. Sullivan BD, Crews LA, Sönmez B, de la Paz MF, Comert E, Charoenrook V, de Araujo AL, Pepose JS, Berg MS, Kosheleff VP. Clinical utility of objective tests for dry eye disease: Variability over time and implications for clinical trials and disease management. Cornea 2012; 31: 1000–1008.
5. Rocha G, Gulliver E, Borovik A, Chan CC. Randomized, masked, in vitro comparison of three commercially available tear film osmometers. Clin Ophthalmol 2017; 11: 243–248.
6. Lee YH, Bang S-P, Shim K-Y, Son M-J, Kim H, Jun JH. Association of tear matrix metalloproteinase 9 immunoassay with signs and symptoms of dry eye disease: A cross-sectional study using qualitative, semiquantitative, and quantitative strategies. PLoS ONE 2021; 16: e0258203.

7. Sambursky R, Davitt WF III, Friedberg M, Tauber S. Prospective, multicenter, clinical evaluation of point-of-care matrix metalloproteinase-9 test for confirming dry eye disease. Cornea 2014; 33: 812–818.
8. Di Zazzo A, Barabino S, Fasciani R, Aragona P, Giannaccare G, Villani E, Rolando M. One soul and several faces of evaporative dry eye disease. J Clin Med 2024; 13: 1220.
9. de la Fuente M, Rodríguez-Agirretxe I, Vecino E, Astigarraga E, Acera A, Barreda-Gómez G. Elevation of tear MMP-9 concentration as a biomarker of inflammation in ocular pathology by antibody microarray immunodetection assays. Int J Mol Sci 2022; 23: 5639.
10. Chotikavanich S, de Paiva CS, Li DQ, Chen JJ, Bian F, Farley WJ, Pflugfelder SC. Production and activity of matrix metalloproteinase-9 on the ocular surface increase in dysfunctional tear syndrome. Investig Ophthalmol Vis Sci 2009; 50: 3203–3209.
11. Lanza NL, McClellan AL, Batawi H, Felix ER, Sarantopoulos KD, Levitt RC, Galor A. Dry eye profiles in patients with a positive elevated surface matrix metalloproteinase 9 point-of-care test versus negative patients. Ocul Surf 2016; 14: 216–223.
12. Mu C, Shi M, Liu P, Chen L, Marriott G. Daylight-mediated, passive, and sustained release of the glaucoma drug timolol from a contact lens. ACS Cent Sci 2018; 4: 1677–1687.
13. Wang TZ, Liu XX, Wang SY, Liu Y, Pan XY, Wang JJ, Nan KH. Engineering advanced drug delivery systems for dry eye: A review. Bioengineering 2022; 10: 53.
14. Kumari A, Sharma PK, Garg VK, Garg G. Ocular inserts—Advancement in therapy of eye diseases. J Adv Pharm Technol Res 2010; 1: 291–296.
15. Mariz M, Murta J, Gil MH, Ferreira P. An ocular insert with zero-order extended delivery: Release kinetics and mathematical models. Eur J Pharm Biopharm 2022; 181: 79–87.
16. Alzahrani A, Youssef AAA, Nyavanandi D, Tripathi S, Bandari S, Majumdar S, Repka MA. Design and optimization of ciprofloxacin hydrochloride biodegradable 3D printed ocular inserts: Full factorial design and in-vitro and ex-vivo evaluations: Part II. Int J Pharm 2023; 631: 122533.
17. Duman G, Yıldır İ, Macit M, Genç E, Sümer E, Kale S, Deniz İ. Development and evaluation of 3D-printed ocular insert containing liposomal moxifloxacin. J Drug Deliv Sci Technol 2024; 92: 105353.
18. Friederich R. The pilocarpine Ocusert: A new drug delivery system. Ann Ophthalmol 1974; 6: 1279–1284.
19. Kamaly N, Yameen B, Wu J, Farokhzad OC. Degradable controlled-release polymers and polymeric nanoparticles: Mechanisms of controlling drug release. Chem Rev 2016; 116: 2602–2663.
20. Kimura H, Ogura Y. Biodegradable polymers for ocular drug delivery. Ophthalmologica 2001; 215: 143–155.
21. Vert M, Doi Y, Hellwich K-H, Hess M, Hodge P, Kubisa P, Rinaudo M, Schué F. Terminology for biorelated polymers and applications (IUPAC Recommendations 2012). Pure Appl Chem 2012; 84: 377–410.
22. Lyu S, Untereker D. Degradability of polymers for implantable biomedical devices. Int J Mol Sci 2009; 10: 4033–4065.
23. Zhao L, Qi X, Cai T, Fan Z, Wang H, Du X. Gelatin hydrogel/contact lens composites as rutin delivery systems for promoting corneal wound healing. Drug Deliv 2021; 28: 1951–1961.
24. Wang Y, Ma M, Wang J, Zhang W, Lu W, Gao Y, Zhang B, Guo Y. Development of a photo-crosslinking, biodegradable GelMA/PEGDA hydrogel for guided bone regeneration materials. Materials 2018; 11: 1345.

25. Yue K, Trujillo-de Santiago G, Alvarez MM, Tamayol A, Annabi N, Khademhosseini A. Synthesis, properties, and biomedical applications of gelatin methacryloyl (GelMA) hydrogels. Biomaterials 2015; 73: 254–271.
26. Tse JW, Rizwan M, Rasmussen J, Jones L, Yim EKF. Gelatin methacrylate as an enzyme-controlled release vehicle of hyaluronic acid for the treatment of recurrent corneal erosion. ACS Appl Bio Mater 2020; 3: 6214–6223.
27. Schwab A, Levato R, D'Este M, Piluso S, Eglin D, Malda J. Printability and shape fidelity of bioinks in 3D bioprinting. Chem Rev 2020; 120: 11028–11055.
28. Leone G, Consumi M, Pepi S, Pardini A, Bonechi C, Tamasi G, Donati A, Rossi C, Magnani A. Modified low molecular weight poly-vinyl alcohol as viscosity enhancer. Mater Today Commun 2019; 21: 100634.
29. Phan C-M, Subbaraman LN, Jones LW. Uptake and release of polyvinyl alcohol from hydrogel daily disposable contact lenses. Optom Vis Sci 2019; 96: 180–186.
30. Pflugfelder SC, Farley W, Luo L, Chen LZ, de Paiva CS, Olmos LC, Li DQ, Fini ME. Matrix metalloproteinase-9 knockout confers resistance to corneal epithelial barrier disruption in experimental dry eye. Am J Pathol 2005; 166: 61–71.
31. Bhaskaran R, Palmier MO, Lauer-Fields JL, Fields GB, Van Doren SR. MMP-12 catalytic domain recognizes triple helical peptide models of collagen V with exosites and high activity. J Biol Chem 2008; 283: 21779–21788.
32. Lauer-Fields JL, Sritharan T, Stack MS, Nagase H, Fields GB. Selective hydrolysis of triple-helical substrates by matrix metalloproteinase-2 and -9. J Biol Chem 2003; 278: 18140–18145.
33. Shokrollahi P, Garg P, Wulff D, Hui A, Phan CM, Jones L. Vat photopolymerization 3D printing optimization: Analysis of print conditions and print quality for complex geometries and ocular applications. Int J Pharm 2025; 668: 124999.
34. Procházková L, Rodríguez-Muñoz Y, Procházka J, Wanner J. Simple spectrophotometric method for determination of polyvinylalcohol in different types of wastewater. Int J Environ Anal Chem 2014; 94: 399–410.
35. Liu Y, Fan Q, Huo Y, Liu C, Li B, Li Y. Construction of a mesoporous polydopamine@GO/cellulose nanofibril composite hydrogel with an encapsulation structure for controllable drug release and toxicity shielding. ACS Appl Mater Interfaces 2020; 12: 57410–57420.
36. Garg P, Shokrollahi P, Darge HF, Phan C-M, Jones L. Controlled PVA release from chemical-physical interpenetrating networks to treat dry eyes. ACS Omega 2024; 10: 1249–1260.
37. Yu K, Zhang XJ, Sun Y, Gao Q, Fu JZ, Cai XJ, He Y. Printability during projection-based 3D bioprinting. Bioact Mater 2022; 11: 254–267.
38. Bose S, Phan CM, Rizwan M, Tse JW, Yim E, Jones L, Pignatello R, Almeida H, Santonocito D, Puglia C. Fabrication and characterization of an enzyme-triggered, therapeutic-releasing hydrogel bandage contact lens material. Pharmaceutics 2024; 16: 26.
39. Zhu MX, Wang YY, Ferracci G, Zheng J, Cho NJ, Lee BH. Gelatin methacryloyl and its hydrogels with an exceptional degree of controllability and batch-to-batch consistency. Sci Rep 2019; 9: 6863.
40. Heidarian P, Kouzani AZ, Kaynak A, Paulino M, Nasri-Nasrabadi B. Dynamic hydrogels and polymers as inks for three-dimensional printing. ACS Biomater Sci Eng 2019; 5: 2688–2707.
41. Chen Q, Chen H, Zhu L, Zheng J. Fundamentals of double network hydrogels. J Mater Chem B 2015; 3: 3654–3676.
42. Mandrycky C, Wang Z, Kim K, Kim D-H. 3D bioprinting for engineering complex tissues. Biotechnol Adv 2016; 34: 422–434.

43. Caprioli M, Roppolo I, Chiappone A, Larush L, Pirri CF, Magdassi S. 3D-printed self-healing hydrogels via Digital Light Processing. Nat Commun 2021; 12: 2462.
44. Ino JM, Sju E, Ollivier V, Yim EK, Letourneur D, Le Visage C. Evaluation of hemocompatibility and endothelialization of hybrid poly(vinyl alcohol)(PVA)/gelatin polymer films. J Biomed Mater Res B Appl Biomater 2013; 101: 1549–1559.
45. Hassan CM, Peppas NA. Structure and applications of poly(vinyl alcohol) hydrogels produced by conventional crosslinking or by freezing/thawing methods. Adv Polym Sci 2000; 153: 37–65.
46. Mandal P, Stokes K, Hernández G, Brandell D, Mindemark J. Influence of binder crystallinity on the performance of Si electrodes with poly(vinyl alcohol) binders. ACS Appl Energy Mater 2021; 4: 3008–3016.
47. Adelnia H, Ensandoost R, Moonshi SS, Gavgani JN, Vasafi EI, Ta HT. Freeze/thawed polyvinyl alcohol hydrogels: Present, past and future. Eur Polym J 2022; 164: 110974.
48. Liu Y, Vrana N, Cahill P, McGuinness G. Physically crosslinked composite hydrogels of PVA with natural macromolecules: Structure, mechanical properties, and endothelial cell compatibility. J Biomed Mater Res B Appl Biomater 2009; 90: 492–502.
49. Thangprasert A, Tansakul C, Thuaksubun N, Meesane J. Mimicked hybrid hydrogel based on gelatin/PVA for tissue engineering in subchondral bone interface for osteoarthritis surgery. Mater Des 2019; 183: 108113.
50. Bernal-Chávez SA, Romero-Montero A, Hernández-Parra H, Peña-Corona SI, Del Prado-Audelo ML, Alcalá-Alcalá S, Cortés H, Kiyekbayeva L, Sharifi-Rad J, Leyva-Gómez G. Enhancing chemical and physical stability of pharmaceuticals using freeze-thaw method: Challenges and opportunities for process optimization through quality by design approach. J Biol Eng 2023; 17: 35.
51. Hu Q, Lu R, Liu S, Liu Y, Gu Y, Zhang H. 3D printing GelMA/PVA interpenetrating polymer networks scaffolds mediated with CuO nanoparticles for angiogenesis. Macromol Biosci 2022; 22: 2200208.
52. Sivak JM, Fini ME. MMPs in the eye: Emerging roles for matrix metalloproteinases in ocular physiology. Prog Retin Eye Res 2002; 21: 1–14.
53. Toth M, Sohail A, Fridman R. Assessment of gelatinases (MMP-2 and MMP-9) by gelatin zymography. Methods Mol Biol 2012; 878: 121–135.
54. Loessner D, Meinert C, Kaemmerer E, Martine LC, Yue K, Levett PA, Klein TJ, Melchels FP, Khademhosseini A, Hutmacher DW. Functionalization, preparation and use of cell-laden gelatin methacryloyl–based hydrogels as modular tissue culture platforms. Nat Protoc 2016; 11: 727–746.
55. Schuurman W, Levett PA, Pot MW, van Weeren PR, Dhert WJ, Hutmacher DW, Melchels FP, Klein TJ, Malda J. Gelatin-methacrylamide hydrogels as potential biomaterials for fabrication of tissue-engineered cartilage constructs. Macromol Biosci 2013; 13: 551–561.
56. Lalitha Sridhar S, Vernerey F. Localized enzymatic degradation of polymers: Physics and scaling laws. Phys Rev Appl 2018; 9: 031001.
57. Ho B, Phan CM, Garg P, Shokrollahi P, Jones L. A rapid screening platform for simultaneous evaluation of biodegradation and therapeutic release of an ocular hydrogel. Pharmaceutics 2023; 15: 2625.
58. Marcos Luciano B. Mathematical models of drug release. In Strategies to modify the drug release from pharmaceutical systems; Woodhead Publishing: Sawston, UK, 2015; 63–86.

Chapter 7

1. White C, Tieppo A, Byrne M. Controlled drug release from contact lenses: A comprehensive review from 1965-present. J Drug Deliv Sci Technol 2011; 21(5): 369–384.
2. Yoo J, Won Y-Y. Phenomenology of the initial burst release of drugs from PLGA microparticles. ACS Biomater Sci Eng 2020; 6(11): 6053–6062.
3. Galante R, Pinto TJ, Colaco R, Serro AP. Sterilization of hydrogels for biomedical applications: A review. J Biomed Mater Res B Appl Biomater 2018; 106(6): 2472–2492.
4. Bento CS, Gaspar MC, Coimbra P, de Sousa HC, Braga ME. A review of conventional and emerging technologies for hydrogels sterilization. Int J Pharm 2023; 634: 122671.
5. Sambursky R, Davitt WF III, Friedberg M, Tauber S. Prospective, multicenter, clinical evaluation of point-of-care matrix metalloproteinase-9 test for confirming dry eye disease. Cornea 2014; 33(8): 812–818.
6. Pflugfelder SC, Farley W, Luo L, Chen LZ, de Paiva CS, Olmos LC, Li DQ, Fini ME. Matrix metalloproteinase-9 knockout confers resistance to corneal epithelial barrier disruption in experimental dry eye. Am J Pathol 2005; 166(1): 61–71.